Technische Universität München
TUM School of Life Sciences

Identification and characterization of novel regulators of ferroptotic cell death

Juliane Tschuck

Vollständiger Abdruck der von der TUM School of Life Sciences der Technischen Universität München zur Erlangung des akademischen Grades einer

Doktorin der Naturwissenschaften (Dr. rer. nat.)

genehmigten Dissertation.

Vorsitz: Prof. Dr. Johan Philipp Benz

Prüfende der Dissertation:

1. Prof. Dr. Nina Henriette Uhlenhaut
2. Priv.- Doz. Dr. Tobias Fromme

Die Dissertation wurde am 04.10.2023 bei der Technischen Universität München eingereicht und durch die TUM School of Life Sciences am 21.01.2024 angenommen.

Table of Content

1. Summary

Ferroptosis is an iron-dependent form of regulated cell death that is significantly different from apoptosis. Important hallmarks of this cell death are impaired defenses against oxidative stress, a labile iron pool present in the cell and subsequently peroxidation of polyunsaturated fatty acid-containing phospholipids in the cellular membrane. Over the last decade it became evident that ferroptosis occurs in several diseases, sometimes as a cause but also as a side effect together with other types of cell death. Even though there is a high research interest in targeting ferroptosis in degenerative diseases or cancer, many fundamental aspects about it remain still unknown, such as the exact physiological role of ferroptosis. To uncover yet unknown mechanisms and regulators of ferroptosis that could serve as possible drug targets we conducted a compound screening with 3,684 small molecules with known mode of actions. We obtained 16 hits, from which we analyzed two compounds in detail: by analyzing the screening hits Turofexorate and Fexaramine, we established that the Farnesoid X receptor increases the transcription of important anti-ferroptotic genes in several liver-related cellular systems, which presents new potential for the treatment of ferroptosis-associated liver diseases. We furthermore found that Seratrodast, an approved asthma drug, is also an inhibitor of lipid peroxidation and discovered that its anti-ferroptotic properties stem from a quinone moiety that confers radical-trapping activity. These findings can be used in a drug repurposing strategy. In a third project, we established that vitamin A is a strong inhibitor of ferroptosis by activating the Retinoic Acid receptor, and thereby increasing a set of ferroptosis-regulatory genes. This process seems to be important during stem cell differentiation into cortical neurons to ensure correct brain formation.

1. Zusammenfassung

Ferroptose ist eine eisenabhängige Form des regulierten Zelltods, die sich deutlich von der Apoptose unterscheidet. Wichtige Merkmale dieses Zelltods sind beeinträchtigte Abwehrmechanismen gegen oxidativen Stress, ein freier Eisenpool in der Zelle und anschließend die Peroxidation von mehrfach ungesättigten Fettsäuren enthaltenden Phospholipiden in der Zellmembran. In den letzten zehn Jahren wurde deutlich, dass Ferroptose bei verschiedenen Krankheiten auftritt, manchmal als Ursache, aber auch als Nebeneffekt zusammen mit anderen Arten des Zelltods. Obwohl es ein großes Forschungsinteresse gibt, Ferroptose bei degenerativen Erkrankungen oder Krebs zu bekämpfen, bleiben viele grundlegende Aspekte noch unbekannt, wie zum Beispiel die genaue physiologische Rolle der Ferroptose. Um bisher unbekannte Mechanismen und Regulatoren der Ferroptose zu entdecken, die als mögliche Zielstrukturen für Medikamente dienen könnten, haben wir ein Compound-Screening mit 2.000 Molekülen mit bekannten Wirkmechanismen durchgeführt. Wir haben 16 Hits erhalten, von denen wir zwei Compounds im Detail analysiert haben: Durch die Analyse der Screening-Treffer Turofexorate und Fexaramine stellten wir fest, dass der Farnesoid-X-Rezeptor die Transkription wichtiger anti-ferroptotischer Gene in leber-bezogenen zellulären Systemen erhöht, was neue Möglichkeiten für die Behandlung von ferroptose-assoziierten Leber-Erkrankungen bietet. Wir fanden außerdem heraus, dass Seratrodast, ein zugelassenes Asthmamedikament, auch ein Inhibitor der Lipidperoxidation ist und entdeckten, dass seine anti-ferroptotischen Eigenschaften von einer Chinon-Gruppe herrühren, die radikalfangende Aktivität hat. Diese Erkenntnisse können in einer Drug-Repurposing-Strategie verwendet werden. In einem dritten Projekt stellten wir fest, dass Vitamin A ein starker Inhibitor der Ferroptose ist, indem es den Retinsäure-Rezeptor aktiviert und dadurch die Expression mehrerer ferroptose-regulierender Gene erhöht. Dieser Prozess scheint während der Stammzell-Differenzierung in kortikale Neurone wichtig zu sein, um eine korrekte Gehirnbildung sicherzustellen.

2. Abbreviations

Abbreviation	Full name
ABCC2	ATP binding cassette subfamily C member 2
ACSL3	Acyl-CoA synthetase long-chain family member 3
ACSL4	Acyl-CoA synthetase long-chain family member 4
ALB	Albumine
APS	Ammonium persulfate
ATRA	All-trans retinoic acid
BA	Bile acids
BH2	Dihydrobiopterin
BH4	Tetrahydrobiopterin
BODIPY	Boron-dipyrromethene
CDC	Chenodeoxycholic acid
cDNA	Complementary desoxyribonucleic acid
CoA	Coenzyme A
CoQ10	Coenzyme Q10/ Ubiquinone-10
CRISPR	Clustered regularly interspaced short palindromic repeats
CYP1A1	Cytochrome P450 family 1 subfamily A member 1
DMSO	Dimethyl sulfoxide
DNA	Desoxyribonucleic acid
dsDNAse	Double strand-specific Desoxyribonuclease
EDTA	Ethylenediaminetetraacetic acid
FBS	Fetal bovine serum
Fer-1	Ferrostatin-1
Fexa	Fexaramine
FIN	Ferroptosis inducing agent
FSP1	Ferroptosis suppressor protein
FXR	Farnesoid X Receptor
FXRi	FXR inhibitor, Guggulsterone
GAPDH	Glyceraldehyde-3-phosphate dehydrogenase
GCH1	GTP Cyclohydrolase 1
GFP	Green fluorescent protein
GPX4	Glutathione peroxidase 4
gRNA	Guide RNA
GSH	Glutathione
GTP	Guanosine triphosphate
HNF4A	Hepatocyte nuclear factor 4 alpha
IAP	Inhibitor of Apoptosis Protein
IC50	Half-maximal inhibitory concentration
IKE	Imidazole ketone erastin
KO	Knock-out

MEF	Mouse embryonic fibroblast
mRNA	Messenger RNA
MUFA	Mono-unsaturated fatty acid
NR1H4	Nuclear Receptor Subfamily 1 Group H Member 4
ns	not significant
NTCP	Sodium taurocholate cotransporting polypeptide
OC	Obeticholic acid
OE	Overexpression
PAGE	Polyacrylamide gel electrophoresis
PI	Propidium iodide
PL	Phospholipid
PPARa	Peroxisome proliferator-activated receptor alpha
PUFA	Poly-unsaturated fatty acid
PVDF	Polyvinylidene fluoride
qRT-PCR	Quantitative real-time polymerase chain reaction
RAR	Retinoic acid receptor
RNA	Ribonucleic acid
ROS	Reactive oxygen species
RP2	Retinitis pigmentosa gene 2
RSL3	RAS-selective lethal compound 3
RXR	Retinoid X receptor
SCD1	Stearoyl-CoA desaturase 1
SD	Standard deviation
SDS	Sodium dodecyl sulfate
Sera	Seratrodast
SHP	Small heterodimer partner
siRNA	Small interfering RNA
SLC7A11	Solute carrier family 7 member 11
SMAC	Second mitochondrial-derived activator of caspases
TBARS	Thiobarbituric acid reactive substances
TBS-T	Tris-buffered saline with Tween20
TCA	Trichloroacetic acid
TEMED	Tetraacetylethylenediamine
TNFa	Tumor necrosis factor alpha
Turo	Turofexorate
wt	Wild-type

3. Introduction

3.1 Ferroptosis

3.1.1 Discovery of ferroptosis

Since the 1970s, when apoptosis was first discovered, there was a consensus among researchers that there only two types of cell death exist: on the one hand necrosis, which happens prematurely and is caused by extreme external stressors, such as injuries or toxins; and on the other hand apoptosis, which is highly regulated and happens in a pointed manner [1]. During necrosis, the cell ruptures and causes an immune response due to release of damage-associated molecular patterns (DAMPs) [2]. Apoptosis, in contrast, does not cause an immune response, since cellular contents are packed into apoptotic bodies and digested by phagocytosis [3]. It has become evident that the controlled deletion of cells is essential for numerous processes in the human body: apoptosis maintains tissue homeostasis by counteracting cell proliferation, it prevents cancer in cells with DNA damage, it protects tissues from spreading infections, and it also shapes the morphology of organs during embryonal development [3, 4]. Therefore, the control of regulated cell death presents a promising option for the treatment of various diseases, which prompted intensive research and drug development in this field.

During the 1990s and 2000s it was discovered that several other types of regulated cell death exist, such as parthanatos [5], pyroptosis [6] and necroptosis [7]. The group of Brent Stockwell in 2012 was also searching for therapeutic uses of regulated cell death [8]. While aiming at the development of molecules that are lethal specifically to RAS-mutant tumor cells, they discovered that the cell death that was achieved by their molecule was not apoptotic and also could not be sorted into any other category of regulated cell death [9] [1]. It was characterized by high cellular levels of reactive oxygen species (ROS) and could be inhibited by iron chelators. This iron dependency led the researchers to coin this type of cell death “ferroptosis”. At the same time, another research group observed that cysteine uptake and the activity of glutathione peroxidase 4 significantly regulate cell survival and sensitivity towards oxidative stress in lymphoma cells [10].

These early findings still form the essential hallmarks for the current definition of ferroptosis: it is a type of non-apoptotic regulated cell death that depends on a labile iron pool in the cell [11]. Ferroptosis is induced when cellular defenses against reactive oxygen species are impaired, which allows excessive peroxidation of phospholipids containing polyunsaturated fatty acids (PUFAs) [11]. These PUFA-phospholipids are located in the plasma membrane as well as in subcellular membranes, such as ER, mitochondria and lysosome membranes. The exact mechanism of how lipid peroxidation leads to ferroptotic cell death has not been resolved yet, but it has been hypothesized that peroxidized PUFA-phospholipids alter membrane stability, leading to thinning, reduced fluidity and finally damage of the membranes [12]. It could also be shown that ferroptosis happens in different phases: early ferroptosis begins at the membranes of the endoplasmic reticulum, and only later lipid peroxidation spreads to the plasma membrane [13]. Besides peroxidation products of PL-PUFAs (such as 4-Hydroxynonenal or Malondialdehyde), further markers of ferroptosis could be established: shrinkage of mitochondria, upregulation and translocation of Transferrin receptor 1 (TfR1) towards the membrane, and changes in the expression of typical regulators of ferroptosis [1].

Until now, there is no general consent about a possible physiological role of ferroptosis and it was discussed whether it only occurs in pathological settings. However, there have been several reports that connect ferroptosis to physiological processes: $CD8^+$ T cells can induce ferroptosis in tumor cells [14]; p53 as major tumor suppressor controls the expression of ferroptosis regulators [15] [16]; aging of mice, rats and nematodes is associated with increased ferroptosis susceptibility [17] [18]; and ferroptosis could even be reported in plants [19].

A growing body of evidence shows that ferroptosis is a driver of neurodegenerative diseases, especially in Parkinson's Disease, Huntington's Disease, Alzheimer's Disease and amyotrophic lateral sclerosis [4]. Besides the brain, a variety of other organs can also be affected by ferroptosis: acute heart failure, acute kidney failure, necrotic liver injury, atherosclerosis and chronic obstructive pulmonary disease were connected to cell death by ferroptosis via *in vivo* mouse studies or human patient samples [4] [20, 21]. Furthermore, studies showed that induction of ferroptosis can kill cancer cells and reduce tumor size; however, different types of cancer display different susceptibility towards ferroptosis. The exact

metabolic, genetic or proteomic profile that is necessary to reliably induce ferroptotic cell death in cancer remains to be solved and might be highly complex [22] [23].

3.1.2 Cellular regulators of ferroptosis

In contrast to apoptosis or necroptosis, ferroptosis does not involve long cascades of kinases and phosphorylation that are induced upon a stimulus and lead to a signal transduction that ends in controlled degradation of a cell [3]. Instead, cells contain several lines of defense against oxidative stress and ferroptosis, which are known as negative regulators of ferroptosis [4]. These regulators are enzymes that produce metabolites with radical-trapping, antioxidant or iron-chelating functions, have these functions themselves or activate the expression of other negative regulators and therefore promote a ferroptosis-inhibiting cellular milieu [24] [9]. The most important direct anti-ferroptotic defenses are Glutathione Peroxidase 4 (GPX4), Ferroptosis Suppressor Protein 1 (FSP1, formerly known as Apoptosis Inducing Factor Mitochondria Associated 2, AIFM2), system xc- (SLC7A11) and GTP-cyclohydrolase 1 (GCH1) [1]. Additional important anti-ferroptotic regulators are enzymes involved in the synthesis of monounsaturated fatty acids (MUFAs), such as Acyl-CoA Synthetase Long Chain Family Member 3 (ACSL3) or Stearoyl-CoA Desaturase (SCD1), since MUFAs inhibit lipid peroxidation at the plasma membrane [25]. An overview about the most important ferroptosis regulators can be found in Figure **1**.

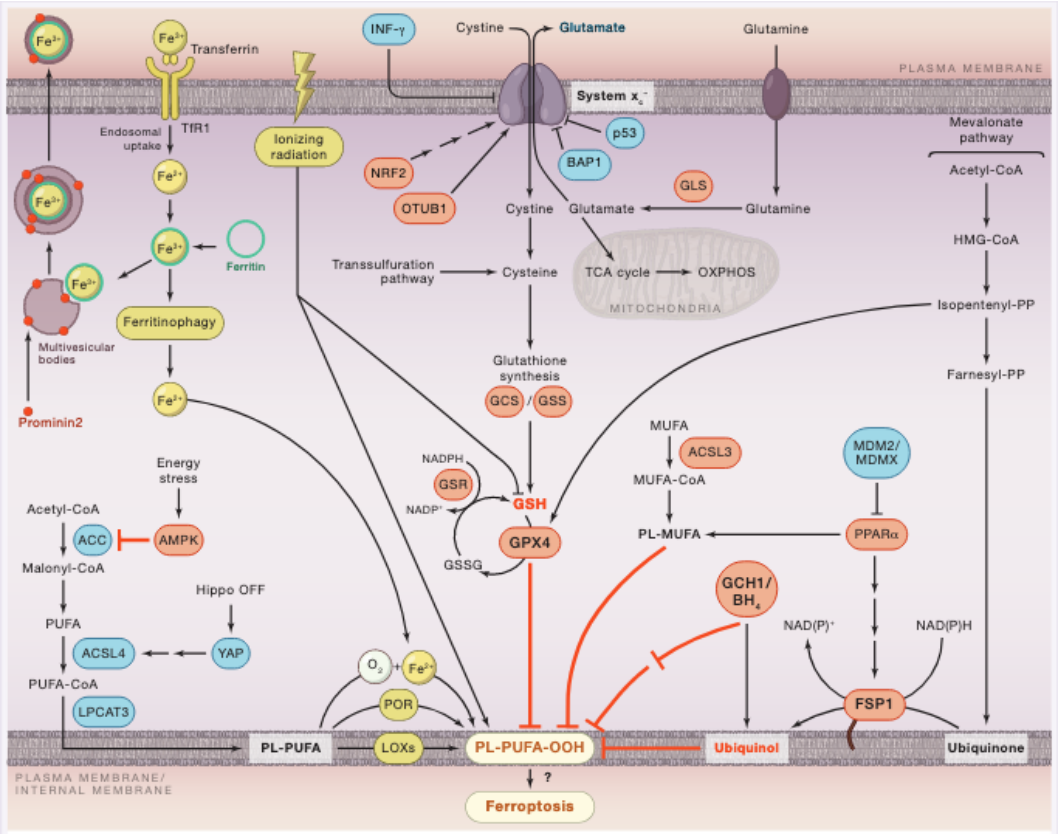

Figure 1: **Central regulators of ferroptosis.** In 2020, Hadian and Stockwell published a SnapShot of the most important regulatory axes in ferroptosis: iron uptake and metabolism, MUFA and PUFA synthesis, system xc-/GPX4, FSP1/ubiquinone and GCH1/tetrahydrobiopterin. [26]

In order to keep cellular homeostasis and antioxidative balance, negative regulators of ferroptosis have to function properly and must be powerful enough to substitute one another in case of a failure of one anti-ferroptotic defense. However, ferroptosis can also be regulated positively by cells, which could represent a possible tumor suppressor function of ferroptosis. Peroxidation of polyunsaturated fatty acid (PUFA)-containing phospholipids (PUFA-PLs) is the main driver of ferroptotic cell death and is caused by reactive oxygen species (ROS), that normally arise as unwanted byproducts during cellular processes such as the electron transport chain in mitochondria or the enzymatic activity of oxidases [27] [11] [5]. In the context of ferroptosis, however, ROS are created by a chemical reaction called Fenton reaction, which involves the oxidation of intracellular iron(II) by oxygen species (such as hydrogen peroxide) into iron(III) and PL-PUFA-hydroperoxides [9]. The Fenton reaction also produces hydroxyl radicals, which subsequently propagate lipid peroxidation of cellular membranes [28]. Lipoxygenases, such as Arachidonate 15-Lipoxygenase (ALOX15), further catalyze the

peroxidation of PL-PUFAs [29]. Since the Fenton reaction is iron-dependent, increased iron uptake by Transferrin Receptor 1 (TfR1) and intracellular release of iron from ferritin enhances the susceptibility to ferroptosis [30]. Enzymes that catalyze the synthesis of PL-PUFAs are also considered positive regulators of ferroptosis, such as Acyl-CoA Synthetase Long Chain Family Member 4 (ACSL4) or Lysophosphatidylcholine Acyltransferase 3 (LPCAT3) [29].

3.1.2.1 The GPX4/ system xc- axis

Mammals express eight confirmed isoforms of glutathione peroxidases, which all serve the purpose of defending the cell against oxidative stress [31]. Glutathione peroxidase 4 (GPX4) specifically inhibits lipid peroxidation and is ubiquitously expressed, which makes it the central enzyme of ferroptosis regulation [10]. A complete knock out of GPX4 is lethal [32], and newborns with GPX4 mutations show severe symptoms and a short life expectancy, which underlines the immense importance of this enzyme [33]. In order to catalyze the reduction of lipid peroxides, GPX4 uses reduced glutathione as a cofactor, which is recycled by glutathione reductase (GSR) at the expense of NADPH. In its catalytic center, GPX4 possesses a triade of selenocysteine, asparagine and tryptophane, and during reduction of peroxides, selenol is oxidized to selenic acid. Glutathione then recycles selenic acid back to selenol [34].

GPX4 can only function together with the reduced form of glutathione, whose synthesis requires cysteine. This is imported into the cell as cystine via system xc- (catalytic subunit SLC7A11), a cystine-glutamate antiporter. By inhibiting system xc- and thereby starving the cell from cysteine, ferroptosis can be induced, since glutathione cannot be recycled and serve as cofactor for GPX4 [35]. The expression of system xc- is, among others, controlled by tumor suppressor p53 and the ubiquitin-proteasome system and presents a regulator of cellular susceptibility to ferroptotic cell death [36] [16].

3.1.2.2 The FSP1/ ubiquinone/ vitamin K axis

Ferroptosis suppressor protein 1 (FSP1) is a flavoprotein oxidoreductase and was known as apoptosis-inducing factor 2 (AIFM2) until it was established that its main function is the suppression of ferroptotic cell death [37]. It could be observed that there are some cancer cell lines that are resistant to ferroptosis induction via inhibition of GPX4, which sparked the question whether different cellular defenses against ferroptosis might exist. In a cDNA library screening in ferroptosis-resistant breast cancer cells it was established that FSP1 serves as a substitute defense to compensate the loss of GPX4 [38]. The mechanism of action of FSP1 is the reduction of ubiquinone to ubiquinol, which is an antioxidant and thereby prevents lipid peroxidation of cellular membranes [39]. Recently it was discovered that FSP1 also reduces vitamin K (*i.e.,* phylloquinone and menaquinone) to hydroquinone, another potent antioxidant and ferroptosis suppressor [40]. The substrates of FSP1 are obtained from the mevalonate pathway, where acetyl-CoA is metabolized first into mevalonate and then further into isopentenyl pyrophosphates, which are basic building blocks for a variety of biomolecules [41]. The anti-ferroptotic function of FSP1 is mainly conferred by its N-terminus [38] [42]: it contains a myristoylation motif, which might facilitate the binding of FSP1 to lipid bilayers of the endoplasmic reticulum and Golgi apparatus, both key organelles of early ferroptosis [13].

3.1.2.3 The GCH1/ Tetrahydrobiopterin/ DHFR axis

Another GPX4-independent line of defense against ferroptosis is formed by GTP cyclohydrolase 1 (GCH1), the rate-limiting enzyme in the conversion of GTP into tetrahydrobiopterin (BH_4) [1]. Originally, GCH1 was found to play a role in modulating pain sensitivity [43], but a CRISPR activation screen in 2020 revealed an additional function in suppressing lipid peroxidation and ferroptotic cell death [44]. This anti-ferroptotic effect of GCH1 is achieved by different mode of actions: on the one hand, the produced BH_4 is a strong radical trapping and antioxidant agent, and suppression of BH_4 synthesis leads to uncoupling of nitric oxide synthases and creates ROS. This finding was also confirmed in an additional study [45]. Furthermore, the GCH1-produced BH_4 leads to lipid remodeling and selectively

protects plasma membrane PL-PUFAs from peroxidation by radicals. As a third mechanism, GCH1 overexpression increases the pool of ubiquinone, another potent cellular antioxidant [44] [46]. These three mechanisms of GCH1 can effectively inhibit ferroptosis, and it was also shown that a combined treatment of GCH1 inhibition and ferroptosis inducer erastin effectively reduces tumor growth [47]. BH_4 can not only be synthesized from GTP, but it can also be regenerated from dihydrobiopterin (BH_2), which is catalyzed by dihydrofolate reductase (DHFR) [45]. These insights together with the findings that overexpression of GCH1 can replace the knock out of GPX4 [44] make GCH1 a significant regulator of ferroptosis and a promising drug target for ferroptosis-related diseases.

3.1.2.4 Lipid metabolism in ferroptosis

Since the peroxidation of PL-PUFAs is the main driver of ferroptosis, enzymes of lipid metabolism and synthesis have a significant impact on the regulation of ferroptosis sensitivity or resistance. It was discovered that the supplementation of cells with monounsaturated fatty acids (MUFAs) protects from ferroptotic cell death, since MUFA-containing phospholipids are less prone to peroxidation by ROS [25]. Enzymes of MUFA synthesis can therefore increase cellular protection against lipid peroxidation [48] [25]. The first rate-limiting enzyme of MUFA synthesis is stearoyl coenzyme A desaturase 1 (SCD1), which inserts a double bond into saturated fatty acids, particularly stearic acid and palmitic acid [49]. In order to be metabolized, long chain fatty acids must be converted into fatty acyl-CoA. This reaction is catalyzed by Acyl-CoA Synthetase Long Chain Family Member 3 (ACSL3), an enzyme which activates MUFAs by ligating coenzyme A (CoA) to them [50]. With increased expression of ACSL3 or SCD1, more MUFAs are synthesized and incorporated into the cell membrane, which creates a ferroptosis-protected cellular state. The expression of SCD1 is regulated either by the dietary hormones insulin and leptin, or by several nuclear receptors and transcription factors, such as LXRα, SREBP or PPARα [51] [52]. ACSL3 is mainly under transcriptional control of PPARδ [53].

In the same way that MUFA-PL protect cells from ferroptosis, increased incorporation of PUFA-PL into cellular membranes sensitizes cells towards ferroptosis, since PUFA-PL are more prone to lipid peroxidation. One ferroptosis-relevant enzyme of PUFA synthesis is Acyl-CoA Synthetase Long Chain Family Member 4 (ACSL4), due to its substrate specificity for arachidonic acid, a 20:4 PUFA. Expression levels of ACSL4 regulate cellular sensitivity towards ferroptosis: knock out of ACSL4 leads to increased ferroptosis resistance in cells, even in combination with a GPX4 knock out, whereas overexpression sensitizes cancer cells to ferroptotic cell death [54]. Downstream of ACSL4 in PUFA-PL are the enzymes lysophosphatidylcholine acyltransferase 3 (LPCAT3) and 15-lipoxygenase (ALOX15), which are also considered ferroptotic regulators. LPCAT3 esterifies PUFA-CoA into phosphatidylethanolamines (PE), whereas ALOX15 directly catalyzes the peroxidation of PUFA-PL [29] [55]. By conducting lipidomic analyses on cells and quantifying the amounts of different MUFA and PUFA species, the "ferroptotic state" of cells, *e.g.,* after compound treatment, can reliably be assessed.

3.1.2.5 Iron metabolism in ferroptosis

Ferroptosis is dependent on the presence of iron in cells, since the Fenton reaction that causes lipid peroxidation is facilitated by iron(II) [9] [28]. Cellular iron metabolism must always be maintained at a certain level, and an imbalance in iron uptake or release can lead to altered ferroptosis sensitivity [56]. Iron uptake into cells primarily happens via endocytosis mediated by transferrin receptor 1 (TfR1), where transferrin-bound iron(III) is imported into the cell [57]. Subsequently, iron is released from endosomes by divalent metal ion transporter 1 (DMT1) and reduced to iron(II) [58]. In order to store iron in the cell in a non-toxic from, it is bound by ferritin as iron(III) [59]. Ferritinophagy, an autophagic process of ferritin degradation, releases iron from ferritin, which then enters the intracellular labile iron pool and significantly contributes to the generation of ROS [60]. Therefore, controlling iron import by regulating TfR1 expression and ferritinophagy regulates ferroptosis resistance. Recently it was also established that TfR1 is one of few ferroptosis markers: upon ferroptosis induction, TfR1 expression is increased,

and image analysis shows that TfR1 accumulates at the plasma membrane [30] . By treating cells with iron chelators, that effectively reduce the labile iron pool, ferroptosis can also be suppressed [61].

3.1.3 Small molecule inducers and inhibitors of ferroptosis

Small molecules that induce ferroptosis are categorized into four different classes according to their different mode of actions [1]. Class I inducers inhibit system xc-, which causes a stop of cystine import into the cell. This leads to depletion of cysteine, which is necessary for glutathione synthesis, an important antioxidant and cofactor of GPX4 [35]. The first class I ferroptosis inducer discovered was erastin, which was also used in experiments that lead to the discovery of ferroptosis [62]. Throughout the years, erastin analogs with optimized selectivity, stability and potency were developed, such as imidazole ketone erastin (IKE) or Piperazine erastin [63]. System xc- can also be inhibited by glutamate, Sulfasalazine or Sorafenib, but less potent and selective than erastin analogs [64] [65]. Class II ferroptosis inducers are small molecules that directly inhibit GPX4. One example of this class is (1S,3R)-RSL3, which is most often used for *in vitro* ferroptosis studies, but is not suitable *in vivo* due to low stability [8]. As alternative class II compounds, there are ML210 and ML162, which still need to be fully investigated [66] [67]. The third class of ferroptosis inducers includes small molecules that cause the depletion of peroxidation-suppressing antioxidant ubiquinol, such as FIN56. It activates squalene synthase, an enzyme of the mevalonate pathway which diverts the flux of metabolites necessary for ubiquinol synthesis more towards sterol production [68]. In a yet unresolved mechanism, FIN56 also lowers GPX4 protein level without depletion of glutathione [4]. Class IV of ferroptosis inducers comprises compounds that induce cell death by causing the peroxidation of PUFAs, such as $FINO_2$. This compound directly oxidizes iron, which triggers the Fenton reaction and subsequently ferroptosis. $FINO_2$ also indirectly inhibits GPX4, however, deeper research into this mechanism is missing yet [69]. Besides these four classes of molecules there are also other targets that, upon inhibition, can contribute to ferroptosis induction or at least sensitize cells towards ferroptosis, such as iFSP1 or FSEN1, which inhibit FSP1 [38] [70], Methotrexate (DHFR inhibitor), which inhibits recycling of anti-

ferroptotic metabolite BH_4 [45], or statins, which disrupt the mevalonate pathway and therefore synthesis of ubiquinol or vitamin K [4].

Inhibition of ferroptosis leads to improvement of degenerative diseases, therefore a great interest in developing small molecule ferroptosis inhibitors exists. Several mechanisms of ferroptosis suppression were already established: general scavenging of ROS by antioxidants, interference in the synthesis of peroxidation-susceptible PUFA-phospholipids, or chelation of intracellular iron. Protection against ROS and lipid peroxidation is efficiently achieved by antioxidants [24]. Two compounds that show the highest potency against ferroptosis are Ferrostatin-1 and Liproxstatin-1, which both trap radicals and therefore suppress lipid peroxidation [71]. Ferrostatin-1 is considered the “gold standard” ferroptosis inhibitor, however, it is not suitable for *in vivo* therapeutical use due to metabolic instability. Currently, Ferrostatin-1 analogues are being developed and tested that display improved pharmacological characteristics, such as UAMC-3203 [72]. Liproxstatin-1 is currently in the preclinical testing phase and improves renal ischemia reperfusion injury in mice [32]. Additionally, treatment with endogenous cellular antioxidants, such as α-Tocopherol, vitamin K, ubiquinol or BH_4 also counteracts ferroptotic cell death [4]. In order to suppress PUFA-PL synthesis, inhibition of ACSL4 is necessary, which is achieved by thiazolidinediones, *e.g.,* Rosiglitazone [54]. The catalyzation of PUFA-PL peroxidation by lipoxygenases is suppressed by Baicalein, a plant-derived flavone [73].

Since ferroptosis is an iron-dependent cell death, chelation of the labile iron pool also suppresses cell death [61]. This was proved by *in vitro* experiments with Deferoxamine, Ciclopirox and Deferiprone [9]. Deferoxamine is also used *in vivo*, however, given the fundamental importance of iron and how little is known about exact iron thresholds during ferroptosis induction, studies into therapeutic applications are still needed [74].

3.2 Nuclear Receptors

3.2.1 The Nuclear Receptor Superfamily

Receptor signaling is an essential process in eukaryotic as well as prokaryotic cells and necessary for sensing, transferring and reacting to external and internal stimuli. Depending on their location and structure, different types of receptors are distinguished: transmembrane receptors, such as G protein-coupled receptors, ligand-gated ion channels or enzyme-linked receptors; and intracellular receptors, which are present in the cytoplasm or nucleus [75]. Nuclear receptors (NRs) belong into the category of intracellular receptors and, in humans, comprise of 48 members, which are distinguished according to their endogenous lipophilic ligands, such as hormones (thyroid hormones, estrogens, cortisol, progesterone, androgens or aldosterone), nutrients (vitamin D, retinoic acid, fatty acids, phospholipids, cholesterol metabolites, bile acids) or others (haem, xenobiotics) (Figure **2**) [76] [77].

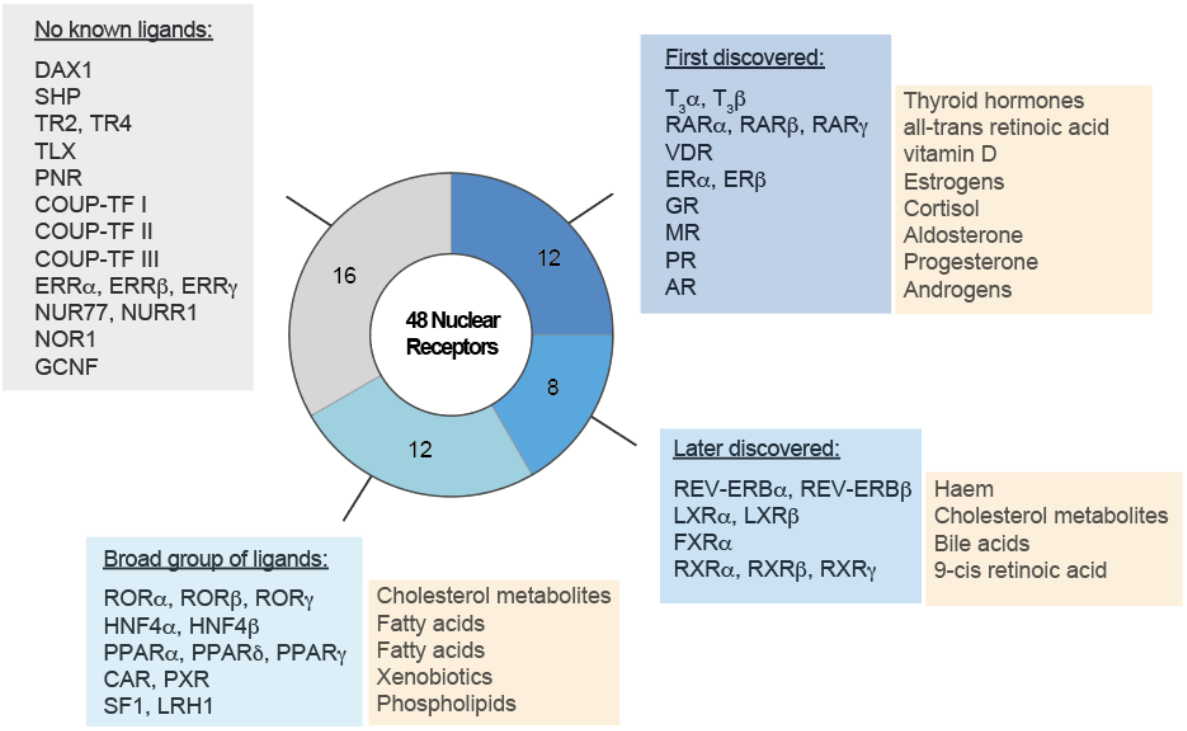

Figure 2: **The Nuclear Receptor Superfamily.** Nuclear receptors can be divided according to their endogenous ligands. Figure was adapted from a review by Scholtes and Giguere, Nat Rev Mol Cell Biol, 2022. [77]

The mechanism of action of nuclear receptors is that of ligand-activated transcription factors: upon binding, they form homo- or heterodimers with other nuclear receptors and translocate

into the nucleus, where they bind specific DNA sequences in the promoter regions of genes [78]. The dense chromatin is remodeled and made accessible for the nuclear receptors by coregulatory proteins, mostly histone acetyltransferases, which modulate the bond between histones and DNA [79]. NRs function as connections between extra- and intracellular environment and genetic regulation, since they "sense" their ligands and achieve a reaction on transcriptional level [80]. This mechanism allows to control the expression of genes necessary for important metabolic pathways, such as cholesterol synthesis, vitamin D and A metabolism or hormonal balance [77]. Nuclear receptors were first identified when researchers searched for receptors of metabolites that play important roles in the human physiology: hormones (such as estrogen, cortisol or progesterone) or nutrients (vitamins, cholesterol, fatty acids) [81]. Over the decades, researchers could match many of the NRs with their respective endogenous ligands, but today there are still "orphan" nuclear receptors that were identified but their ligands are still unknown, or receptors that only have a very broad group of ligands, such as the Peroxisome Proliferator Activated Receptors (PPARs) [77].

NRs are conserved from metazoans to humans and already existed approximately 500 million years ago, which underlines their immense significance [77]. It is even speculated that NRs contributed to the formation of diversity among multicellular organisms. Even though different species possess differently sized NR superfamilies (humans encode 48, mouse 49, *Drosophila* 20, and *C. elegans* 267 NR genes), they all share a common structure (Figure **3**) [77] [80].

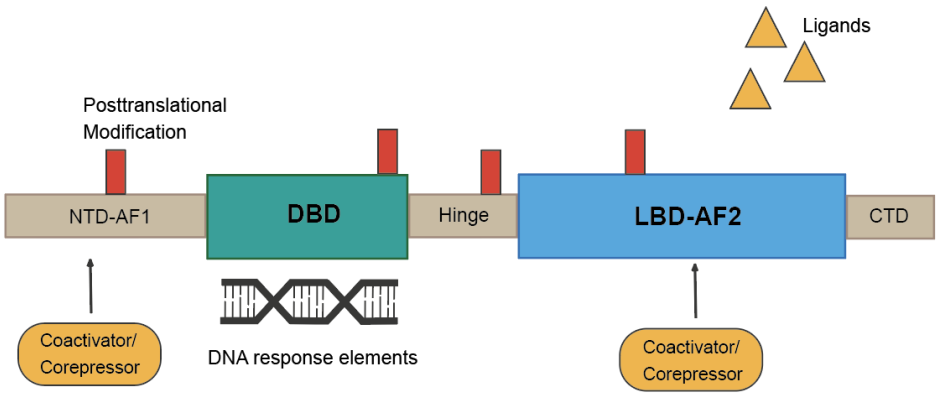

Figure 3: **Structural characterization of Nuclear Receptors.** Among every species, NRs share similar domains: the amino-terminal domain (NTD), the DNA-binding domain (DBD) with two zinc finger motifs, a flexible hinge region, the ligand-binding domain (LBD) and the C-terminal domain (CTD). Figure was adapted from a review by Scholtes and Giguere, Nat Rev Mol Cell Biol, 2022. [77]

3.2.2 Farnesoid X Receptor

The Farnesoid X receptor (FXR), also known as bile acid receptor or nuclear receptor subfamily 1, group H, member 4 (NR1H4), used to be an orphan nuclear receptor with no known ligand until 1995, when the lab of Cary Weinberger discovered in a candidate ligand screening that farnesol metabolites activate FXR [82]. In 1999, this group of ligands was further specified to bile acids, which are synthesized by oxidizing cholesterol [83]. FXR is primarily expressed in liver, kidney and small intestine, and there also have been reports about expression in immune cells, such as macrophages or natural killer cells [84].

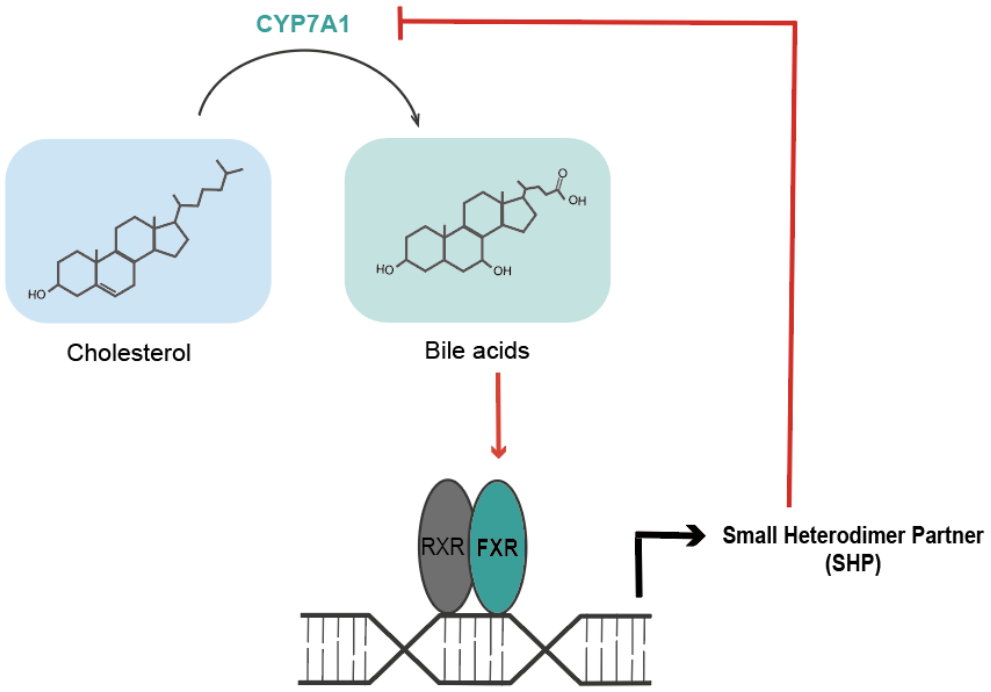

Figure 4: **Transcriptional regulation of bile acid levels by FXR.** Cholesterol is oxidized into bile acids by CYP7A1. Bile acids activate FXR, which dimerizes with RXR and binds to DNA response elements in the promoter region of SHP, which subsequently inhibits CYP7A1 and thereby lowers bile acid levels. Figure was adapted from Sungsoon Fang, J Lipid Atheroscler., 2017 [85].

The main function of the FXR is the transcriptional regulation of bile acid metabolism [86]. This is achieved by upregulating the expression of enzymes involved in the synthesis of cholesterol. FXR serves as a sensor for bile acid levels in the cell: upon activation by bile acids, the FXR forms a heterodimer with other nuclear receptors, most commonly with the Retinoid X receptor (RXR), and binds to response elements in the promoter regions of its target genes. One of its

direct target genes is the orphan nuclear receptor Small Heterodimer Partner (SHP) [87] [85]. To prevent hepatotoxicity, high levels of bile acids have to be downregulated. SHP inhibits the transcription of CYP7A1, the rate-limiting enzyme in bile acid synthesis, which in turn lowers bile acid levels [88] (Figure **4**).

A further role of FXR lies in influencing glucose and lipid metabolism: FXR activation increases transcription of genes involved in hepatic gluconeogenesis and insulin receptor signaling, as well as fibroblast growth factor 15 (FGF15), which is a hormone in JNK pathway signaling [86]. It was reported that FXR knock out mice show higher blood cholesterol levels and decreased gene expression of lipoprotein metabolism, which hints at an immense meaning of FXR in whole body metabolism [89]. When it became clearer that gut microbiome and intestinal immunity are tightly connected, researchers could also show that intestinal FXR plays a role in cellular communication between gut bacteria and immune cells, and controls inflammatory responses [84]. These diverse tasks and involvements make FXR a promising target for the treatment of many diseases, such as liver or colon cancer, obesity, cholestasis or nonalcoholic steatohepatitis [85]. Currently, there is research being conducted into synthesizing FXR agonist that bind with higher affinity than bile acids in order to control the FXR-regulated target gene activation. The endogenous bile acid with the highest affinity to FXR is chenodeoxycholic acid (CDC), with an EC_{50} of 10 µM [90]. Recently, a synthetic bile acid derivative named obeticholic acid (OC) was developed and approved for therapeutic purposes by the Food and Drug Administration (FDA), since it binds FXR with a much higher efficacy [91]. Furthermore, several synthetic non-bile acid FXR agonists are known that are still in clinical or preclinical testing, such as Tropifexor, Nidufexor, Fexaramine, Turofexorate or GW4064 [92]. It has been believed that inhibition of FXR by antagonists would also have beneficial effects on blood cholesterol levels, however, the commercially available FXR antagonist Guggulsterone showed no significant effects in clinical studies [93]. Guggulsterone is the only available specific FXR inhibitor with high bioactivity and useful pharmacologic properties.

3.2.3 Retinoic Acid Receptor

Long before the Retinoic Acid Receptor (RAR) was discovered in 1987, researchers had already established the importance of vitamin A in vision and eye health [81]. It was also known that an impaired vitamin A metabolism leads to severe damage during embryo development, but it was not understood how vitamin A could cause these profound effects. In the years 1985 and 1986, researchers elucidated the structures of the glucocorticoid and estrogen receptor by cDNA cloning, which paved the way for the lab of Petkovich to structurally resolve the RAR as well [94] [95]. These events marked the beginning of decade-long research into the exact structure, mechanism and target genes of RAR. Later it was established that the RAR has three subtypes: RARα, RARβ and RARγ, with RARα being expressed in almost all tissues of the human body, whereas RARβ and RARγ are more specifically expressed [81]. The three subtypes are encoded in three different genes and are varying in their N terminal region, and each subtype additionally gives rise to several isoforms, which adds to the complexity of RAR signaling [96]. Similar to FXR, retinoic acid receptors also dimerize with Retinoid X receptors (RXR) upon ligand-mediated activation before binding to DNA response elements and subsequently enhancing target gene expression [97].

The ligand group that activates RAR are retinoids, which encompass all forms of vitamin A or related vitamers, including retinol, retinal, retinoic acid and β-carotene as precursor [98]. Retinoic acid is metabolized from retinol by oxidation via retinal into retinoic acid. It has different isomers, including all-*trans* retinoic acid (ATRA) and 9-*cis* retinoic acid (9cRA) [98]. ATRA is considered the biologically active form of vitamin A, since it activates all three subtypes of RAR to regulate gene expression [96]. 9cRA activates RAR as well as RXR, however, RXR activation alone is not sufficient to activate transcription, since additional activation of RAR is always required. The reason for this RXR subordination lies in the agonistic activation process: without a RAR agonist, the RAR-RXR heterodimer binds to corepressors and factors that cause a condensed chromatin structure. When agonists bind to RAR, these factors are replaced by coactivators that open the chromatin structure and allow binding of the

heterodimer to the DNA. RXR agonists are not able to cause the release of corepressors, therefore, RXR activation alone cannot activate transcription [99] [100].

Regulation of gene expression by RAR has an impact of numerous biological processes, most importantly embryonic development. The murine embryonal cancer cell line F9 was extensively studied to find out that especially visceral endodermal differentiation, growth arrest and differentiation induction are under the transcriptional control of RAR [96].

4. Aim of this study

Over the last decade, there has been a growing body of evidence that ferroptosis can be the cause or side effect of several severe diseases, such as neurodegenerative diseases, autoimmune disorders, organ injury, or infectious diseases. Opposed to this, it has also been shown that inducing ferroptosis in cancer cells by small molecules is effective to reduce tumor size. Intense research into this novel type of cell death, its regulations and possible therapeutic interventions is being conducted and already produced several promising drug candidates. However, many aspects of ferroptosis are still not fully understood, among them the question if ferroptosis is a physiological process or only occurs during pathological conditions.

To gain further insight into the regulatory processes of ferroptosis, we aimed at discovering novel cellular regulators that inhibit ferroptotic cell death and planned to characterize their mechanism of action and potential physiological role. Furthermore, we had the goal of finding an approved drug for drug repurposing towards a therapeutically applicable ferroptosis inhibitor, since current available drugs are either in preclinical testing phases or not suitable for *in vivo* application.

5. Results

5.1 Vitamin A rescues cells from ferroptotic cell death by receptor activation

5.1.1 Dose-dependent inhibition of ferroptosis by ATRA

In this joined project with the group of Dr. Michelle Vincendeau (Research group Human Endogenous Retroviruses, Helmholtz Munich) it was found that suppression of ferroptosis is necessary during neuronal differentiation to ensure correct forebrain patterning during brain development (Tschuck et. al. – manuscript is currently under revision). This inhibition of ferroptotic cell death seemed to be achieved by vitamin A, since RNA sequencing (performed by the group of Dr. Michelle Vincendeau, data not shown) showed an upregulation of RARB (Retinoic Acid Receptor B) and BCO2 (beta-carotene oxygenase 2, an enzyme involved in vitamin A biosynthesis) in immature neurons that were cultivated in medium supplemented with vitamin A. The active metabolite of vitamin A is all-trans retinoic acid (ATRA) [101], therefore this metabolite was chosen for all experiments.

In order to evaluate the anti-ferroptotic potency of ATRA, different ferroptosis assays were performed in the well-characterized fibrosarcoma cell line HT-1080 before validation experiments were performed in immature neurons. Ferroptotic cell death was induced over 18 hours by treatment with RSL3 or IKE, and cells could be rescued by co-treatment with ATRA (Figure **5A** and **B**). As a positive control, cells were co-treated with Ferrostatin-1, a gold standard ferroptosis inhibitor.

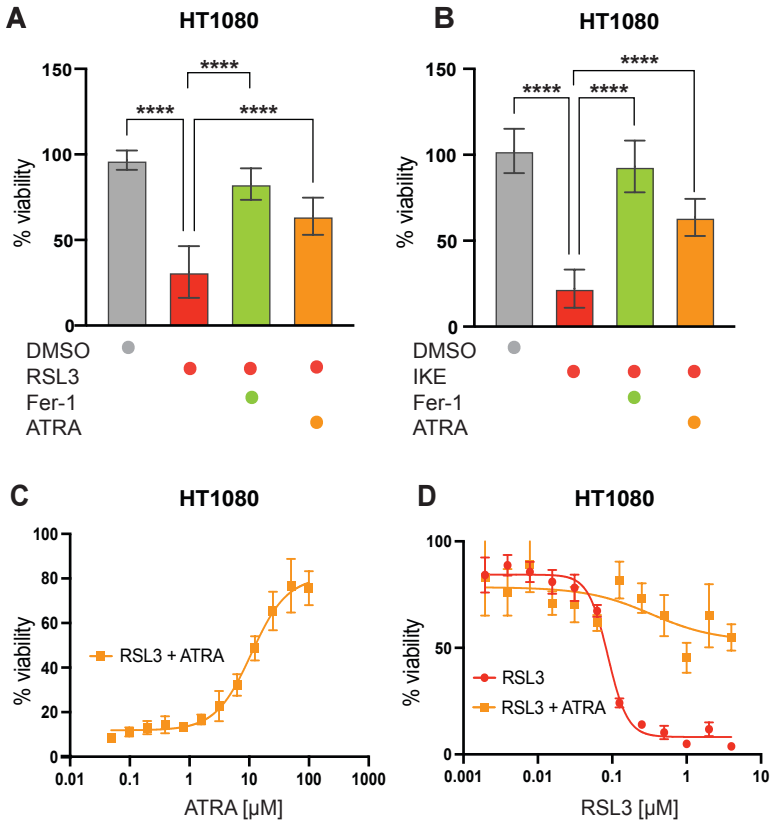

Figure 5: **All-trans retinoic acid (ATRA) inhibits ferroptotic cell death**. **A and B** Ferroptosis was induced in HT1080 cells with 200 nM RSL3 or 1 µM IKE for 18 hours. Co-treatment with 2 µM Ferrostatin-1 as a positive control or 20 µM ATRA inhibited ferroptosis. **C** HT-1080 were treated with 200 nM RSL3 and a 12-point dilution series of ATRA starting from 100 µM for 18 hours. **D** HT-1080 were treated with 20 µM ATRA and a 12-point dilution series of RSL3 starting at 4 µM for 18 hours. In all experiments viability was normalized to DMSO-treated control cells. 3 biological replicates were performed independently. Data plotted are mean values ± SD. **** p≤0.0001 (One-way ANOVA).

To find the most effective treatment concentration of ATRA, cells were treated with a 12-point concentration series after ferroptosis was induced (Figure **5C**), and 20 µM of ATRA achieved the highest rescue of cellular viability, thus this concentration was used in all further experiments. In a dose-response experiment where the concentration of ferroptosis inducer RSL3 was varied and ATRA concentration was kept constant, it could also be observed that ATRA potently inhibited ferroptosis, even at RSL3 concentrations that normally induced 90% cell death. (Figure **5D**).

5.1.2 Validating the mode-of-action of ATRA

To address the question whether ATRA acts as an antioxidant and thereby suppresses ferroptosis or if this effect is receptor-mediated, we performed a cell-free BODIPY C11 Assay (Figure **6A**). In this assay 2,2'-Azobis(2-amidinopropane) dihydrochloride (AAPH) generates radicals and oxidizes the fluorescent dye BODIPY C11, which leads to a fluorescent signal. If a compound is present that acts as an antioxidant, the generated radicals are trapped and BODIPY C11 is not oxidized to its fluorescent form. Since Ferrostatin-1 is an antioxidant and radical trapping agent, it was used as a positive control. The experiment showed that ATRA was not able to trap the generated radicals (Figure **6A**), meaning that its anti-ferroptotic activity is possibly not conferred by antioxidant properties.

These findings were further confirmed with a cell-free DPPH assay (Figure **6B**). In this assay, compounds of interest are incubated together with 2,2-diphenyl-1-picrylhydrazyl (DPPH), a stable radical source with an absorption at 517 nm. If compounds of interest are able to trap the radicals and therefore neutralize DPPH, this absorption decreases. As shown in Figure 2B, Ferrostatin-1 had a radical-trapping effect on DPPH, whereas ATRA could not lower the absorption signal. This led to the conclusion that the anti-ferroptotic effect might be mediated by ATRA activating the Retinoic Acid Receptor (RAR).

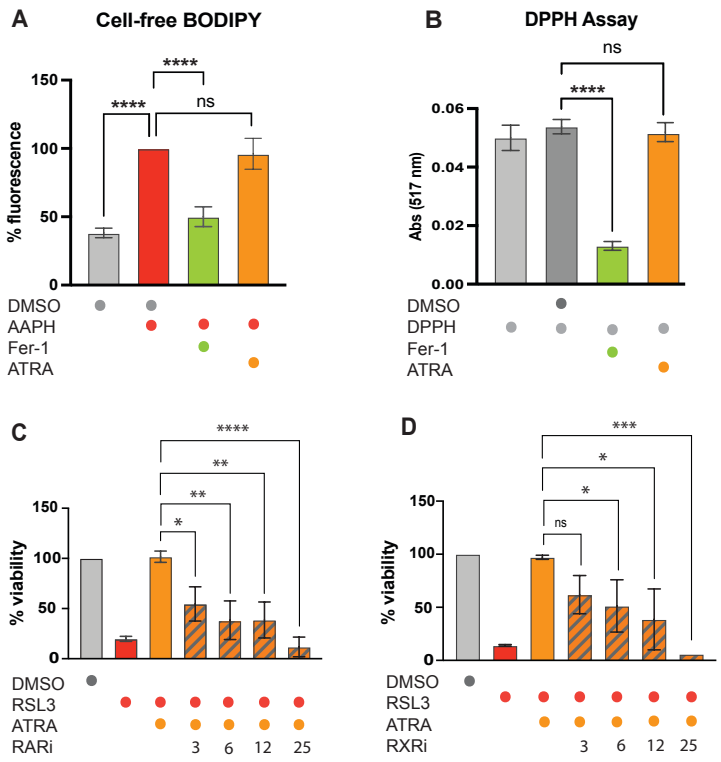

Figure 6: **Anti-ferroptotic effect of ATRA is receptor-mediated**. **A** ATRA did not show antioxidant effects in a cell-free BODIPY assay. Both ATRA and positive control Ferrostatin-1 were tested in a concentration of 25 µM. Measured values were normalized to fluorescence of the AAPH sample. **B** ATRA did not show radical-trapping activity in a DPPH assay. Both positive control Ferrostatin-1 and ATRA were tested in a concentration of 50 µM. **C and D** HT-1080 cells were treated with 200 nM RSL3 to induce ferroptosis and co-treated with 20 µM ATRA and serial dilutions of RAR inhibitor (AGN 193109) or RXR inhibitor (HX 531) as indicated for 18 hours. Viability was normalized to DMSO-treated cells. All experiments were performed independently in 3 biological replicates. Data shown are mean values ± SD. * p≤0.05, ** p≤0.01, *** p≤0.001, **** p≤0.0001 (One-way ANOVA).

To test whether the rescue effect of ATRA is dependent on different receptors, we induced ferroptosis in cells and co-treated them with ATRA and small molecule inhibitors against all 3 isoforms of the Retinoic Acid Receptor (AGN 193109, Figure **6C**) and against all 3 isoforms of the Retinoid X Receptor (HX 531, Figure **6D**). In a dose-dependent manner, the receptor antagonists reverted the anti-ferroptotic effect of ATRA, meaning that both receptors are important to convey a downstream effect leading to ferroptosis inhibition.

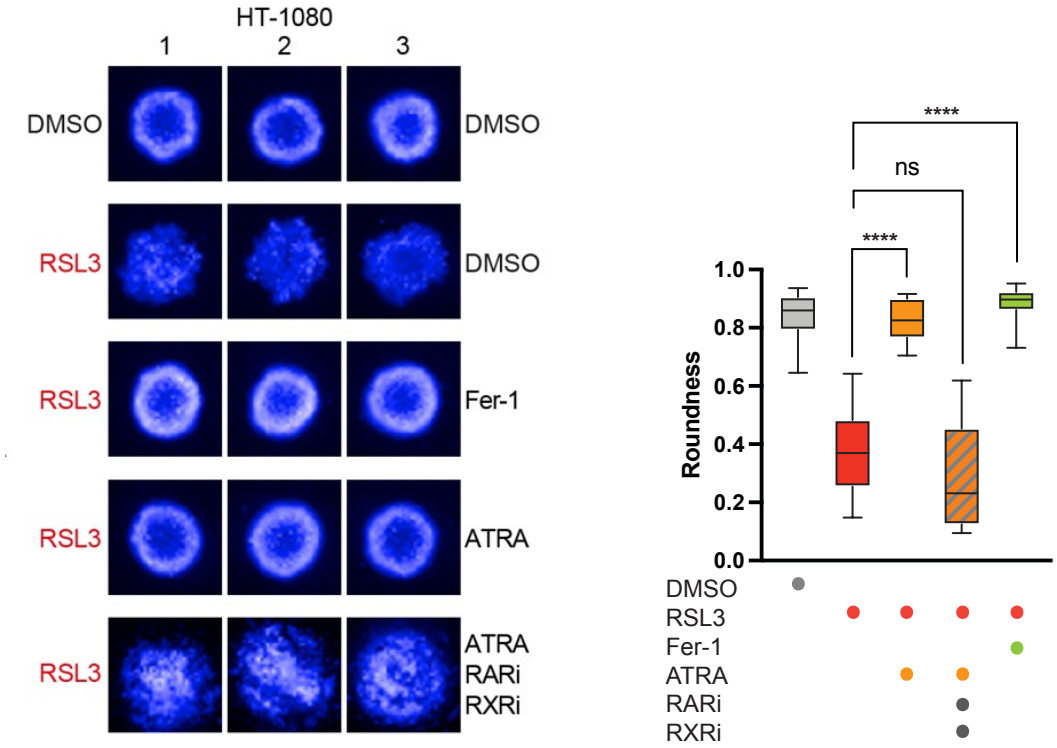

Figure 7: **ATRA can rescue ferroptosis receptor-dependently in a HT-1080 spheroid model.** Spheroids formed from HT-1080 cells were co-treated with 200 nM RSL3 and 2 µM Ferrostatin-1 or 20 µM ATRA and 10 µM RAR inhibitor and 10 µM RXR inhibitor for 48 hours and stained with Hoechst. Experiment was performed independently in 3 biological replicates, each consisting of 8 spheroids per condition. Data plotted are mean values ± SD. **** $p \leq 0.0001$ (One-way ANOVA).

In a spheroid model of HT-1080 cells that resembled a more tumor-like and three-dimensional environment, we made the same observations as in the two-dimensional cell culture experiments (Figure **7**): RSL3-induced ferroptosis impaired the proper formation of spheroids, which could be averted by treatment with ATRA. When both RAR and RXR were inhibited, treatment with ATRA was not sufficient anymore to rescue spheroids from ferroptosis. This could also be quantified by image analysis and measuring the roundness of spheroids in different treatment conditions.

5.1.3 Inhibition of lipid peroxidation

Since peroxidation of phospholipids is an important hallmark of ferroptosis, we performed different assays to examine the ability of ATRA to suppress lipid peroxidation in cell membranes (Figure **8**). The TBARS Assay quantifies thiobarbituric acid-reactive substances, such as Malondialdehyde (MDA), which are typical byproducts of lipid peroxidation. When ferroptosis was induced by RSL3-treatment, the MDA content of HT-1080 cells increased significantly, but after co-treatment with ATRA, the MDA could be lowered again (Figure **8A**).

The same treatment was performed in a flow cytometry experiment, where HT-1080 cells were stained with the fluorescent dye C11-BODIPY that acts as a sensor of reactive oxygen species (ROS) in lipids. Induction of ferroptosis with RSL3 increased the fluorescence signal, indicating for increased ROS and therefore lipid peroxidation, whereas cotreatment with ATRA shifted the curve back towards lower fluorescence intensity (Figure **8B**).

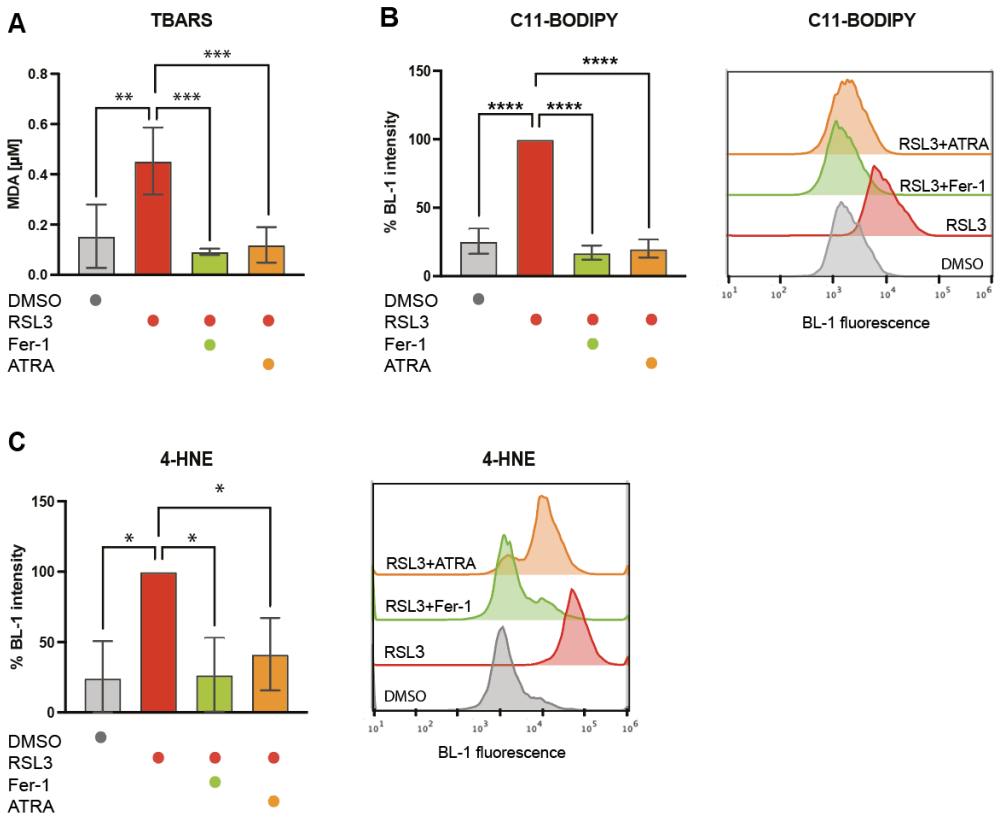

Figure 8: **Treatment with ATRA suppresses lipid peroxidation. A** TBARS assay of HT-1080 cells treated with 100 nM RSL3 and 2 µM Fer-1 or 20 µM ATRA for 4 hours. Data plotted are mean values ± SD. **B** Flow cytometry measurement of HT-1080 treated with 200 nM RSL3 and 2 µM Fer-1 or 20 µM ATRA for 2.5 hours. Cells were stained with C11-BODIPY. **C** Immunostaining of 4-HNE and flow cytometry measurement of HT-1080 treated with 250 nM RSL3 and 2 µM Fer-1 or 20 µM ATRA for 2.5 hours. Data plotted is the median fluorescence intensity ± SD normalized to the RSL3-treated samples. All experiments were performed independently in 3 biological replicates. *p≤0.05, **p≤0.01, ***p≤0.001, ****p≤0.0001 (One-way ANOVA).

4-Hyroxynonenal (4-HNE) is another product of lipid peroxidation in cell membranes that is increased when cells undergo ferroptosis. Upon immunostaining of 4-HNE we could observe in flow cytometry experiments that treatment of ferroptotic cells with ATRA could significantly decrease cellular 4-HNE levels (Figure **8C**).

In a live cell staining of HT-1080 with C11-BODIPY we were able to visualize the effects that we saw in the flow cytometry experiment before: Cells that undergo RSL3-induced ferroptosis showed a high fluorescence signal, indicating high lipid ROS content. By cotreatment with ATRA, this fluorescence could be diminished (Figure **9**). This could be quantified by analyzing the number of fluorescent objects per image.

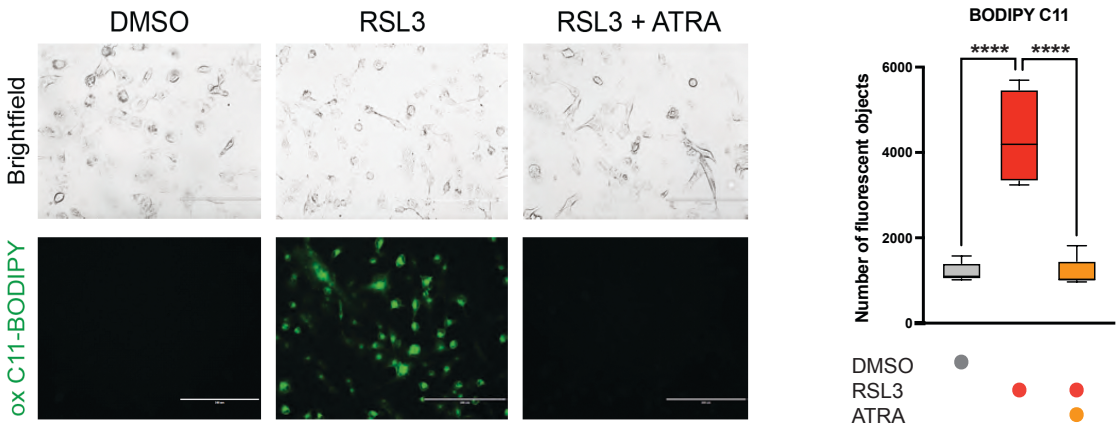

Figure 9: **C11-BODIPY staining visualizes inhibition of lipid peroxidation by ATRA.** HT-1080 cells were stained with C11-BODIPY and treated with 200 nM RSL3 and 20 µM ATRA for 2 hours before imaging. Representative images are shown of 3 biological replicates. Data plotted are mean values ± SD. ****p≤0.0001 (One-way ANOVA).

Summarizing, all four assays with different readouts clearly show that treatment with ATRA rescues cells from ferroptosis by inhibiting lipid peroxidation and suppressing the generation of ROS.

5.1.4 Upregulation of anti-ferroptotic genes by ATRA

As a next step, we wanted to examine the exact mechanism of how ATRA suppresses lipid peroxidation and ferroptotic cell death. Since we could already validate that this effect is receptor-mediated, and because RAR and RXR are nuclear receptors, we concluded that ATRA acts as a ligand for the Retinoic Acid Receptor, which then dimerizes with the Retinoid X Receptor and subsequently binds to response elements in the promoter region of specific downstream ferroptosis-relevant target genes.

To proof this theory, we treated cells with ATRA and measured mRNA levels of various canonical anti-ferroptotic genes in a qRT-PCR (Figure **10**). Indeed, we found that the transcription of the three main axes of ferroptosis defense, GPX4, FSP1 and GCH1 [26], were significantly upregulated after ATRA treatment. Furthermore, mRNA levels of three genes that are involved in lipid metabolism were also increased: PPARα as a transcription factor itself and major regulator of fatty acid metabolism [102]; and ACSL3 and SCD1 as enzymes necessary for the synthesis of mono-unsaturated fatty acids, which are known to have anti-ferroptotic properties [25].

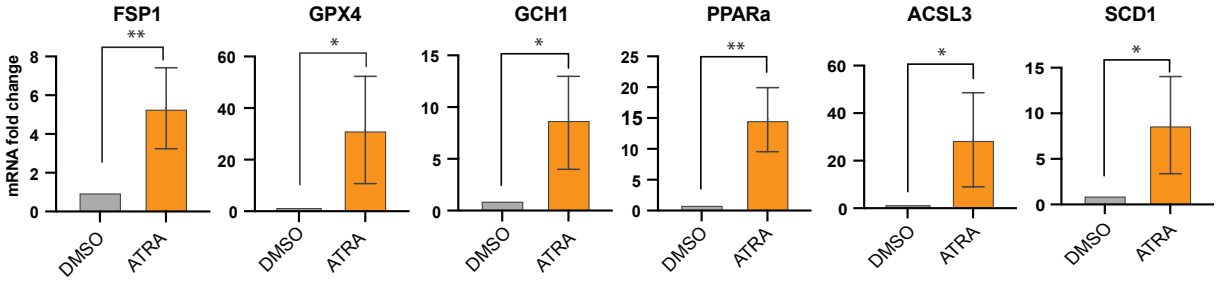

Figure 10: **Treatment of HT-1080 with ATRA leads to upregulation of anti-ferroptotic target genes.** HT-1080 were treated with 20 µM ATRA for 6 hours before total RNA was isolated, transcribed into cDNA and analyzed in a qRT-PCR. Experiment was repeated independently in 3 biological replicates. Data plotted are mean values ± SD. **p≤0.01, *p≤0.05 (One-way ANOVA).

To ensure that the observed effect was a direct result of ATRA treatment and not a side effect or artefact, ferroptosis was induced by RSL3-treatment and cells were cotreated with ATRA and small molecule inhibitors of either FSP1 or PPARα (Figure **11A and B**).

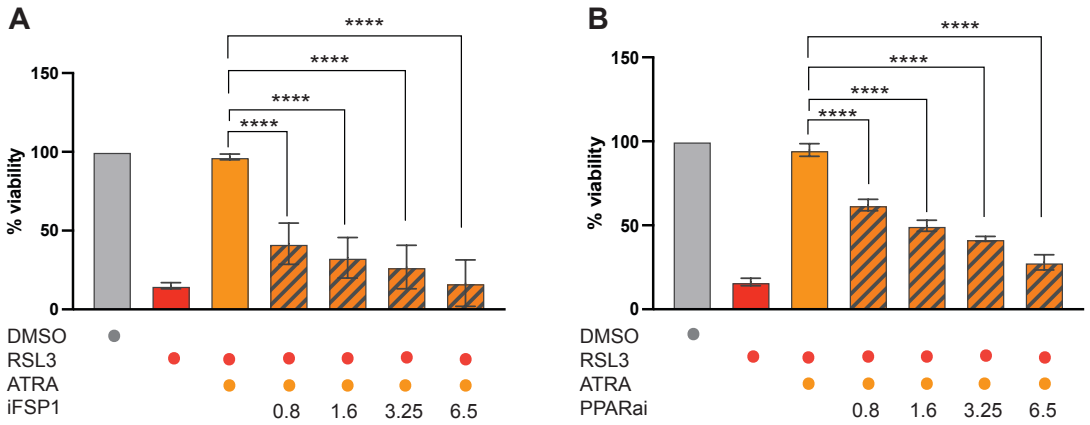

Figure 11: **Treatment with inhibitors against FSP1 or PPARα significantly reduces effect of ATRA. A and B** Ferroptosis was induced in HT-1080 cells by 200 nM RSL3. Cells were cotreated with 20 µM ATRA and a serial dilution of iFSP1 or PPARα inhibitor GW6471 as indicated. Experiments were repeated independently in 3 biological replicates. Data shown are mean values ± SD. ****p≤0.0001 (One-way ANOVA).

These experiments clearly showed that without functional FSP1 or PPARα, ATRA is not able to rescue cells from ferroptosis anymore. This further validates our theory that ATRA acts as an activator of RAR, which in turn acts as a transcription factor for several anti-ferroptotic genes. By activating these genes, cells can defend themselves against lipid peroxidation and ferroptosis. The lab of Dr. Michelle Vincendeau (Helmholtz Munich) also confirmed these findings in differentiating neurons and forebrain organoids, which hints at an important role of ferroptosis suppression during early brain development.

5.1.5 Different metabolites of vitamin A

Vitamin A is an essential vitamin for humans and refers to a chemically related group of metabolites: retinol, retinal, retinoic acid and retinyl esters [103]. Among them, all-trans retinoic acid (ATRA) is the transcriptionally active form of vitamin A. Retinoic acid can also have different isoforms, such as 9-cis retinoic acid [104].

To test whether other metabolites of vitamin A could also act as ferroptosis inhibitors, we treated cells with RSL3 and serial dilutions of ATRA, retinol, retinal or 9-cis retinoic acid (Figure **12A**). Measurement of viability showed that all tested forms of vitamin A could suppress ferroptosis to some extent, with retinol showing the highest potency. We hypothesized that these results can be explained by the different chemical properties of the different compounds:

retinol and retinal possess conjugated double bonds and functional groups that favor the trapping of radicals, which can inhibit ferroptosis [104].

In contrast, only the isoforms of retinoic acid can act as ligands for the Retinoic Acid Receptor, and therefore activate downstream anti-ferroptotic target genes, which could explain why a higher concentration of these compounds is needed to inhibit ferroptosis.

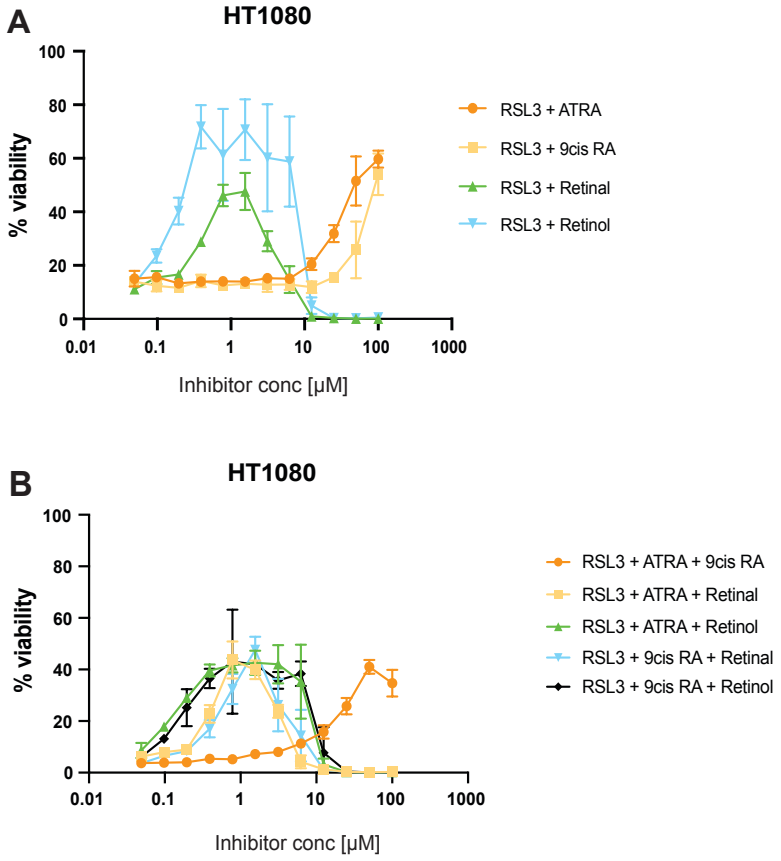

Figure 12: **Different metabolites of Vitamin A as ferroptosis inhibitors. A** HT-1080 cells were cotreated with 200 nM RSL3 and serial dilutions of different vitamin A metabolites for 18 hours. **B** Cells were treated in the same way as in A, but serial dilutions of 2 forms of vitamin A were added at the same time. Measured viability was normalized to DMSO-treated control cells. Data shown are mean ± SD of 3 technical replicates.

Combined treatment with two forms of vitamin A did not lead to a stronger or synergistic rescuing effect in ferroptotic cells (Figure **12B**). Furthermore, when a RAR-activating compound was paired with an antioxidant compound, the optimal rescuing concentration was similar to that of the antioxidant alone, since the radical trapping is happening faster in the cell than the receptor activation and subsequent downstream activation.

5.2 Seratrodast is a ferroptosis inhibitor suitable for drug repurposing

5.2.1 Selection of Seratrodast as a repurposing molecule

With the identification of vitamin A as a successful inhibitor of lipid peroxidation, we discovered an endogenous metabolite as a ferroptosis suppressor. As a next step, we aimed at finding an anti-ferroptotic synthetic molecule with known mode of action that is already clinically approved. The last decade of ferroptosis research showed that many degenerative diseases are accompanied, or even caused, by regulated cell death, and most of the anti-ferroptotic drugs to date are not stable enough *in vivo* or still need to be pre-clinically tested [4]. The repurposing of already approved drugs therefore presents a promising strategy to bring ferroptosis inhibitors into therapeutic application.

We approached this project by rationally looking at clinically approved small molecules and their structures to select one with potential antioxidant, radical-trapping or iron chelating properties. Several established ferroptosis inhibitors (Idebenone, Ubiquinone, vitamin K) contain a quinone moiety [38, 40, 105]; therefore, we selected Seratrodast, an inhibitor of the Thromboxane A2 receptor (TBXA2R) containing a quinone head group, as a possible drug for a ferroptosis repurposing strategy [106]. Seratrodast is an approved asthma drug in Japan, China and India that displays only moderate side effects and advantageous pharmacokinetics [107]. These drug properties convinced us to experimentally validate Seratrodast as a suppressor of lipid peroxidation and ferroptotic cell death for potential use as a repurposing anti-ferroptotic drug in the future.

5.2.2 Seratrodast successfully rescues cell death induced by different FINs

In order to identify a possible pathway that is targeted by Seratrodast during ferroptosis, cell death was induced by different classes of ferroptosis inducers (FINs). For this experiment HT-1080 cells were treated with class I FIN IKE (inhibition of system xc^-), class II FIN RSL3 (direct inhibition of GPX4), class III FIN FIN56 (CoQ_{10} depletion, GPX4 protein depletion) and class IV FIN $FINO_2$ (iron oxidation, loss of GPX4 function) in a serial dilution. Cotreatment with Seratrodast could rescue cell viability in all cases, even when high concentrations of inducers were present (Figure **13A-D**).

Cells were also cotreated with Ferrostatin-1, a compound that specifically suppresses ferroptosis, and Seratrodast was able to inhibit ferroptosis in the same or even more potent manner as Ferrostatin-1 (Figure **13A-D**).

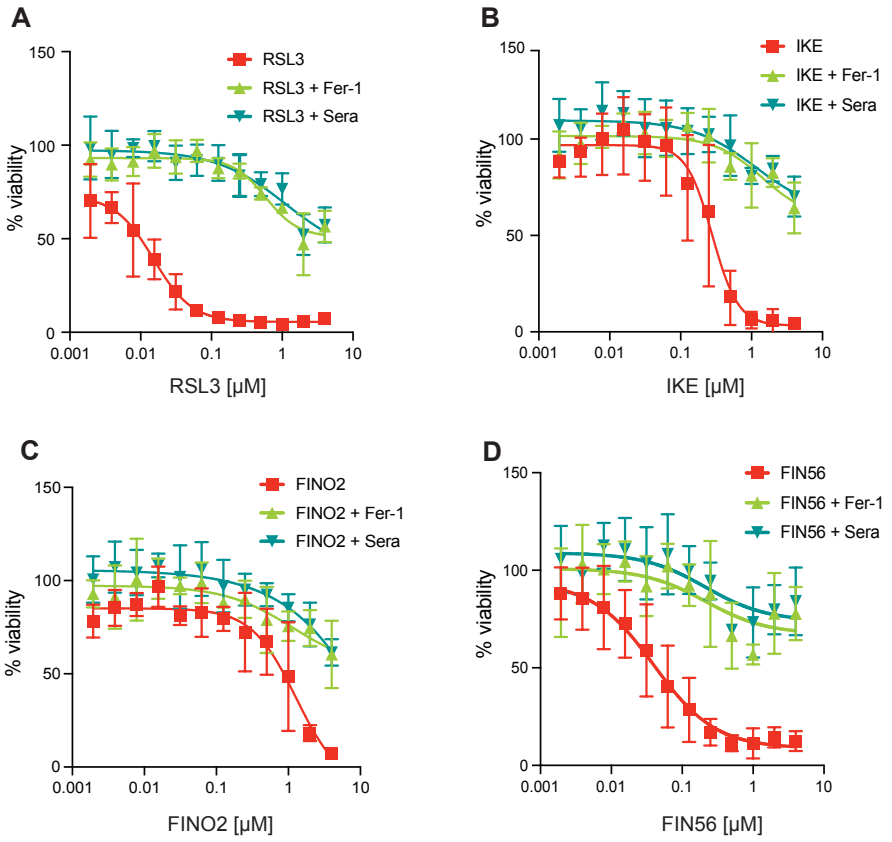

Figure 13: **Seratrodast is a potent inhibitor against different ferroptosis inducers.** HT-1080 were treated with serial dilutions of RSL3 **(A)**, IKE **(B)**, FINO2 **(C)** or FIN56 **(D)** (red) and cotreated either with 2 µM Ferrostatin-1 (green) or 6 µM Seratrodast (blue) for 18 hours. Measured viability was normalized to DMSO-treated control cells. Data plotted are mean values ± SD of 3 independent biological replicates.

Furthermore, Seratrodast was tested in a spheroid model in order to examine the anti-ferroptotic activity in a 3-dimensional cell culture model (Figure **14**). Treatment with RSL3 impaired the formation of intact spheroids, whereas cotreatment with Seratrodast could revert this effect, again to the same extent as Ferrostatin-1.

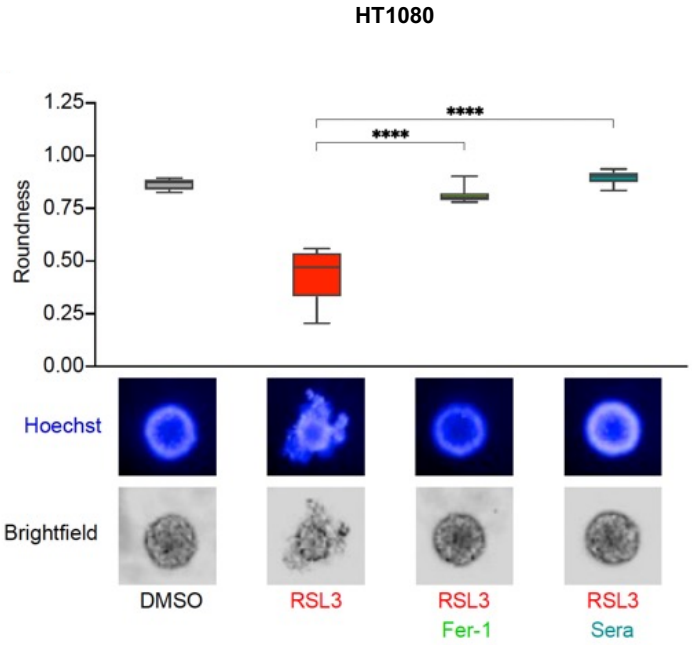

Figure 14: **Seratrodast inhibits ferroptosis in a spheroid model.** HT1080 were grown into spheroids over 48 hours and treated with 200 nM RSL3, 2 µM Fer-1 and 6 µM Seratrodast for another 48 hours. Data shown are mean values ± SD of 3 independent biological replicates, each replicate consisting of 8 spheroids. Representative images are shown for each treatment condition. ****p≤0.0001 (One-Way ANOVA).

5.2.3 Investigation of target activity

An anti-ferroptotic effect of small molecules can either be achieved through antioxidant or iron-chelating characteristics of the compound, or by acting on a cellular target that in turn has a ferroptosis-suppressing effect. To examine whether the observed effect of Seratrodast is caused by inhibition of its target Thromboxane A2 receptor (TBXA2R), several other inhibitors against the same target were tested for anti-ferroptotic activity (Figure **15**). Ferroptosis was induced by treatment with RSL3, and TBXA2R inhibitors were added in a serial dilution.

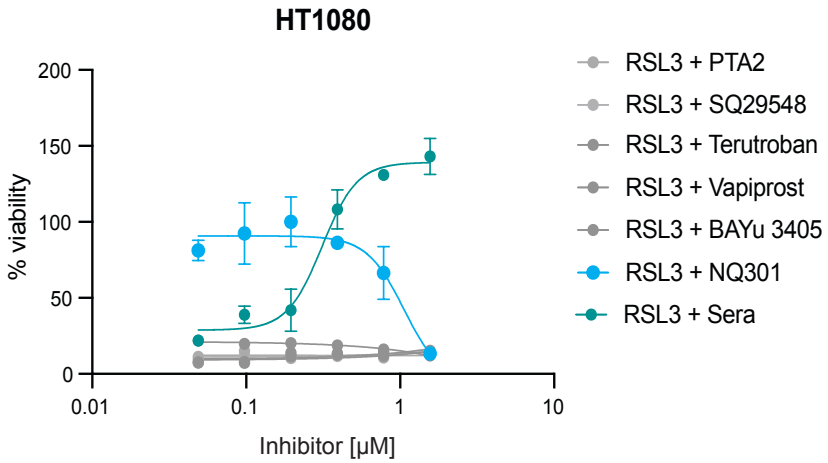

Figure 15: **Anti-ferroptotic effect of Seratrodast is not receptor-mediated.** HT-1080 cells were treated with 200 nM RSL3 and serial dilutions of different TBXA2R inhibitors for 18 hours. Measured viability was normalized to DMSO-treated control cells. Data shown are mean values ± SD of 3 technical replicates.

NQ301 was the only TBXAR2 inhibitor that could rescue cells from ferroptosis in a dose-dependent manner, with an even higher potency than Seratrodast (shown in blue and green in Figure **15**). These findings led us to the hypothesis that the TBXA2R is not a cellular ferroptosis regulator, but instead the chemical structure of Seratrodast and NQ301 is contributing to the inhibition of ferroptosis. The direct comparison of the chemical structures of all tested TBXA2R inhibitors showed that only NQ301 and Seratrodast possess a quinone moiety (Figure **16**): according to IUPAC, a quinone is defined as “fully conjugated cyclic dione structure, […], derived from aromatic compounds by conversion of an even number of -CH= groups into -C(=O)- groups […]” [108]. Since quinones are redox-active and able to scavenge free radicals, it can be hypothesized that this moiety leads to the observed anti-ferroptotic effect by trapping free radicals and thereby suppressing lipid peroxidation in the cellular membrane.

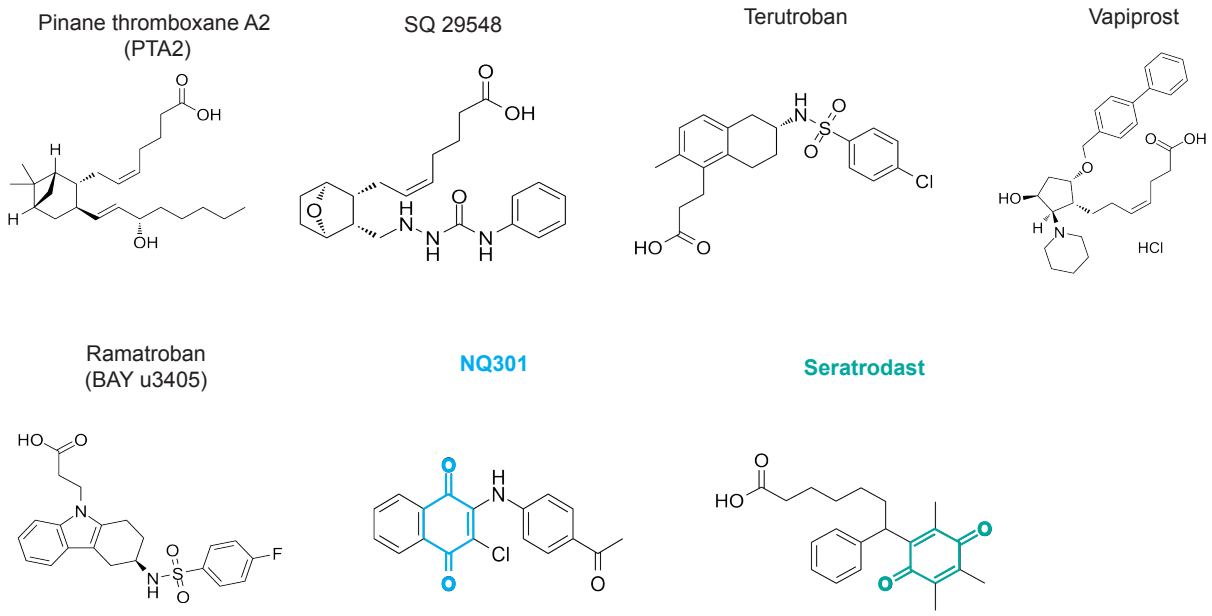

Figure 16: **Chemical structures of thromboxane receptor inhibitors.** The quinone structure of NQ301 and Seratrodast (marked in blue or green) confers radical-trapping and antioxidant activity that leads to efficient inhibition of ferroptosis in cells.

5.2.4 Inhibition of lipid peroxidation

To validate the presumed direct antioxidative activity of Seratrodast we performed an assay in a cell-free setting (Figure **17**). The cell-free C11-BODIPY assay shows that Seratrodast acts as a free radical scavenger and significantly suppresses oxidation of the fluorescent probe (Figure **17**).

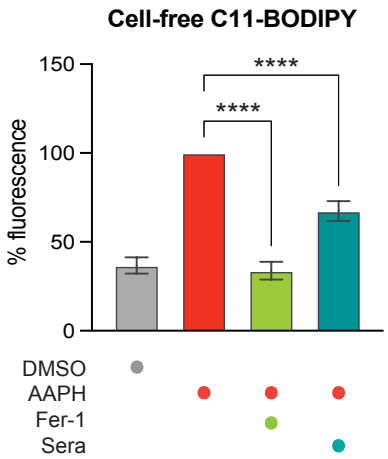

Figure 17: **Seratrodast shows antioxidative activity in a cell-free assay.** Cell-free C11-BODIPY assay with 25 µM Seratrodast and 25 µM Ferrostatin-1 as positive control. Measured values were normalized to fluorescence of the AAPH sample. Data plotted are mean values ± SD of 3 independent biological replicates. ****p≤0.0001 (One-Way ANOVA).

To translate these findings into cultured cells and to examine the antioxidative properties of Seratrodast with regards to ferroptosis, we cotreated cells with RSL3 and Seratrodast and performed several assays to quantify lipid peroxidation (Figure **18**). In a TBARS assay, we measured cellular malondialdehyde (MDA) levels and observed a significant reduction after cotreatment with Seratrodast (Figure **18A**). Staining with C11-BODIPY and subsequent flow cytometry also showed that Seratrodast diminishes ROS and lipid peroxidation in ferroptotic cells (Figure **18B**). Finally, an immunostaining of 4-Hydroxynonenal (4-HNE) confirmed that Seratrodast potently inhibits lipid peroxidation (Figure **18C**).

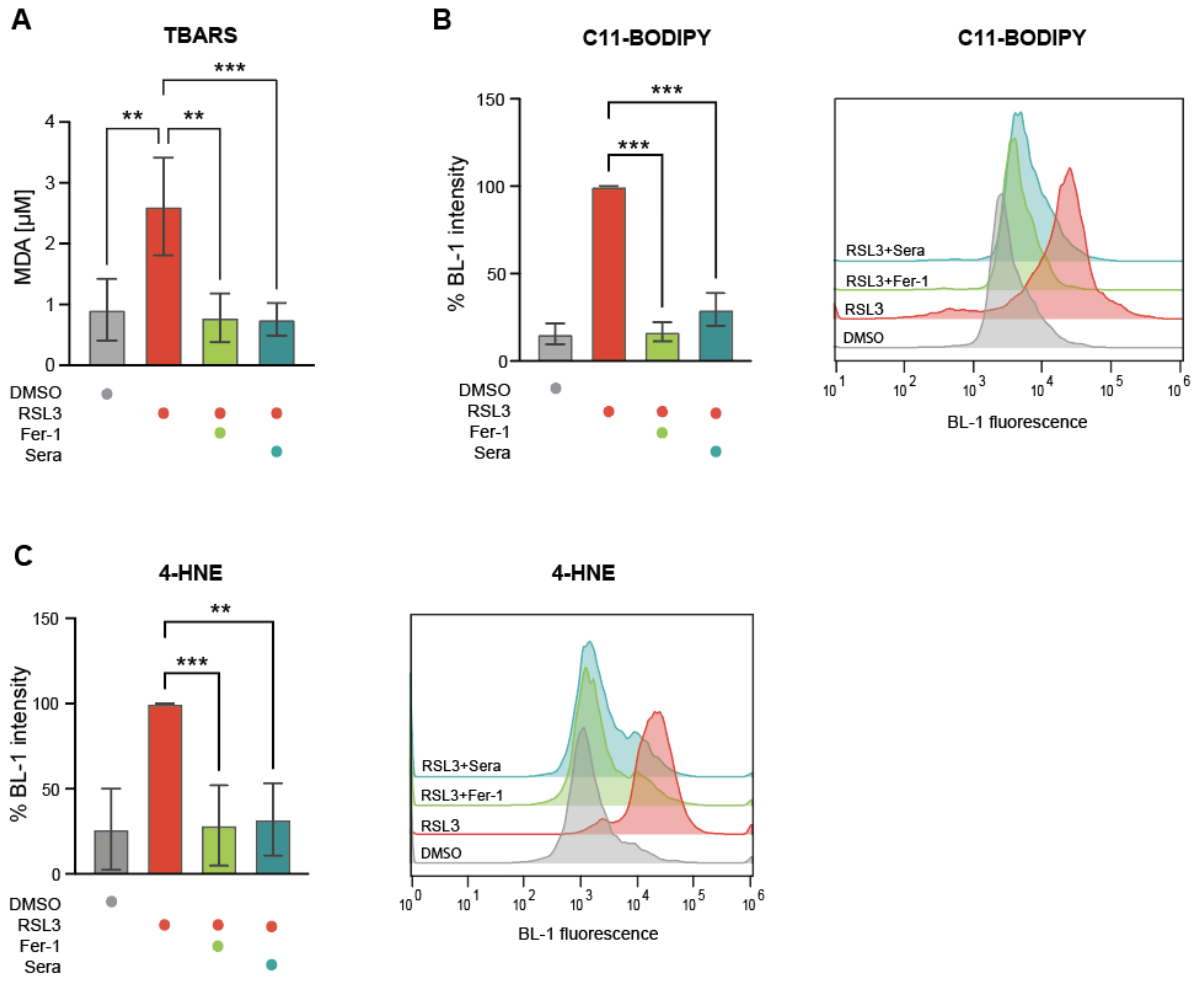

Figure 18: **Seratrodast inhibits lipid peroxidation. A** HT-1080 cells were treated with 250 nM RSL3 and 2 µM Ferrostatin-1 or 6 µM Seratrodast for 2.5 hours before a TBARS assay was performed. **B** HT-1080 cells were treated with 200 nM RSL3 and 2 µM Ferrostatin-1 or 6 µM Seratrodast for 2.5 hours before C-11 BODIPY staining and flow cytometry was performed. A representative histogram is shown. **C** HT-1080 cells were treated with 300 nM RSL3 and 2 µM Ferrostatin-1 or 6 µM Seratrodast for 2 hours before immunostaining of 4-HNE and flow cytometry was performed. A representative histogram is shown. All experiments were performed in 3 independent biological replicates. Data shown are mean values ± SD. **p≤0.01, ***p≤0.001 (One-way ANOVA).

Summarizing, Seratrodast could be validated as a potent ferroptosis inhibitor against different classes of FINs. This effect is not caused by binding its target TBXA2R, but instead stems from a quinone moiety in the chemical structure of Seratrodast, which provides antioxidative potential and radical trapping abilities. This allows Seratrodast to directly suppress lipid peroxidation in cell membranes of ferroptotic cells.

5.3 Farnesoid X Receptor as a novel regulator of ferroptosis

5.3.1 Compound Screening for small molecule ferroptosis inhibitors

In contrast to the identification of Seratrodast as a ferroptosis inhibitor, where we rationally selected a compound with attention to its chemical structure, we next aimed at a more unbiased approach of discovering novel ferroptosis inhibitors: we conducted a small molecule compound screening and tested approximately 3,684 compounds (in-house library selection) with known mode of actions for the ability to rescue ferroptotic cell death. By analyzing the known targets of these compounds in further experiments, we wanted to find and characterize yet unknown cellular regulators of ferroptosis.

After thoroughly establishing the optimal cellular density and inducer concentrations in 384-well plates to achieve approximately 80% ferroptotic cell death after 18 hours, the 3,684 compounds were transferred onto HT-1080 cells using an automated liquid handling system. Subsequently, ferroptosis was induced with the class-I-FIN IKE over night before viability was assessed. As a positive control, cells were co-treated with inducers and Ferrostatin-1, a gold standard ferroptosis inhibitor. Since all compounds were solved in DMSO, we used DMSO-treated cells as an “untreated” control. After 18 hours of incubation, cell viability was measured by lysing cells and detecting luminescence proportional to amounts of released ATP in the culture medium. Only compounds that could rescue cellular viability to a value higher than the plate median (of all compound-treated wells) plus 3x standard deviation were considered as hits (Figure **19**).

When inserting standard deviations and means of the positive (IKE + Fer-1 treatment) and negative controls (IKE treatment) into the commonly used formula for Z-prime value calculations, we obtained a Z-prime value of 0.3 to 0.7, which is considered “excellent” and confirmed that our chosen controls and conditions were suitable for this type of screening assay.

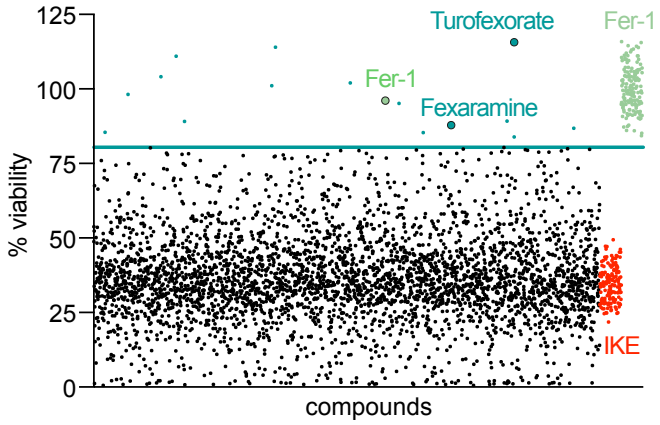

2-TEDC	ATT	**Fexaramine**	H 89
Dipyridamol	Oxymetazoline	**Turofexorate**	ICI-89406
LY231617	Moxisylyte	L-778123	AZD1208
Cetaben	Fer-1	WHI-P154	TTA

Figure 19: **Compound screening for small molecules that inhibit ferroptosis.** HT-1080 cells were treated with a compound library and ferroptosis was induced by 1.5 µM IKE for 18 hours before viability was measured. 2 µM Ferrostatin-1 was used as a positive control. Viability was normalized to positive control wells (Fer-1, 100%). Every dot represents a well treated with compounds and IKE. Cut-off (marked as green line) was chosen as median of all compound-treated wells + 3x SD. The box below shows all hits selected for validation experiments.

After excluding unwanted hits such as frequent hitters, toxic-marked compounds or compounds without known targets or mode of action, the screening yielded 16 initial hits. For further validation of these hits and to obtain an EC_{50} value that can be used in future experiments, HT-1080 cells were treated with a 10-point serial dilution of each compound while ferroptosis was induced either by RSL3 or IKE (Figure **20**). During screening, compounds were tested in a standard concentration of 10 µM, therefore we now chose a concentration range of approximately 100 nM to 50 µM for our validation experiment while cotreating with constant ferroptosis inducer concentrations. This method can also give insights about the highest concentration that can be used before the compound has toxic effects on the cells.

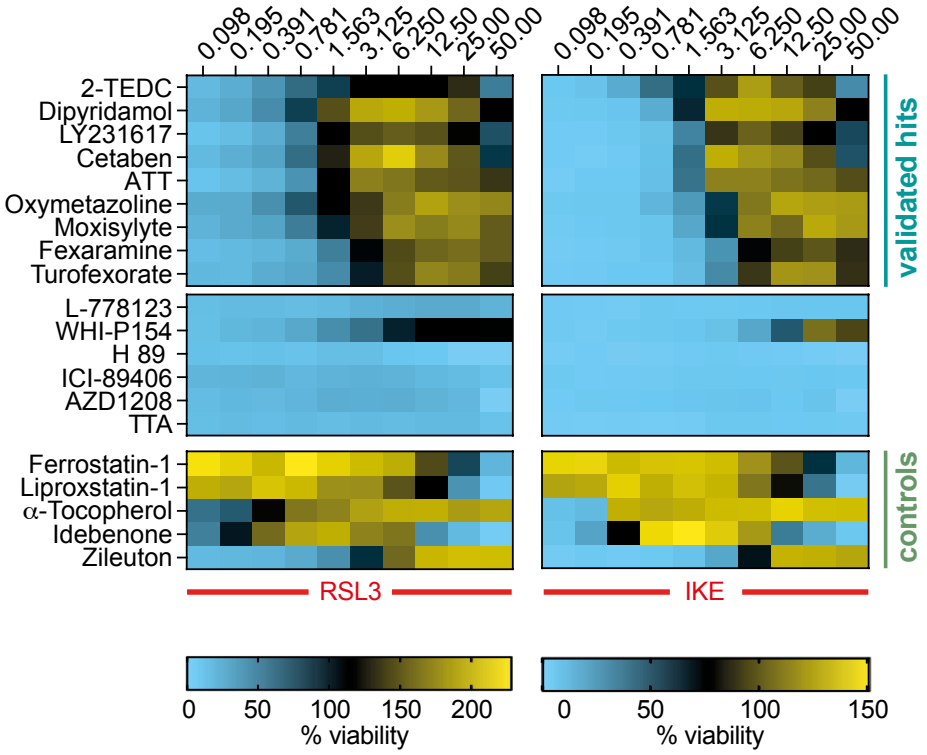

Figure 20: **Hit validation of initial screening hits in a dose-response experiment.** HT-1080 cells were treated with 10-point serial dilutions of compounds and ferroptosis was induced either by 100 nM RSL3 or 1.5 µM IKE for 18 hours. Ferrostatin-1, Liproxstatin-1, Idebenone, Zileuton and α-Tocopherol are known ferroptosis inhibitors and were used as positive controls. Data shown are mean values of 3 technical replicates. Measured viability was normalized to DMSO-treated control cells.

It was validated that 9 of the initial 16 screening hits showed dose-dependent rescuing activity after RSL3- or IKE-induced ferroptosis. To obtain an impression of the compounds' potency, we also tested five already established ferroptosis inhibitors in parallel and compared their EC_{50} values and cytotoxicity. Ferrostatin-1, Liproxstatin-1 and Idebenone showed a higher potency than the screening hits, however, these positive controls also exhibit cytotoxicity at higher concentrations, whereas most of the screening hits showed less or no loss of cell viability at high concentrations (Figure **20**). Compound concentrations that could restore the highest viability were used as optimal concentrations in follow-up experiments. The exact concentration for every compound can be found in Supplementary Table **S1.**

Since no reliable and robust ferroptosis markers are established up to date, the primary option to verify the occurrence of ferroptosis is to rescue cells with ferroptosis-specific inhibitors and to exclude other types of cell death. To exclude screening hits that non-specifically inhibit cell death, we induced apoptosis and necroptosis in different experiments. Apoptotic cell death

was induced by treatment with kinase inhibitor Staurosporine, and after cotreatment with hit compounds we measured caspase 3/7 activity in a luminescence-based assay (Figure **21**). As a known apoptosis inhibitor and therefore positive control, the pan-caspase inhibitor z-VAD-FMK was included. One compound (Anethole-trithione, ATT) significantly lowered caspase 3/7 activity and was therefore ruled as unspecific and not considered for further in-depth analyses regarding ferroptosis.

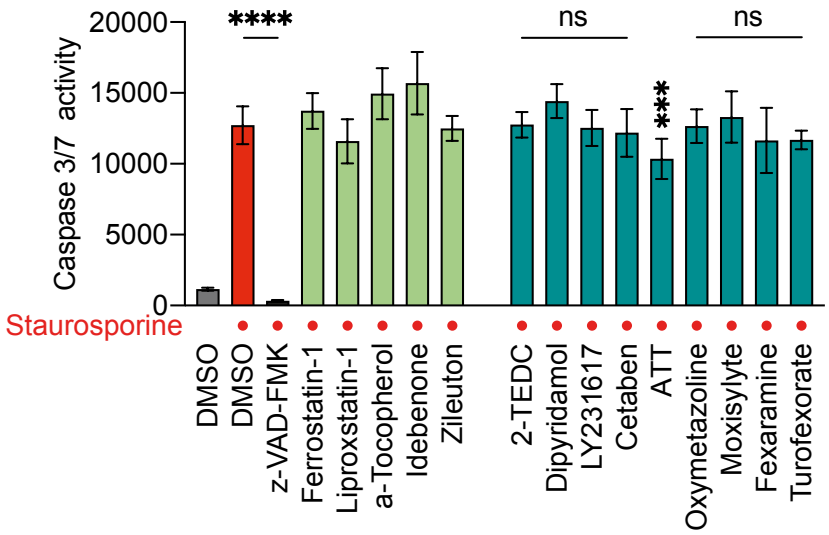

Figure 21: **Anti-apoptotic activity of initial screening hits.** Apoptosis was induced in HT-1080 by treatment with 1 µM Staurosporine for 18 hours. As a positive control, cells were co-treated with 50 µM z-VAD-FMK. As negative controls, cells were cotreated with ferroptosis inhibitors. Data shown are mean values of 5 technical replicates ± SD. ***p≤0.001, ****p≤0.0001 (One-way ANOVA).

To examine whether the initial screening hits had also anti-necroptotic activity, we induced necroptosis in mouse embryonic fibroblasts (MEF). This cell line was chosen because HT-1080 are usually necroptosis-resistant due to a lack of sufficient RIPK3 expression, which is necessary for the kinase-cascade leading to phosphorylation of MLKL, an important hallmark of necroptotic cell death [109]. MEF are also sensitive to treatment with tumor necrosis factor α (TNFα). Induction of necroptosis in MEF was achieved by combination treatment with TNFα, z-VAD-FMK and LCL161 (SMAC mimetic and IAP inhibitor).

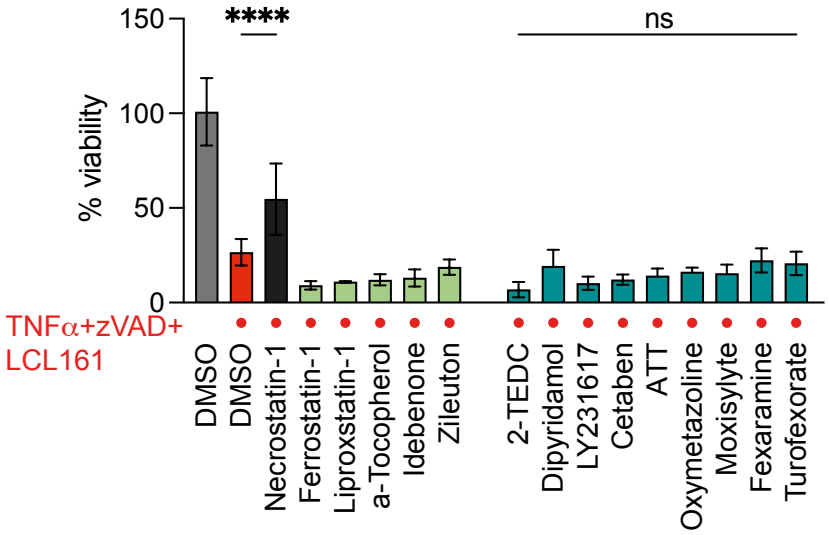

Figure 22: **Anti-necroptotic activity of initial screening hits.** Necroptosis was induced in MEF by treatment with 20 ng/ml TNFα, 10 µM z-VAD-FMK and 10 µM LCL161 for 18 hours. As a positive control, cells were cotreated with 10 µM Necrostatin-1. As negative controls, cells were cotreated with ferroptosis inhibitors. Data shown are mean values of 8 technical replicates ± SD. ****p≤0.0001 (One-way ANOVA).

Viability measurement showed that among all screening hits, only the positive control Necrostatin-1, a necroptosis-specific inhibitor, could rescue cells. Therefore, all tested compounds except for ATT were considered ferroptosis-specific inhibitors (Figure **22**).

As a next step of validation, we tested whether the initial screening hits could not only rescue cells from ferroptosis that was induced by compounds belonging into class I (IKE) or II (RSL3) of FINs, but also class III FINs. If we observed that some compounds can only rescue ferroptosis induced by IKE (for example), this could reveal information about a possible mechanism of ferroptosis inhibition.

For this experiment HT-1080 cells were treated with FIN56 (class III FIN, induces ferroptosis by degrading GPX4 and depleting ubiquinone) and cotreated with the initial screening hits (Figure **23**). As positive controls, we also cotreated in parallel with the known ferroptosis inhibitors Ferrostatin-1, Liproxstatin-1, α-Tocopherol, Idebenone and Zileuton. Most of the tested screening compounds showed a protective effect against FIN56-induced ferroptosis, except for Oxymetazoline and 2-TEDC.

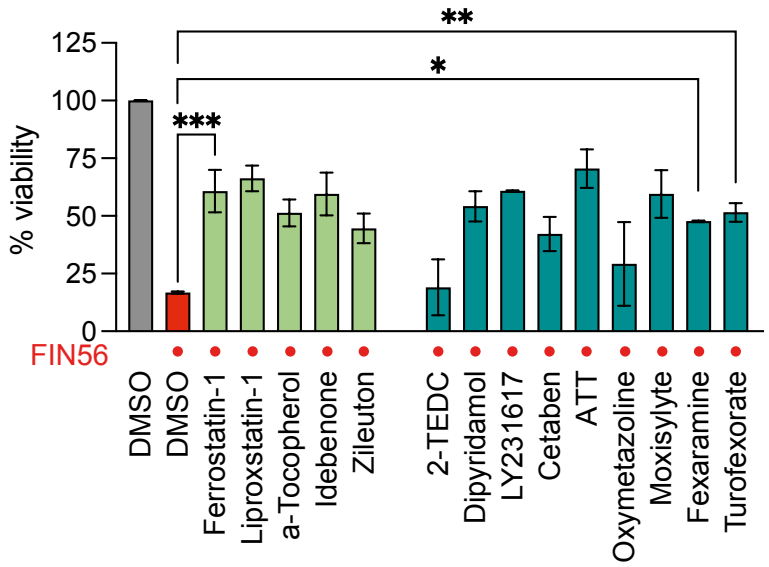

Figure 23: **Activity of initial screening hits after ferroptosis induction by FIN56.** Ferroptosis was induced in HT-1080 by treatment with 200 nM FIN56 for 18 hours. Cells were cotreated with known ferroptosis inhibitors as positive controls or initial screening hits. Data shown are mean values of 2 biological replicates ± SD. *p≤0.05, **p≤0.01, ***p≤0.001 (One-way ANOVA).

Since lipid peroxidation is one of the important hallmarks of ferroptosis, we also subjected the initial screening hits to a C11-BODIPY assay as part of the hit validation (Figure **24**). In this assay, ferroptosis was induced in HT-1080 either by treatment with RSL3 or IKE. After cotreatment with known ferroptosis inhibitors or the initial screening hits, cells were stained with the lipid ROS sensor C11-BODIPY. By detecting fluorescence in a flow cytometer, we analyzed which compounds were able to suppress generation of ROS and therefore lipid peroxidation of cellular membranes. The flow cytometry experiments were evaluated by observing peak shifts between different treatments (higher fluorescence means a shift to the right, which means higher lipid peroxidation and vice versa) (Figure **24**).

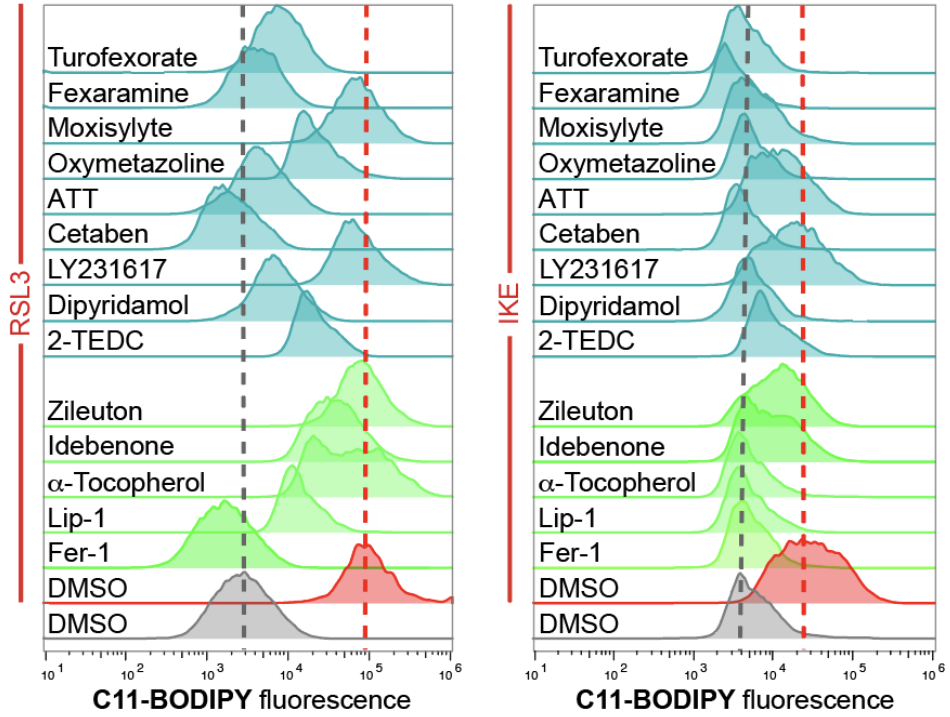

Figure 24: **Flow cytometry histograms of screening hits tested in C11-BODIPY assay.** HT-1080 cells were treated either with 250 nM RSL3 for 2 h, or 2.5 µM IKE for 6 h and cotreated with initial screening hits or known ferroptosis inhibitors. Cells were stained with C11-BODIPY for 30 min before flow cytometry was performed. Dashed lines represent mean intensities of DMSO-treated samples (grey) or ferroptotic cell samples (RSL3- or IKE-treated, red).

Since not every initial screening hit suppressed lipid peroxidation despite showing anti-ferroptotic properties in experiments before, we measured fluorescence at 520 nm of every compound in a cell-free setting (Supplementary Figure **S1**). This ensures that the compounds do not show fluorescence that could interfere with the C11-BODIPY assay, which is measured at an excitation wavelength of 520 nm. The measurement showed that only Dipyridamol and 2-TEDC emit at 520 nm (Supplementary Figure **S1**).

Summarizing, we screened 3,684 compounds in a cell-viability-based assay to discover inhibitors of ferroptosis, which should guide us to novel ferroptosis regulators based on their known targets. We received 16 hits from which 9 compounds showed dose-dependent anti-ferroptotic activity in follow-up experiments. These remaining hits were tested for ferroptosis-specificity, activity against FIN56, and for suppression of lipid peroxidation. Based on literature research and validation performance, we decided to further analyze Turofexorate and Fexaramine, which are both agonists of the Farnesoid X Receptor (FXR).

5.3.2 FXR agonists potently inhibit ferroptosis

We analyzed two agonists of the Farnesoid X receptor (FXR), Turofexorate and Fexaramine (Turo and Fexa), which significantly inhibited ferroptosis in our compound screen. These two compounds were selected because of their promising performances in the hit validation experiments and due to the important role of FXR in cholesterol and lipid metabolism, which prompts a connection to ferroptosis.

To measure the potency of Turo and Fexa, we treated HT-1080 cells with a serial dilution of RSL3 or IKE and cotreated with the previously determined optimal concentration of Turo or Fexa (Figure **25A** and **B**). Even at normally lethal doses of ferroptosis inducers, both FXR agonists were able to rescue cell death.

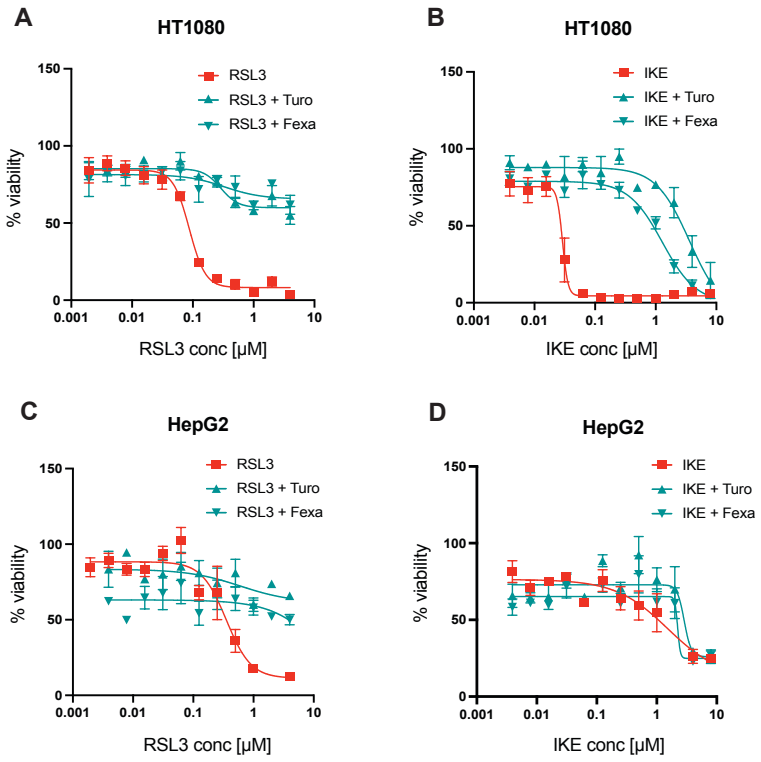

Figure 25: **FXR agonists potently inhibit ferroptosis in HT-1080 and HepG2.** HT-1080 or HepG2 were cotreated with serial dilutions of RSL3 or IKE (red) and 12 µM Turo or Fexa (green) for 18 hours. Measured viability was normalized to DMSO-treated control cells. Data shown are mean values of 3 technical replicates ± SD.

Since the FXR is typically expressed in liver, kidney and small intestine [82] [110], we chose the hepatocellular carcinoma cell line HepG2 as an additional *in vitro* model to study ferroptosis inhibition by FXR activation. Interestingly, when HepG2 were treated with serial dilutions of

RSL3 and IKE, we could observe a higher resistance to ferroptosis induction than in HT-1080 (Figure **25C** and **D**), which could already hint at an anti-ferroptotic function of FXR in these cells.

Since HT-1080 normally only express very low levels of FXR [111], the question was raised how Turo and Fexa could rescue HT-1080 cells from ferroptosis. To address this, we treated HT-1080 or HepG2 with FXR agonists alone and analyzed expression of FXR on mRNA and protein level (Figure **26**).

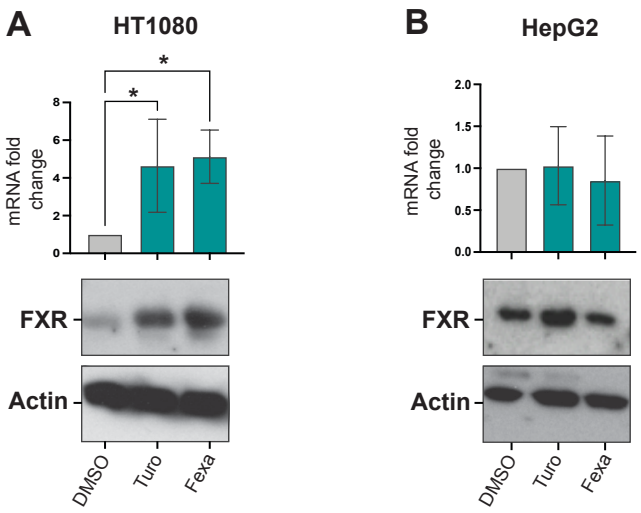

Figure 26: **mRNA and protein level of FXR after treatment with Turo or Fexa**. Cells were treated with 12 µM FXR agonists for 7 hours before they were harvested for qRT-PCR or Western Blotting. Levels of mRNA were normalized to GAPDH expression. qRT-PCR data shown are mean values of 3 biological replicates ± SD. *p≤0.05 (One-way ANOVA). Western Blots shown are representative images of 3 biological replicates.

Upon stimulation with Turo or Fexa, FXR expression was significantly upregulated on mRNA and protein level in HT-1080 cells (Figure **26A**). When HepG2 were treated with Turo or Fexa, FXR was not upregulated. This observation can be explained by the negative feedback loop that regulates FXR expression in cells [110], and since the FXR levels in HepG2 are already high, they won't be further increased by FXR activation.

To examine whether general FXR activation could rescue cells from ferroptosis or if it only occurs after activation by chemical agonists such as Turo or Fexa, ferroptosis was induced in HepG2 by RSL3-treatment and co-treated with two bile acids, obeticholic acid and chenodeoxycholic acid (Figure **27**).

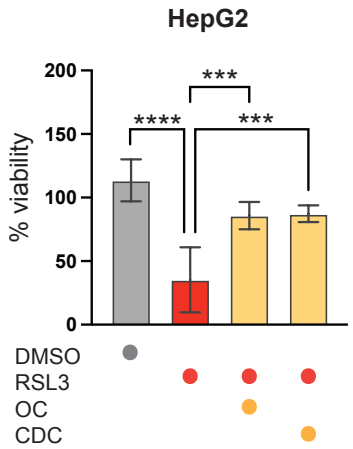

Figure 27: **Endogenous ligands of FXR also rescue cells from ferroptosis.** HepG2 were treated with 65 nM RSL3 and 2 µM Obeticholic acid (OC) or 20 µM Chenodeoxycholic acid (CDC) for 5 hours. Data shown are mean values of 5 technical replicates ± SD. ****p≤0.0001, ***p≤0.001 (One-way ANOVA).

Treatment with endogenous ligands of FXR, the bile acids, also rescued HepG2 cells from ferroptosis, which hints at a receptor-mediated anti-ferroptotic effect.

5.3.3 Dimerization of FXR with RXR

As a nuclear receptor, FXR binds to DNA response elements in order to transcriptionally activate its downstream target genes. This DNA binding can happen as a FXR monomer or as a FXR dimer; but mostly it occurs in dimers with other nuclear receptors, such as the Retinoid X receptor (RXR) [112]. In order to test whether the RXR is involved in anti-ferroptotic downstream signaling, we induced ferroptosis in HT-1080 cells and cotreated with Turo or Fexa and a small molecule inhibitor of RXR (Figure **28**).

When RXR is inhibited, Turo or Fexa treatment could not rescue cells from ferroptosis anymore. This effect was dose-dependent and significant, therefore we hypothesized that the heterodimerization between FXR and RXR is indeed necessary to exert the anti-ferroptotic effect of FXR activation by Turo or Fexa.

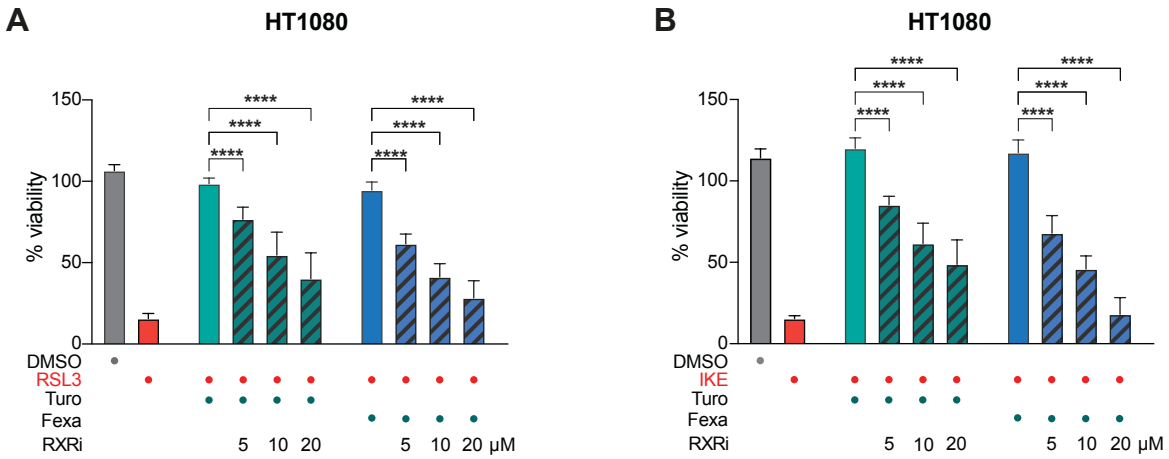

Figure 28: **Dimerization of RXR with FXR is necessary to suppress ferroptosis via Turo or Fexa treatment.** HT-1080 were cotreated with 250 nM RSL3 **(A)** or 1 µM IKE **(B)**, 12 µM Turo (green) or Fexa (blue) and a serial dilution of RXR inhibitor as indicated for 18 hours. Data shown are mean values of 3 biological replicates ± SD. ****p≤0.0001 (One-way ANOVA).

5.3.4 Target specificity of Turo and Fexa

To further characterize the anti-ferroptotic activity of Turo and Fexa, we performed different cell-free assays. These assays will answer the question whether the compounds can suppress ferroptosis through certain chemical properties, which allow them to trap radicals or to chelate iron. In the cell-free C11-BODIPY assay and DPPH assay, we could conclude that Turo and Fexa do not display antioxidative or radical trapping activities (Figure **29A** and **B**). In an Iron Chelator Assay we determined that Turo and Fexa also do not chelate ferrous iron in a cell-free set up (Figure **29C**). This was tested because ferroptosis is an iron-dependent cell death, and the presence of high ferrous iron levels in cells leads to Fenton-reaction-generated ROS, which then leads to lipid peroxidation and ferroptosis [113]. Using iron chelators such as Deferoxamine, ferroptosis can be suppressed [9]. The results that Turo and Fexa do not chelate iron or act as antioxidants further hint at a receptor-mediated ferroptosis-inhibiting effect.

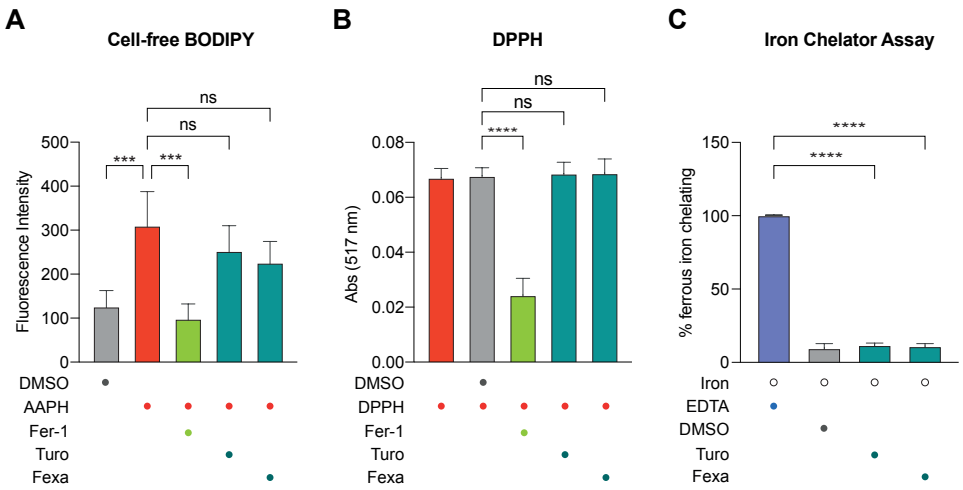

Figure 29: **Cell-free assays show that Turo and Fexa are no RTA or iron chelators. A** C11-BODIPY was oxidized by 7.5 mM AAPH. 25 µM Turo or Fexa were tested in PBS for radical trapping activity. 25 µM Fer-1 was used as a positive control. **B** 50 µM of Turo or Fexa was diluted in 0.05 mM DPPH in methanol to test for antioxidative activity. 50 µM of Fer-1 was used as a positive control. **C** 12 µM of Turo or Fexa was tested for iron chelating activity in a ferrozine-based assay. 100 µM EDTA was used for normalization. In all 3 experiments, data plotted are mean values of 3 biological replicates ± SD. ***p≤0.001, ****p≤0.0001 (One-way ANOVA).

To prove whether activation of the target of Turo and Fexa, the FXR, is mediating ferroptosis suppression, a HepG2 FXR knock-out cell line was generated using CRISPR-Cas9 (3% residual FXR levels since a full knock-out seemed to be lethal, Figure **30C**). When ferroptosis was induced by RSL3 in FXR-KO HepG2 cells, the knock-out cells showed a higher ferroptosis sensitivity compared to wild-type HepG2 (Figure **30A**).

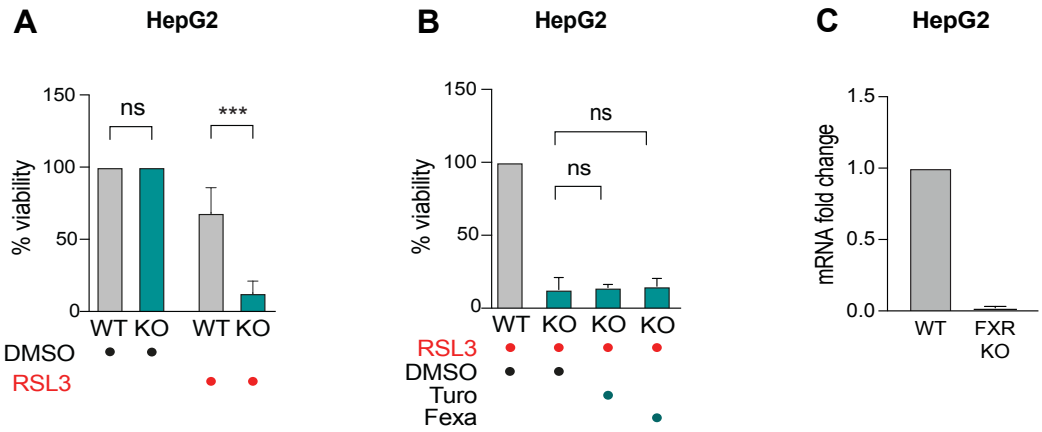

Figure 30: **FXR-KO cell line has higher sensitivity to ferroptosis and cannot be rescued by Turo or Fexa. A** HepG2 FXR-KO cell line has a higher sensitivity to RSL3-induced ferroptosis compared to wildtype HepG2. Cells were treated with 125 nM RSL3 for 18 hours. Data plotted are mean values of 3 technical replicates ± SD. ***p≤0.001 (One-way ANOVA). **B** Ferroptotic FXR-KO cells cannot be rescued by Turo or Fexa treatment anymore. Cells were treated with 125 nM RSL3 and 12 µM Turo or Fexa for 18 hours. Data shown are mean values of 3 technical replicates ± SD. p > 0.05 (One-way ANOVA). **C** FXR knock out was validated via qRT-PCR and revealed 97% knock out in an expanded single clone. mRNA levels were normalized to cellular RP2 levels. Data shown are mean values of 4 biological replicates.

Furthermore, treatment of FXR-KO cells with Turo or Fexa did not rescue from ferroptosis anymore (Figure **30B**), suggesting that Turo and Fexa specifically bind to their expected target FXR and thereby regulate ferroptosis inhibition. Without FXR expression, treatment with both compounds did not affect cell viability after RSL3-induced ferroptosis.

Since agonistic activation of FXR suppressed ferroptosis, we hypothesized whether antagonistic inhibition of FXR would have a sensitizing effect on cells. We cotreated HepG2 cells with RSL3, Turo and a small molecule inhibitor of FXR (Guggulsterone) and observed that not only the rescuing activity of Turo was diminished (Figure **31A**), but also treatment with FXR inhibitor alone sensitized the cells towards ferroptotic cell death induced by RSL3 (Figure **31B**).

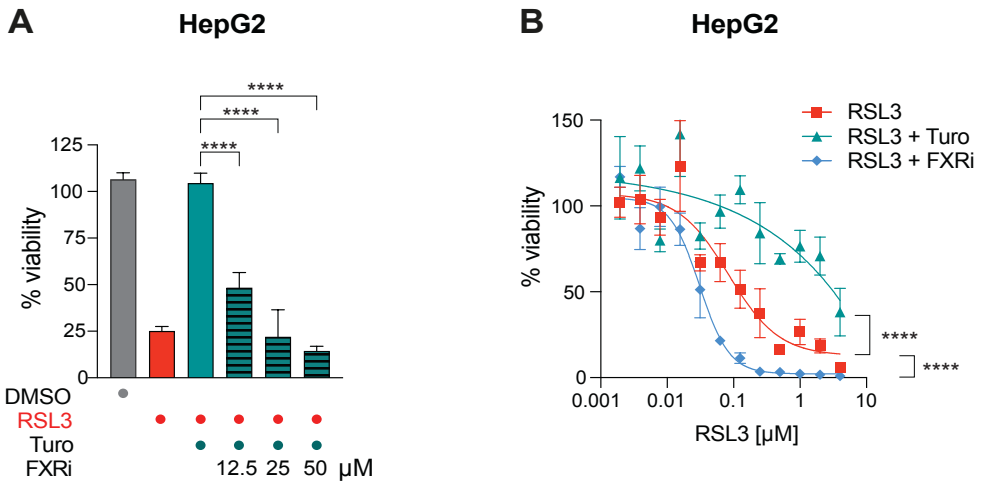

Figure 31: **Small molecule FXR inhibitor sensitizes cells to ferroptosis. A** HepG2 were cotreated with 1 µM RSL3, 12 µM Turo and indicated concentrations of FXR inhibitor for 18 hours. Data shown are mean values of 3 biological replicates ± SD. ****p≤0.0001 (One-way ANOVA). **B** HepG2 were treated with a serial dilution of RSL3, 12 µM Turo or 50 µM FXR inhibitor for 18 hours. Measured viability was normalized to DMSO-treated control cells. Data shown are mean values of 3 technical replicates ± SD. ****p≤0.0001 (One-way ANOVA).

Furthermore, we wanted to verify if treatment with Turo or Fexa activates canonical downstream targets of the FXR to further corroborate our hypothesis of an on-target effect. We treated HepG2 with Turo or Fexa and measured mRNA levels of Small Heterodimer Partner (SHP) and CYP7A1 (Supplementary Figure **S2**). SHP is upregulated upon FXR activation by bile acids and then in turn inhibits expression of CYP7A1 as part of the negative feedback regulation of FXR [114]. Indeed, we observed an upregulation of SHP and

downregulation of CYP7A1 upon treatment with Turo or Fexa, indicating on-target activity of these agonists.

In summary, Turo and Fexa are inhibiting ferroptosis not by trapping radicals or chelating iron, but presumably by binding their target FXR. In the absence of FXR or when FXR is inhibited, cells were more sensitive towards RSL3-induced ferroptosis and could not be rescued by Turo or Fexa anymore. Finally, mRNA levels of known downstream target genes of FXR were altered upon treatment with Turo or Fexa.

5.3.5 FXR activation suppresses lipid peroxidation

In addition to regulation of bile acid metabolism, the FXR is also known to influence lipid metabolism [115]. Since Turo and Fexa alone could not suppress radical reactions, we hypothesized that activation of FXR is needed to inhibit peroxidation of membrane phospholipids and therefore ferroptosis. To test this hypothesis, we performed the previously utilized set of cellular lipid peroxidation assays: an immunostaining of 4-HNE with subsequent flow cytometry, a TBARS assay to detect MDA levels and C11-BODIPY flow cytometry staining in HT-1080 and HepG2 (Figure **32A-D**). We observed that treatment of ferroptotic cells with FXR agonists markedly lowered levels of 4-HNE and MDA. Staining with the fluorescent ROS sensor C11-BODIPY further confirmed that treatment with Turo or Fexa suppressed lipid peroxidation in HT-1080 as well as HepG2.

To gain further insights into cellular lipid composition upon treatment with ferroptosis inducer RSL3 and rescue via Turo or Ferrostatin-1, we performed global lipidomic profiling on HT-1080 cells (Figure **32E and F**, lipidomics performed and analyzed by Dr. Constanze Müller, Research Unit Analytical BioGeoChemistry, Helmholtz Munich). The resulting Principal Component Analysis (PCA) showed that DMSO-treated control samples cluster together with samples that were treated with RSL3 and Ferrostatin-1, meaning that they show a similar lipidomic phenotype. RSL3-treated samples show a highly changed phenotype in comparison to control cells, and RSL3 and Turo-treated cells form an entirely different cluster (Figure **32E**).

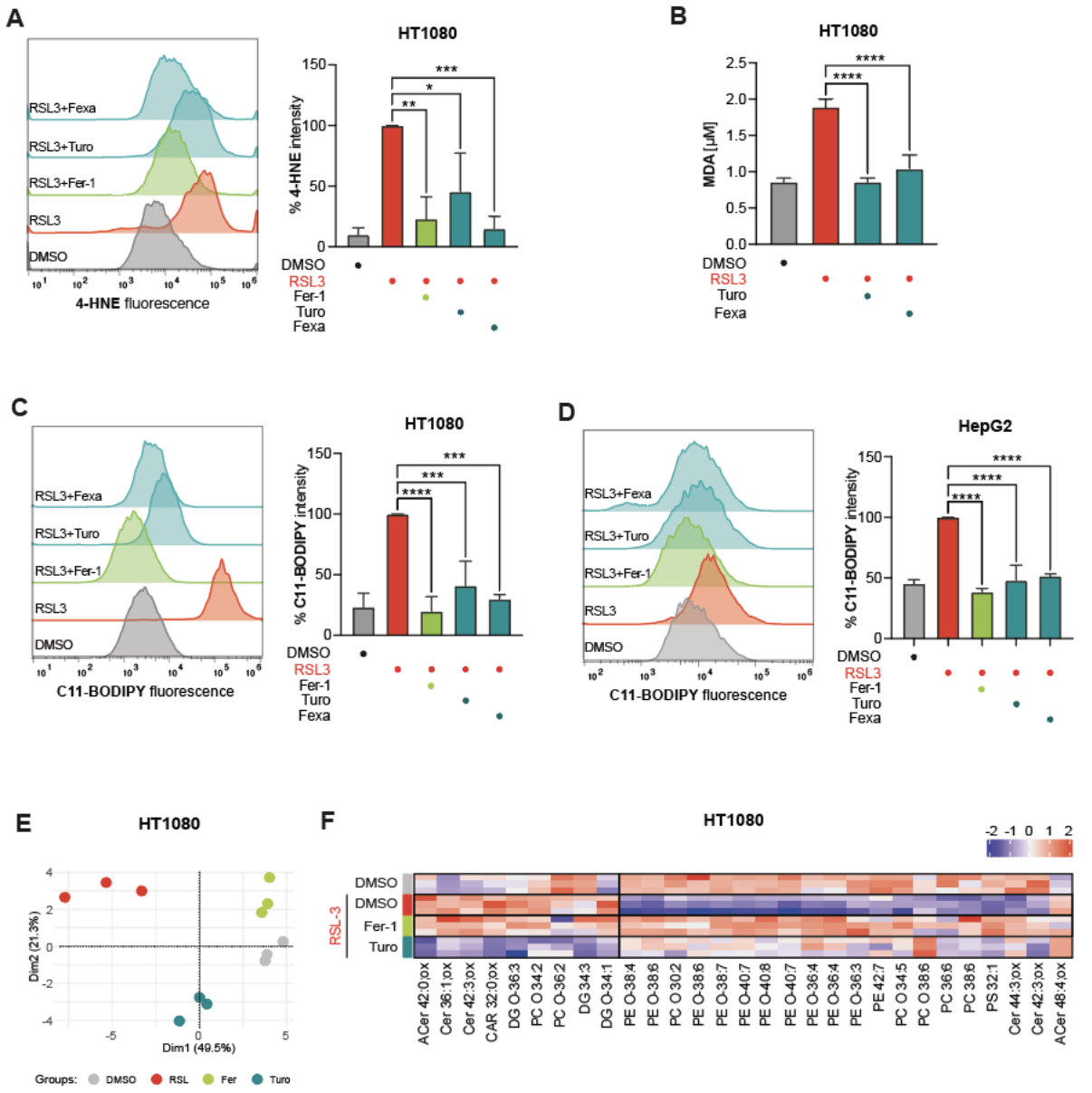

Figure 32: **FXR agonists suppress lipid peroxidation and modify PUFA composition. A** Flow cytometry histograms and quantification of 4-HNE immunostaining after treatment of HT1080 with 300 nM RSL3 and 2 µM Fer-1 or 12 µM Turo or Fexa for 2 hours. **B** TBARS assay of HT1080 treated with 250 nM RSL3 and 12 µM Turo or Fexa for 2.5 hours. **C and D C11-**BODIPY staining and flow cytometry of HT1080 and HepG2. Cells were treated with 250 nM RSL3 and 12 µM Turo/Fexa or 2 µM Fer-1 for 2 hours. Histograms shown in all experiments are representative of 3 biological replicates. Bar graphs shown in all experiments are mean values of 3 biological replicates ± SD. *p≤0.05, **p≤0.01, ***p≤0.001, ****p≤0.0001 (One-Way ANOVA). **E** Principal component analysis of lipidomics data derived from HT1080 treated with 200 nM RSL3 and 12 µM Turo or 2 µM Fer-1 for 2 hours. **F** Change of lipid composition in HT1080 after treatment with 200 nM RSL3 and 12 µM Turo or 2 µM Fer-1 for 2 hours visualized in a heat map. Red fields indicate high amounts of indicated lipids, blue fields indicate low amounts. Lipidomic profiling was performed in 3 technical replicates.

When visualizing the relative abundance of different lipid classes in a heat map, we could observe that upon treatment, the composition of PUFA-containing phospholipids was altered (Figure **32F**). Under ferroptosis induction by RSL3, some classes of PUFA-PL were increased (left block), whereas other classes of PUFA-PL were depleted due to degradation (right block).

Treatment with Ferrostatin-1 or Turo could revert these changes back to the state of control cells (right block), or even improve it (Turo, left block). Notably, the lipid changes between treatment with Turo or treatment with Ferrostatin-1 were not similar, hinting at different peroxidation-suppressing mechanisms.

5.3.6 FXR upregulates ferroptosis-inhibitory target genes

Next, we aimed to examine the mechanism of how FXR activation leads to a suppression of lipid peroxidation and therefore inhibition of ferroptosis. As a nuclear receptor, FXR binds to response elements in the DNA and acts as a transcription factor for different genes that regulate bile acid metabolism and other pathways [82]. We searched different databases that collect results of ChIP-Seq experiments (Catalogue of Transcriptional Regulatory Interactions (Catrin), Eukaryotic Promoter Database (EPD)) and map FXR binding sites. Interestingly, we found predicted FXR response elements in the promoters of several anti-ferroptotic genes: FSP1 and GPX4 (two of the most important ferroptotic defense genes), PPARA (a central regulator of lipid metabolism and a nuclear receptor itself) and ACSL3 and SCD1 (enzymes of the MUFA synthesis pathway).

Based on this knowledge, we conducted qRT-PCR to measure mRNA levels of these predicted downstream genes of FXR. Since FXR expression is normally low in HT-1080, we transfected cells with an overexpression plasmid to enhance possible transcriptional effects (Figure **33A**).

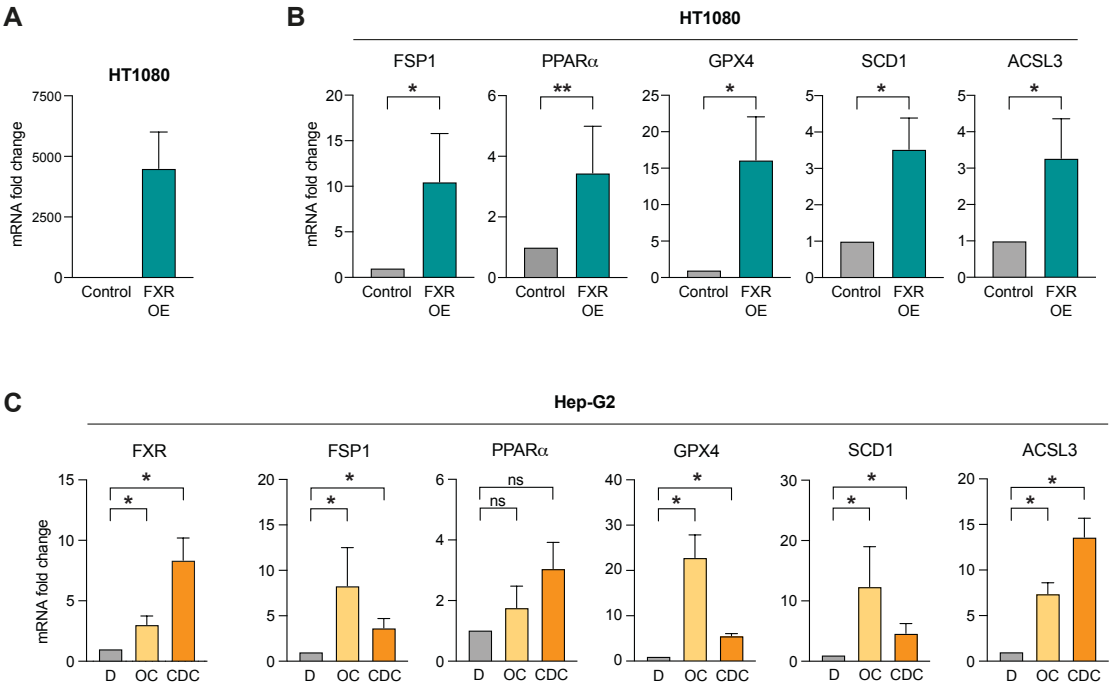

Figure 33: **Overexpression of FXR or treatment with FXR ligands upregulates anti-ferroptotic genes. A** Overexpression of FXR in HT1080 by transient plasmid transfection. **B** qRT-PCR of ferroptosis-regulating genes in FXR-overexpressing HT1080. **C** qRT-PCR of ferroptosis-regulating genes. HepG2 were treated with bile acids (2 µM Obeticholic acid or 20 µM Chenodeoxycholic acid) for 8 hours. For all experiments: Data shown are mean values of 3 biological replicates ± SD. mRNA levels are normalized to GAPDH expression. **p≤0.01, *p≤0.05 (One-way ANOVA).

The results of the qRT-PCR could confirm our hypothesis of FXR activating the transcription of anti-ferroptotic genes: Upon FXR overexpression, mRNA levels of FSP1, GPX4, PPARA, SCD1 and ACSL3 increased significantly (Figure **33B**). In a more endogenous setting, where HepG2 cells were treated with bile acids, we could also observe an upregulation of these genes on mRNA level (Figure **33C**).

To validate that downstream target activation by FXR is necessary to inhibit ferroptosis, we treated ferroptotic cells with Turo and small molecule inhibitors of FSP1 or PPARα (Figure **34A and B**). We detected that the anti-ferroptotic effect of Turo was reduced in a dose-dependent manner with impaired activity of FSP1 or PPARα. This further underlines our finding that FXR activates the transcription of ferroptosis-regulating genes.

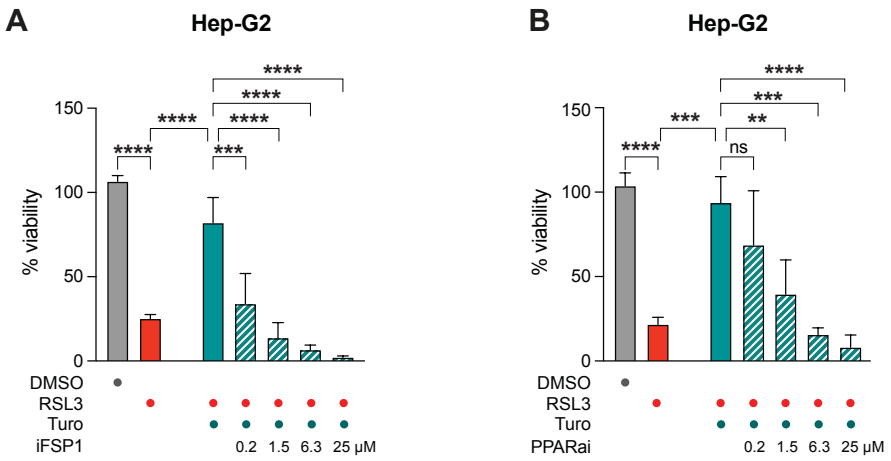

Figure 34: **Inhibitors against FSP1 or PPARα revert the anti-ferroptotic effect of FXR activation.** HepG2 cells were treated with 1 µM RSL3, 12 µM Turo and indicated concentrations of FSP1 inhibitor (iFSP1) or PPARα inhibitor (GW6471) for 18 hours. Data shown are mean values of 3 biological replicates ± SD. **p≤0.01, ***p≤0.001, ****p≤0.0001 (One-Way ANOVA).

Since upregulation of transcription alone is not sufficient to inhibit ferroptosis, we also performed Western Blot experiments to examine whether our detected target genes also showed increased protein levels. For this, we treated HepG2 cells either with Turo, Fexa or bile acids (Obeticholic acid or Chenodeoxycholic acid) and analyzed levels of FSP1 and GPX4 in whole cell lysates (Figure **35A and B**). Quantification of band intensities showed that FSP1 and GPX4 protein levels were also increased in comparison to DMSO-treated control cells.

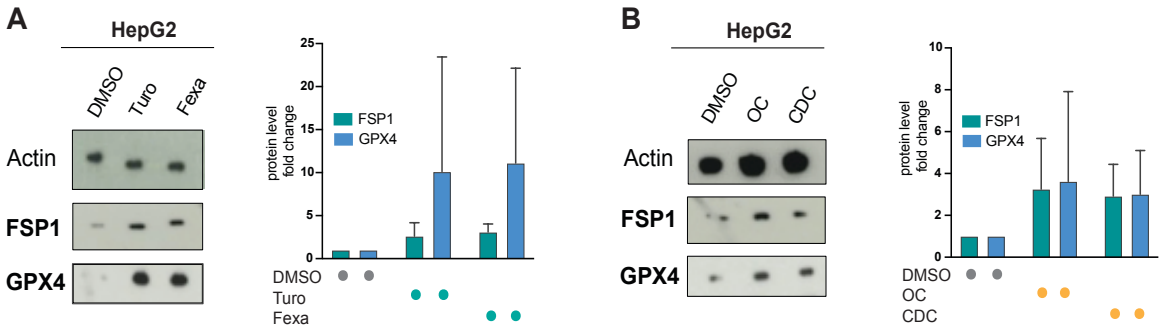

Figure 35: **Upregulation of FXR targets after agonist treatment on protein level. A** HepG2 were treated with 12 µM Turo or Fexa for 2 hours. **B** HepG2 were treated with 2 µM OC or 20 µM CDC for 2 hours. Band intensities were quantified and visualized as protein fold change compared to DMSO treated cells. FSP1 and GPX4 levels were normalized to β- Actin levels. Blots shown are representative images of 3 biological replicates. Blot images of every biological replicate can be found in Supplementary Figures **S3** and **S4**. Data shown are mean values of 3 biological replicates ± SD.

We further analyzed protein levels of all target genes in FXR-overexpressing HT1080 cells to validate the results of the previously performed qRT-PCR. Similar to the agonist treatments in

HepG2 cells, the FXR-OE cells also showed elevated protein levels of FSP1, GPX4, ACSL3, PPARα and SCD1 (Figure **36**). These results support our hypothesis of FXR acting as a transcription factor for anti-ferroptotic regulators.

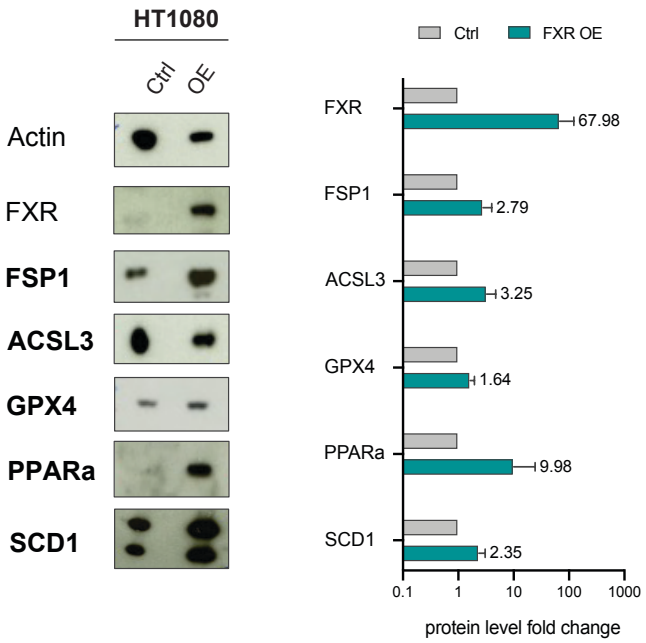

Figure 36: **Upregulation of target genes in FXR OE cells could be validated on protein level.** HT1080 overexpressing FXR show upregulated protein levels of anti-ferroptotic genes. Band intensities were quantified and visualized as protein fold change compared to control cells. FXR, FSP1, ACSL3, GPX4, PPARα and SCD1 levels were normalized to β- Actin levels. Blot shown is a representative image of 3 biological replicates. Blot images of all biological replicates can be found in Supplementary Figure **S5**. Data shown are mean values of 3 biological replicates ± SD.

To address the question whether the upregulation of target genes is mediated specifically by FXR, we treated FXR-overexpressing HT-1080 cells with FXR antagonist Guggulsterone and measured mRNA levels of our selected target genes in a qRT-PCR (Figure **37**).

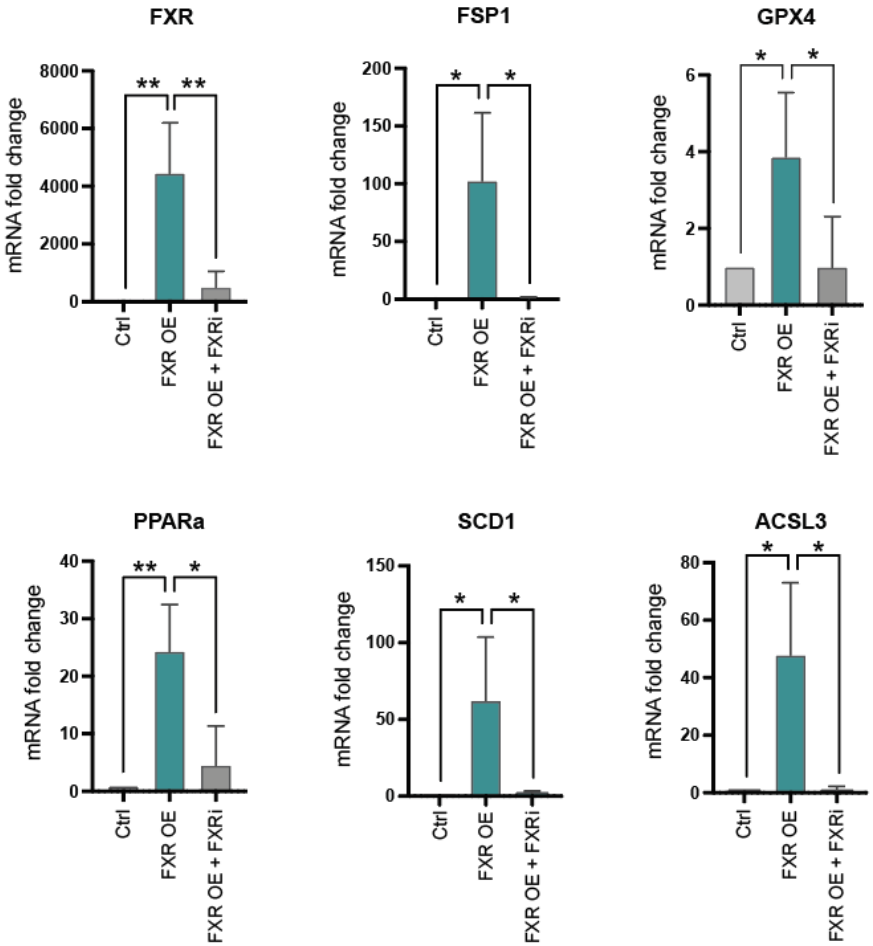

Figure 37: **FXR inhibitor treatment reduces upregulated genes in FXR-OE cells.** HT1080-FXR-OE cells were treated with 50 µM FXR inhibitor for 24 hours. Target gene levels were normalized to RP2 levels. Data shown are mean values of 3 biological replicates ± SD. **p≤0.01, *p≤0.05 (One-Way ANOVA).

Interestingly, we observed that the transcription level of every target gene was reduced after inhibitor treatment, almost to the levels of control cells.

Summarizing, we discovered that several anti-ferroptotic regulators show binding sites of FXR in their promoter sequences. We found that FXR upregulates these target genes upon FXR agonist treatment or FXR overexpression. This was confirmed on protein level and could be reversed by FXR inhibition.

5.3.7 Validation in primary and 3D cellular systems

Finally, we wanted to verify our *in vitro* observations in different cellular systems of primary origin to underscore the physiological relevance of FXR-mediated ferroptosis inhibition. To achieve this, we isolated hepatocytes from healthy mice (with the help of the lab of Prof. Zischka at TUM) and induced ferroptosis. Notably, these hepatocytes had a much lower ferroptosis sensitivity than HT-1080 or HepG2. Treatment with synthetic FXR agonists Turo or Fexa as well as treatment with endogenous FXR ligands could rescue hepatocytes from cell death (Figure **38A**). When these primary hepatocytes were treated with Turo or Fexa alone, we observed a significant upregulation of FSP1 and PPARα on transcriptional level (Figure **38B**). These results in an *ex vivo* model confirmed our previous findings of FXR as a ferroptosis suppressor.

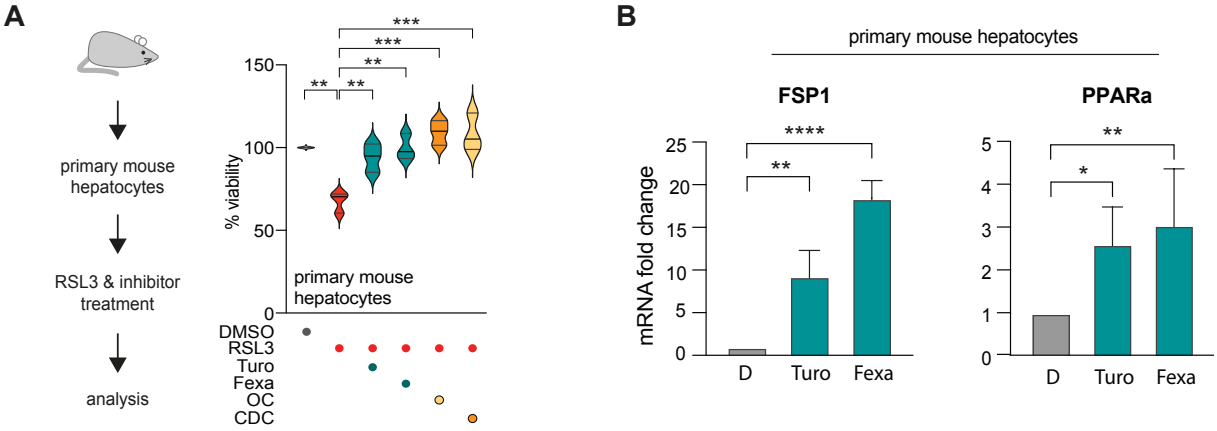

Figure 38: **FXR activation suppresses ferroptosis in murine hepatocytes by upregulation of target genes. A** Primary hepatocytes from 2 healthy mice were isolated and treated with 1 µM RSL3, 12 µM Turo or Fexa, 2 µM Obeticholic acid or 20 µM Chenodeoxycholic acid for 18 hours. **B** Murine primary hepatocytes were treated with 12 µM Turo or Fexa for 6 hours. Measured mRNA levels were normalized to GAPDH expression. Data shown in both experiments are mean values of 3 technical replicates ± SD. ****p≤0.0001, ***p≤0.001, **p≤0.01, *p≤0.05 (One-way ANOVA).

These results in an *ex vivo* model confirmed our previous findings of FXR as a ferroptosis suppressor.

To test the anti-ferroptotic function of Turo and Fexa in a three-dimensional tumor-like environment, we generated spheroids from HT1080 and induced cell death by RSL3 treatment. Hoechst staining and high-content image analysis showed that cotreatment with Turo or Fexa

could rescue spheroids destruction in the same manner as cotreatment with Ferrostatin-1 (Figure **39A**). These results were quantified by measuring the ration of spheroid width to length, which showed significant reduction of spheroid destruction after suppression of ferroptosis by Turo or Fexa treatment (Figure **39B**).

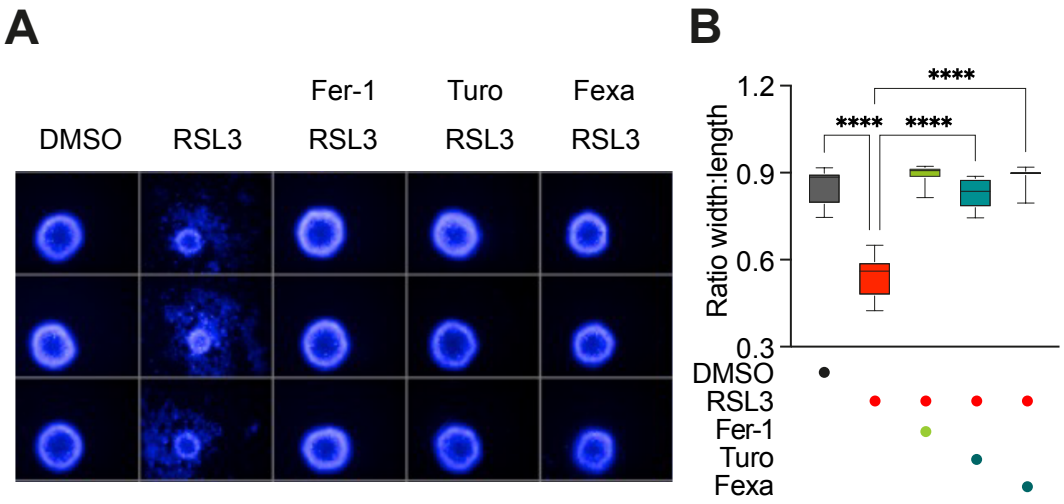

Figure 39: **Turo and Fexa rescue ferroptotic cell death in HT1080-derived spheroids. A** Representative microscopic images of spheroids treated with 200 nM RSL3, 2 µM Ferrostatin-1 or 12 µM Turo or Fexa for 48 hours. Spheroids were stained with Hoechst 33342. **B** Analysis of spheroid images by measurement of width:length ratio. Data shown are mean values of n=24 (3 biological replicates with 8 spheroids per condition) ± SD. ****p≤0.0001 (One-way ANOVA).

As a third cellular system we wanted to examine the effect of FXR activation or inhibition in human non-cancerous hepatocytes. To achieve this, we differentiated induced pluripotent stem cells (iPSCs) into functional hepatocytes (with the help of the lab of Dr. Vincendeau at Helmholtz Munich), induced ferroptosis and cotreated with FXR agonists or FXR inhibitor Guggulsterone (Figure **40A**). Quantitative RT-PCR of canonical hepatocyte markers confirmed differentiation state and functionality of the hepatocytes (Supplementary Figure **S6**). Subsequent staining with Propidium iodide revealed that cotreatment with Turo or Fexa could significantly lower the number of dead hepatocytes, whereas cotreatment with RSL3 and the FXR inhibitor sensitized cells even more towards cell death (Figure **40B**). This experiment confirms our previous findings and shows that ferroptosis regulation by FXR is also active in human non-cancerous hepatic cells.

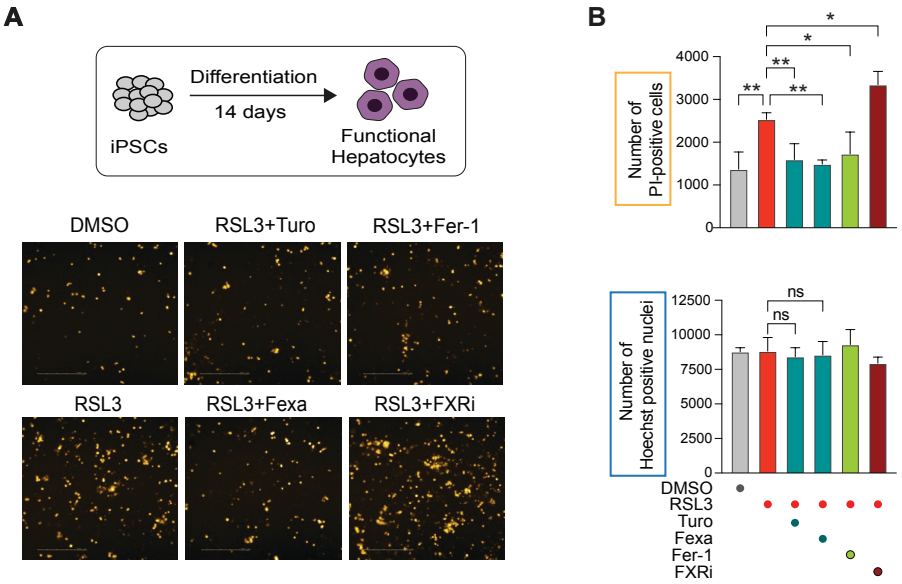

Figure 40: **FXR regulates ferroptosis in human differentiated hepatocytes. A** Induced pluripotent stem cells were differentiated over 14 days into hepatocytes. Cells were treated with 1 µM RSL3, 12 µM Turo or Fexa, 2 µM Ferrostatin-1 and 50 µM FXR inhibitor for 6 hours before they were stained with Propidium iodide or Hoechst. Representative images of 8 replicates (2 biological replicates with 4 technical replicates each) are shown. **B** Image analysis of PI-stained cells. Hoechst stain was used for normalization of cell numbers. Data shown are mean values ± SD. **p≤0.01, *p≤0.05 (One-way ANOVA).

Summarizing, we found that our screening hits Turofexorate and Fexaramine inhibit ferroptosis by agonistic activation of the nuclear receptor FXR. With serveral cell-free experiments and a FXR-knock-out cell line we prove an on-target effect of these compounds to activate FXR, which then acts as a transcription factor for important ferroptotic defenses (such as GPX4 and FSP1) and regulators of MUFA synthesis (such as ACSL3, PPARα, SCD1) to suppress lipid peroxidation. These findings could be validated in murine hepatocytes, spheroids and human hepatocytes differentiated from iPSCs.

6. Discussion

6.1 Chemical-genetic screening reveals novel ferroptosis regulator

To date, many small molecules that can induce ferroptosis are known and intensive research into therapeutic applications, e.g. in cancer treatment, is conducted [116] [73]. However, ferroptosis is not only valuable to target aberrant cells, but it is also implied to occur in degenerative diseases [32] [117] [118]. By discovering cellular inhibitors of ferroptosis, which ideally can be activated by small molecules, excessive cell death and organ damage may be prevented.

We approached the goal of discovering novel cellular ferroptotic regulators by performing a chemical genetics screen of 3,684 small molecules with known targets and mode of actions on ferroptotic HT-1080 cells. Many of our tested compounds are already FDA-approved or are in a stage of preclinical or clinical trial, which would be favorable for a possible repurposing as an anti-ferroptotic drug in the future. Based on our calculated Z-prime factor of 0.3 to 0.7, we evaluated our screening results as reliable and continued to validate 9 hits out of initial 16 hits. The selection of screening hits was based on objective criteria, such as exclusion of compounds without known targets and a cut-off at a certain activity level. We also based the hit selection on literature research and possible links to ferroptosis, which may have introduced some bias into our final hit list. Nevertheless, 9 compounds could be validated in several ferroptosis assays: a 10-point dose-response measurement, exclusion of necroptosis or apoptosis inhibition, induction of ferroptosis with FIN56, and a C11-BODIPY staining to measure lipid peroxidation. Furthermore, we ensured that selected compounds for follow-up experiments showed no fluorescence at wavelengths that overlap with our assays.

Based on the targets and mode of actions of several hit compounds we were able to identify and validate several cellular ferroptotic regulators, and especially concentrated on the agonistic activation of the Farnesoid X Receptor.

6.2 Radical trapping agents as ferroptosis inhibitors

In contrast to apoptosis, ferroptosis is not a consequence of intrinsically activated signaling cascades. Instead, it is rather perceived as a cellular state after the tightly regulated balance of defenses against oxidative stress is lost. The role of the main anti-ferroptotic enzymes is to provide or recycle substances that reduce reactive oxygen species or trap radicals in order to inhibit lipid peroxidation: glutathione as a cofactor of GPX4 [119], ubiquinone is reduced by FSP1 [38], tetrahydrobiopterin is produced by GCH1 [44]. Therefore, it can be concluded that ferroptosis can be averted by providing a sufficient amount of antioxidative substances to the cell, which has already been proven by vitamin E or vitamin K treatments [40] [24]. The gold standard ferroptosis inhibitor that was used in almost all of our experiments as a positive control, Ferrostatin-1, is also a radical-trapping antioxidant and showed efficacy against ischemia-reperfusion injury and acute iron poisoning in mice [120] [72]. Another ferroptosis-inhibiting antioxidant is Liproxstatin-1, which shows higher metabolic stability *in vivo* and alleviates renal and hepatic ischemia-reperfusion injury in mice [32]. These examples underline the potential and importance of radical-trapping antioxidants in physiological context as well as in the context of disease treatment.

We rationally selected Seratrodast for possible drug repurposing and discovered it to potently inhibit lipid peroxidation *in vitro* (Figure **18**) as well as in a cell-free setting (Figure **17**). Originally, Seratrodast was approved as a drug for asthma treatment in Japan, China and India, because it inhibits the thromboxane A2 receptor and thereby reduces bronchoconstriction and airway hyperresponsiveness [107]. Our results however do not link the anti-ferroptotic effect of Seratrodast to this receptor, since other canonical TBXA2R inhibitors (Terutroban, Ramatroban, Vapiprost, SQ29548 and 15(R)-Pinane Thromboxane A2) were not able to rescue ferroptotic cells (Figure **15**). We hypothesized that the anti-ferroptotic effect we observed stems from the quinone moiety in the chemical structure of Seratrodast, because NQ301, another TBXA2R inhibitor possessing a quinone moiety, could also rescue cells from ferroptosis. This hypothesis is also supported by a previous study from 2017, which links Seratrodast to antioxidant activity [121]. Quinones are strong oxidizing agents and are

involved in fundamental physiological functions, such as cellular respiration (ubiquinone [122]) and photosynthesis (plastoquinone [123]). They react with peroxide radicals and can thereby stop the radical-driven lipid peroxidation of the cellular membrane that happens during ferroptosis [124]. Recently the reduced form of vitamin K was discovered as a potent radical scavenger, and the anti-ferroptotic function was also ascribed to the quinone head group [40].

In contrast to our findings, another study was published which showed that knockdown of the thromboxane A2 receptor protected neurons from ferroptosis via upregulation of GPX4 on protein level [125]. Similarly, they observed a recovery of SLC7A11 and GPX4 protein levels by Seratrodast treatment after ferroptosis induction by erastin. Interestingly, they also tested different TBXA2R inhibitors besides Seratrodast and could not show anti-ferroptotic effects for every compound. In principle, we cannot exclude that Seratrodast also has an impact on ferroptosis regulators by off-target effects that are not related to the thromboxane A2 receptor, but our data show that the antioxidant activity of Seratrodast is the primary mechanism to suppress ferroptosis. For future experiments it could be useful to validate the antioxidative capacity of Seratrodast with other technologies rather than a cell-free C11-BODIPY assay. A possible method is the FENIX (Fluorescence-enabled inhibited autooxidation) assay, which mimics the phospholipid bilayer of cellular membranes more accurately than C11-BODIPY [126].

Since Seratrodast could inhibit ferroptosis in a 3D spheroid model of HT1080 cells, we are planning in future studies to test Seratrodast in an *in vivo* mouse model. Ideally, this should be a model of a ferroptosis-related degenerative disease, such as kidney ischemia-reperfusion injury, where excessive cell death needs to be inhibited [120]. Seratrodast is an already approved drug in India, China and Japan, which means that studies about pharmacokinetics, pharmacodynamics, contraindications and adverse effects are already available. If these planned *in vivo* experiments are successful, Seratrodast could be a promising compound for a drug repurposing approach and could have therapeutic value in ferroptosis-related diseases. A similar case of an antioxidant repurposed drug is Idebenone, a benzoquinone that was originally approved for the treatment of Leber's hereditary optic neuropathy because of its

protective effects against hypoxia [127]. When it became evident that Idebenone is also an inhibitor of lipid peroxidation, it was also successfully tested against ferroptosis-associated pathologies, such as excessive cell death after myocardial infarction [105]. In a similar way, we also aim to repurpose Seratrodast for future clinical applications.

6.3 Nuclear receptors as ferroptosis regulators

6.3.1 Retinoic Acid Receptor activation by vitamin A suppresses ferroptosis

In a joined project with the group of Dr. Michelle Vincendeau (Helmholtz Munich) we discovered that the active metabolite of vitamin A, all-trans retinoic acid (ATRA), suppresses ferroptosis and lipid peroxidation. We excluded the possibility of ATRA acting as a radical-trapping antioxidant, because it showed no effect in a cell-free C11-BODIPY assay or DPPH assay. Upon inhibition of RAR or RXR the anti-ferroptotic effect of ATRA was reduced, which hints at a receptor-mediated effect. When cells were treated with ATRA, we observed an upregulation of major anti-ferroptotic genes, such as GPX4, FSP1 and GCH1, as well as genes involved in lipid metabolism and MUFA synthesis (PPARα, SCD1 and ACSL3).

We hypothesize that the transcriptional upregulation of these genes is caused by the activation of RAR by binding of ATRA, the subsequent dimerization of RAR with RXR and, as a nuclear receptor, binding to response elements in the promoter regions of our observed target genes (RAREs). It is already known that RAR and RXR regulate hundreds of genes involved in very fundamental processes, such as embryo development, but until now, there has not been a direct connection to ferroptosis [101].

Only very recently, two studies were published that partly support our hypothesis of vitamin A as a ferroptosis inhibitor [128] [129]: Jakaria et al. tested metabolites of vitamin A for ferroptosis inhibition in neuronal cells and observed that retinol, all-trans retinal and all-trans retinoic acid showed radical trapping activity, with ATRA displaying the lowest potency of cell rescue compared to the other metabolites [128]. Interestingly, they also cotreated cells with

anhydroretinol, which serves as a competitive antagonist of vitamin A [130], and observed a sensitizing effect similar to our results in Figure **6C** and **D** when we inhibited RAR or RXR.

In a second study, Bi et al. discovered that the knock-out of retinol saturase (RETSAT) protected cells from ferroptosis because it saturates all-trans retinol to all-trans 13,14-dihydroretinol [129]. Retinol shows radical-trapping activity, whereas dihydroretinol does not; thereby they concluded that without RETSAT there is a higher concentration of antioxidants present in the cell, which stabilizes the cellular protection against ferroptosis. Furthermore, they could show that ATRA activates the transcription of stearoyl-CoA desaturase (SCD1), which in turn catalyzes the rate-limiting step of MUFA synthesis, which has anti-ferroptotic effects [25].

We take these publications as a further confirmation of our findings, but do not see that ATRA inhibits ferroptosis via radical trapping. It has been a long-standing question in literature whether vitamin A can be considered an antioxidant or not, but a recent review on this topic argued that ATRA (as the active metabolite of vitamin A) can only be termed an indirect antioxidant [103]. According to Dinkova-Kostova et al., direct antioxidants are defined with the following characteristics: “(i) they are redox active; (ii) they are either consumed or chemically modified in the process of their anti-oxidant action; and (iii) they have to be replenished or regenerated” [131]. On the basis of our results in several cell-based and cell-free assays, we are convinced that ATRA acts as an indirect antioxidant by transcriptionally activating genes which then act as antioxidative defenses or influence lipid metabolism to counteract peroxidation of PUFA phospholipids. We also tested other metabolites of vitamin A for ferroptosis inhibition (Figure **12**) and found out that 9-cis retinoic acid inhibited ferroptotic cell death in a similar concentration range to ATRA (20 to 100 µM). Retinol and retinal suppressed ferroptosis already at lower doses, which could be another hint at different mode of actions: 9-cis RA is an agonist of RXR [132], thus ferroptosis inhibition stems from RXR activation, dimerization with RAR (or potentially other nuclear receptors) and upregulation of target genes. Since retinol and retinal do not activate RAR or RXR, they seem to suppress ferroptosis by their antioxidant properties. Another explanation could be the fact that all-trans retinol and all-

trans retinal can be oxidized to ATRA; hence, when cells are treated with retinal or retinol, the actual active metabolite inhibiting ferroptosis would still be ATRA [101].

In collaboration with the group of Dr. Michelle Vincendeau (Helmholtz Munich), it was furthermore revealed that our proposed mechanism of ferroptosis inhibition by vitamin A plays a crucial role in neuronal differentiation (Tschuck et al., manuscript is currently under revision). It could be shown that when pluripotent stem cells develop into mature neurons, it is important that ferroptosis is suppressed, otherwise forebrain patterning during development is impaired. This ferroptosis inhibition seems to be achieved either by antioxidants (vitamin E, glutathione or Ferrostatin-1) or by higher levels of vitamin A. It has already been established that neurons require a tightly regulated balance of vitamins and antioxidants as well as genetic regulation during early stages of differentiation and brain formation to prevent oxidative damage by ROS [133] [101]. Based on our results in this project we can now present a mechanism explaining these requirements (as depicted in Figure **41**).

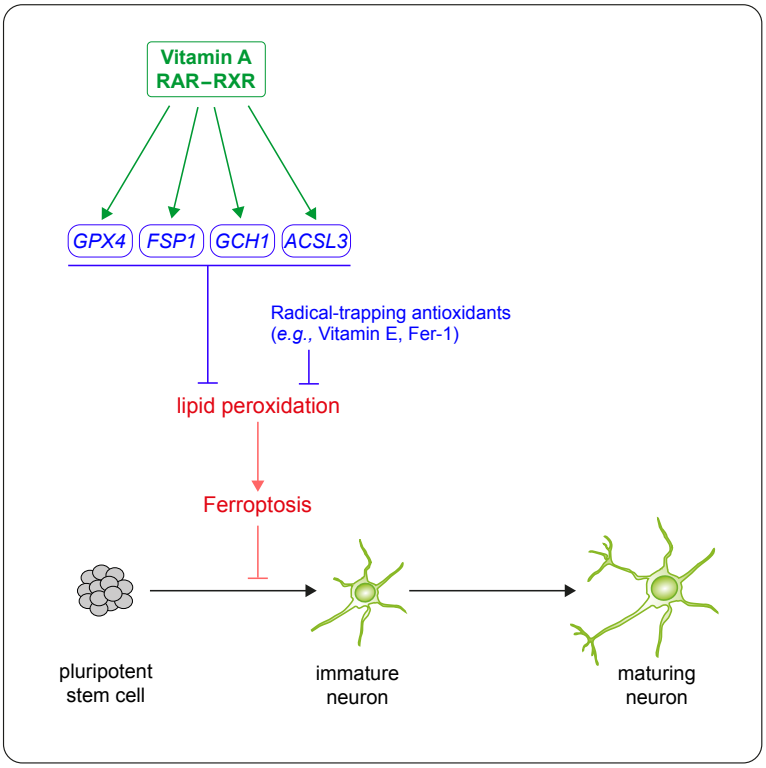

Figure 41: **Mechanism of ferroptosis suppression by vitamin A.** The active metabolite of vitamin A, retinoic acid, binds to the Retinoic Acid Receptor, which dimerizes with the Retinoid X Receptor and binds to specific DNA response elements in the promoter regions of downstream genes. Among other genes, important anti-ferroptotic regulators are transcriptionally activated and thereby protect differentiating neurons from cell death.

In accordance with our findings, a recent study showed that a vitamin E (*i.e.,* antioxidants) deficiency in zebra fish leads to cognitive impairments caused by lipid peroxidation [134], which further hints at the importance of ferroptosis inhibition during early developmental processes.

In summary, we could reveal that the active metabolite of vitamin A suppresses ferroptosis by activating the nuclear receptors RAR and RXR. This leads to downstream transcriptional activation of several anti-ferroptotic genes: FSP1, GPX4, GCH1, ACSL3, PPARα and SCD1. These findings are mostly in line with other studies that were published in parallel to our project and the findings could also be reproduced in an organoid model of differentiating neurons by our project partners. We conclude that this suppression of lipid peroxidation and subsequently ferroptosis inhibition is necessary during early brain development.

6.3.2 The Farnesoid X Receptor is part of an anti-ferroptotic network

The small molecule screening for novel ferroptosis regulators yielded two promising compounds: Turofexorate and Fexaramine. Both compounds are agonists of the Farnesoid X receptor (FXR), and our studies focused on investigating the mechanism by which these to molecules inhibit ferroptosis. We revealed that both FXR agonists dose-dependently inhibited ferroptosis by potently suppressing lipid peroxidation (Figure **32A-F**). This effect was not achieved by radical scavenging or iron chelating activity, but rather by agonistic activation of FXR. This could be demonstrated in several experiments: upon knock-out of FXR, Turo or Fexa treatment could not rescue cells from induced ferroptosis anymore (Figure **30**). Furthermore, HepG2 cells displayed a high level of ferroptosis resistance, but when cotreated with ferroptosis inducer RSL3 and FXR inhibitor Guggulsterone, these cells could be sensitized towards ferroptotic cell death (Figure **31**). Also, the pharmacological inhibition of RXR diminished the rescuing effect of Turo and Fexa, which further undermines our hypothesis of a receptor-mediated mechanism. In cell-free assays (DPPH, C11-BODIPY and iron chelating assay) Turo and Fexa showed no activity, excluding the possibility of antioxidant or iron chelating properties leading to ferroptosis inhibition (Figure **29**). Notably, ferroptosis could also

be suppressed by treating HepG2 with bile acids, the endogenous ligands of FXR. This result shows that not Turo or Fexa treatment alone is responsible for the ferroptosis-suppressing effect, but rather activation of FXR in general is sufficient to rescue cells. This observation suggests that ferroptosis suppression might be an additional physiological role of FXR, since the liver is exposed to high levels of ROS due to its tasks in detoxification and storage of iron and copper [135].

We further observed that after activation of FXR, a dimerization of FXR with RXR is necessary for the anti-ferroptotic effect, which is then carried out by binding to response elements (FXREs) in the promoter regions of ferroptosis-regulating genes: GPX4 as the central anti-ferroptotic defense, FSP1, which generates ubiquinol to suppress lipid peroxidation, PPARα as a master regulator of lipid metabolism and a nuclear receptor itself, and ACSL3 and SCD1 as enzymes of MUFA synthesis. We observed a significant upregulation of these genes upon FXR overexpression or agonistic activation of FXR (either synthetically by Turo or Fexa or endogenous by bile acids), which could also be confirmed on protein level. These target genes were selected based on database searches (Catalogue of Transcriptional Regulatory Interactions (Catrin) and Eukaryotic Promoter Database (EPD)) that predicted FXR binding sites in the promoter regions of anti-ferroptotic genes. For FSP1 and PPARα we could confirm a direct correlation between FXR activation and transcriptional upregulation, since cotreatment with small molecule inhibitors of FSP1 (iFSP1) or PPARα (GW6471) dose-dependently reverted the anti-ferroptotic effect (Figure **34**). An inhibition of GPX4 could not be tested, since small molecule inhibitors (such as RSL3) or a knock-down would directly induce ferroptosis. Importantly, we could show that treatment with a small molecule inhibitor of FXR, Guggulsterone, could revert the upregulated target genes almost back to basal levels (Figure **37**). In future studies, the question of a direct relationship between FXR and GPX4, ACSL3 and SCD1 upregulation could be addressed by performing ChIP experiments or luciferase reporter assays, which could confirm a direct binding of FXR in the promoter regions of these targets.

In recent ferroptosis studies it was established that PPARα as a nuclear receptor can also upregulates the transcription of FSP1 [136] and GPX4 [137], which makes it difficult to discriminate between target gene upregulation caused by FXR activation or PPARα activation. Since PPARα plays a role in lipogenesis, SCD1 expression can also be regulated by PPARα [102]. Based on these results we established a model of an anti-ferroptotic network that is under the control of FXR (Figure **42**) and includes GPX4-dependent and GPX4-independent (FSP1, PPARα, ACSL3 and SCD1) suppression of ferroptosis, which either generate antioxidants or regulate lipid composition and the synthesis of MUFAs, which in turn inhibits lipid peroxidation.

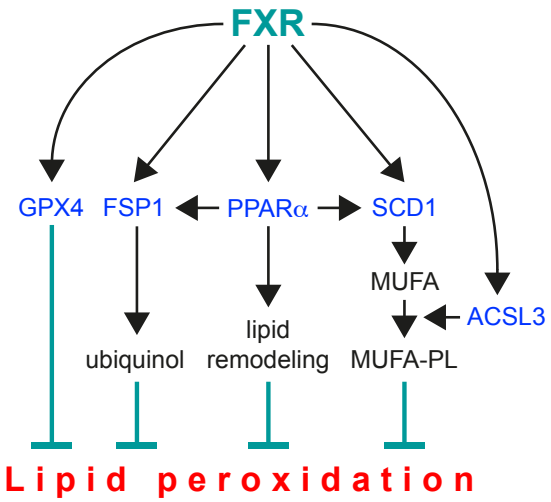

Figure 42: **Mechanism of FXR-mediated ferroptosis inhibition.** Upon activation by endogenous bile acids or synthetic ligands, the Farnesoid X Receptor dimerizes with the Retinoid X Receptor and binds as a nuclear receptor to specific DNA response elements in the promoter regions of downstream target genes. Among these are major ferroptosis-regulating genes, which inhibit lipid peroxidation and lead to suppression of ferroptosis.

As a validation to our study, another paper was independently published about the protective effect of FXR in cisplatin-induced ferroptosis [138]. While the authors could also observe an upregulation of FSP1 upon FXR activation in acute kidney injury, they furthermore described an effect on gamma-glutamyltransferase 6 and glutathione S-transferase 4 expression, which are important enzymes for glutathione homeostasis and critical for liver health and detoxification [139, 140]. This again could be a hint towards a physiological role of FXR in ferroptosis suppression.

Until recently, the nuclear receptor superfamily was not implied to be involved in ferroptosis regulation, PPARα was only mentioned as a co-regulator [136]. In line with the study mentioned previously [138], we report FXR and RXR as the first nuclear receptors that negatively regulate ferroptotic cell death. However, several transcription factors have already been described to modulate the expression of pro- and anti-ferroptotic genes [141] [21]. The transcription factor which is most prominently involved in ferroptosis is nuclear factor erythroid-derived 2-like 2 (NFE2L2, also known as Nrf2), since this is a master regulator of oxidative stress response, iron metabolism and redox homeostasis [142] [143]. Nrf2 has long been considered the main transcription factor in ferroptosis, because it upregulates the expression of a wide range of anti-ferroptotic genes, such as SLC7A11 (system xc^-), GPX4 or FTH1 (subunit of ferritin) [144] [143]. In view of a therapeutical application of ferroptosis regulators, it could be shown that cotreatment with ferroptosis inducers and inhibitors of Nrf2 could induce cell death in hepatocellular carcinoma and head and neck cancer [144, 145]. However, since Nrf2 is highly expressed in many tissues and organs (according to the Broad Institute database depmap portal) and is involved in fundamental processes such as NADPH production, targeting of Nrf2 may lead to many side effects and unwanted risks for patients. Another ferroptosis-involved transcription factor is the established tumor suppressor p53. This factor plays a two-sided role in ferroptosis, since its activation can promote or reduce expression of pro- as well as anti-ferroptotic genes [141] [16]. Therefore, the role of p53 in ferroptotic cell death is context-dependent but presents a promising target for tumor therapy.

Notably, we showed that our proposed model of ferroptosis inhibition by FXR activation does not only apply *in vitro* in HT-1080 and HepG2 cells, but also in a 3D spheroid model, in primary murine hepatocytes and in healthy human hepatocytes differentiated from induced pluripotent stem cells. These results indicate that FXR may be a promising druggable target for degenerative diseases in tissues with high FXR expression, such as kidney, liver or small intestine. First successes in treating kidney and liver diseases with small molecule ferroptosis inhibitors could already be achieved in acute kidney injury [138] and in hepatic ischemia-reperfusion injury in mice [32]. Moreover, a combined treatment with Ferrostatin-1 and

obeticholic acid (an endogenous ligand of FXR) could alleviate non-alcoholic steatohepatitis (NASH) and significantly reduced inflammation in obese mice [146]. Since we not only inhibited ferroptosis by activation of FXR, but also sensitized HepG2 cells towards cell death by inhibiting FXR, this receptor may also be used for targeted ferroptosis induction in hepatic tumors.

7. Conclusion & Outlook

Ferroptosis is a type of regulated cell death that raised a huge research interest during the last decade. Using controlled elimination of aberrant tumor cells or inhibiting excessive cell death in degenerative diseases promises huge progression in otherwise fatal diseases. Since the definitive physiological role of ferroptosis is not yet resolved, we aimed at unraveling novel cellular regulators that inhibit ferroptosis and can be targeted by small molecules. This study resulted in the discovery of two nuclear receptors acting as ferroptosis inhibitors by transcriptionally upregulating anti-ferroptotic genes upon agonistic stimulation.

We found that one of the important roles of vitamin A during neurodifferentiation lies in protecting cells from ROS-caused lipid peroxidation and subsequent ferroptosis, since it increases gene expression of anti-ferroptotic defenses, such as GPX4, FSP1 or GCH1, by activating the Retinoic Acid Receptor. These results were shown in cancer cell-derived spheroids, pluripotent stem cells differentiated into neurons, and forebrain organoids. For future experiments, valuable knowledge could be received by confirming these findings *in vivo*, for example in embryonal mice or zebrafish. It would also be interesting to further investigate the impact of ferroptosis on differentiation processes in other organs and to examine whether and how protection against ferroptosis (*e.g.,* vitamin A, E, or K) is important there. Different nuclear receptors could also be focus of future ferroptosis studies.

Secondly, we established the Farnesoid X receptor as part of an anti-ferroptotic network. Upon activation, either by synthetic ligands or endogenous bile acids, FXR acts as a transcription factor for several ferroptosis-suppressing and lipid-remodeling genes, such as GPX4, FSP1, PPARα, ACSL3 and SCD1. Receptor inhibition or knock out abolished this effect and even sensitized cells to ferroptosis. Since we confirmed the anti-ferroptotic effect in cancer cell-derived spheroids, in *ex vivo* murine hepatocytes, and human hepatocytes differentiated from pluripotent stem cells, the next favorable step would be to test if FXR activation inhibits ferroptosis *in vivo* and if this would be a potential treatment for ferroptosis-related liver diseases (*e.g.,* acute liver failure). Since the liver is an organ with elevated levels of ROS and iron, it can

be speculated whether protection against ferroptosis has an increased importance and if further liver-specific proteins display ani-ferroptotic properties. Furthermore, it has become evident that bile acid metabolism is regulated by gut microbiota and vice versa [147], which sparks interest in the question if ferroptosis can be regulated by diets and specific composition of the gut microbiome. A research approach into this direction is already being discussed among ferroptosis researchers [148].

Thirdly, we found that Seratrodast, an approved drug for asthma treatment in India, Japan and China, potently inhibits ferroptosis due to a quinone head group that scavenges radicals and therefore suppresses lipid peroxidation. We are currently aiming for an *in vivo* testing of Seratrodast in an ischemia reperfusion mouse model, and since the pharmacological profile of Seratrodast is known and seems to be favorable, we expect positive results. For the future we hope to start a drug repurposing strategy, that would allow us to test Seratrodast in a clinical setting and would fast-track the approval of Seratrodast as a drug against ferroptosis-related diseases.

8. Material & Methods

8.1 Material

8.1.1 Instruments and Equipment

Table 1: List of used instruments and equipment.

Instrument/ Equipment	**Supplier**
96-well Round Bottom Ultra Low Attachment Microplates	Corning costar
Adhesive foil for 96-well PCR plates	4titude
Agarose gel chambers	Neolab
Amersham Hyperfilm	GE Healthcare
Attune acoustic flow cytometer	Applied Biosystems
Cell counting chamber Fast-Read 102	Biosigma
Cell Culture Flow Hood Safe 2020	Thermo Fisher Scientific
Cell Culture Plates 96-well, clear, flat bottom	Corning costar
Cell scraper	Sarstedt
Centrifuge 5417 R	eppendorf
CO2 incubator C170i	eppendorf
Cryovials	Greiner
CulturPlates 384-well, white, tissue culture treated	Perkin Elmer
Cyclone 3G working station	Perkin Elmer
Cytomat™ automated incubator	Thermo Fisher Scientific
Developer Optimax Typ TR	MS Laboratory Instruments
Dry incubator	Heraeus Instruments
Electronic Multichannel Pipette 200 µl	BRAND
Envision 2104 plate reader	Perkin Elmer
Eppendorf tubes 1.5 ml, 2 ml	eppendorf
EVOS FL fluorescence microscope	Thermo Fisher Scientific
Falcon tubes 15 ml, 50 ml	FALCON
FrameStar 96 well semi-skirted PCR plates	4titude
Fridge and freezers (4°C, -20°C)	Liebherr
Gel documentation system	Intas
Glass Bottle 250 ml, 500 ml, 1 l	Schott
Ice machine Scotsman AF20	Scotsman ICE Systems
Incubator shaker Innova 40	New Brunswick
Light microscope	Leica
Lightcycler 480	Roche Diagnostics
Magnetic stirrer	IKA Labortechnik
Microwave	SHARP

MultiFlo™ Dispenser	BioTek Instruments
Nanodrop 2000	Thermo Scientific
Needle 26 gauge	B. Braun Sterican
Operetta High Content Analysis System	Perkin Elmer
Petri dishes	Greiner Bio-One
pH meter PB11	Sartorius
PhenoPlate 384-well and 96-well, black, optically clear flat-bottom, tissue-culture treated	PerkinElmer
Pipette tips	Eppendorf
Pipettes 1000 µl, 200 µl, 100 µl, 20 µl, 10 µl, 2.5 µl	Eppendorf
Pipetting aid accu-jet pro	Brand
Plastic pipettes 50 ml, 25 ml, 10 ml, 5 ml, 2 ml	Greiner Bio-One
Power Supply	Consort
Precision scale	KERN
PVDF membrane	Millipore
Refrigerated centrifuge 3K15	Sigma Laborzentrifugen
Rotary Agitator Unitwist 3-D	Uniequip
Rotator	Neolab
Scalpel	B. Braun
Sciclone G3 Liquid Handler	Perkin Elmer
SDS-PAGE gel chamber	Roth
Sealing foil aluminium gold	LVL Technologies
Semi-dry Blotter	Roth
Sonifier U9200S	Hielscher Ultrasonics
StorPlate-384 V	PerkinElmer
Syringes	B. Braun
Thermomixer comfort	eppendorf
Tissue Culture Dish, 100 mm, 150 mm	FALCON
Tissue Culture Flasks, 75 cm2, 175 cm2	FALCON
Tissue Culture Plate, 12-well or 6-well	FALCON
Ultra Low Temperature Freezer (-80°C)	New Brunswick Scientific
Ultra-pure water system MilliQ Plus	Merck Millipore
Vi-Cell cell counting system	Beckman Coulter
Vortexer	Scientific Industries
Whatman Paper	Roth
X-ray films	Amersham

8.1.2 Chemicals

Table 2: List of used chemicals and respective suppliers.

Chemical	**Supplier**
2,2-diphenyl-1-picrylhydrazyl (DPPH)	Sigma-Aldrich
2,2'-Azobis(2-methylpropionamidine) dihydrochloride (AAPH)	Sigma-Aldrich
Accutase solution	Sigma-Aldrich
Acrylamide/ Bisacrylamide	Roth
Ammonium persulfate (APS)	BioRad
Ampicillin	Roth
BODIPY 581/591 C11	Thermo Fisher Scientific
Bovine Serum Albumin (BSA)	Sigma-Aldrich
CellTiter-Glo 2.0 Reagent	Promega
Dexamethasone	Sigma-Aldrich
DMSO	Roth
DNA Agarose	Biozym
DNA Ladder 1kb Plus	New England Biolabs
dNTP Mix 10 mM	Thermo Fisher Scientific
Dulbecco's modified Eagle Medium (DMEM)	Gibco
Dulbecco's modified Eagle Medium (DMEM) high glucose	Gibco
Dulbecco's modified Eagle Medium (DMEM) high glucose/ F12	Gibco
Ethanol absolute	Merck
Ethylendiamine tetraacetic acid (EDTA)	Roth
Fetal bovine serum (FBS)	Gibco
Glutamine	Gibco
Glycerol	Roth
growth factor-reduced Matrigel	Corning
Hoechst 33342	Sigma-Aldrich
Isopropanol	Merck
Kanamycin	Roth
KnockOut Serum Replacement 10%	Gibco
LB agar	Roth
LB medium	Roth
Lipofectamine™ CRISPRMAX™ Cas9 Transfection Reagent	Thermo Fisher Scientific

Lipofectamine™ RNAiMAX™ Transfection Reagent	Thermo Fisher Scientific
Methanol absolute	Merck
Milk powder Blotting grade	Roth
MOPS SDS Running Buffer 1X	Invitrogen
Non-essential amino acids (NEAA)	Life Technologies
Nonidet P40 substitute (NP-40)	Sigma-Aldrich
Normal goat serum 10%	Thermo Fisher Scientific
Opti-MEM reduced serum media	Life Technologies
PageRuler Prestained Protein Marker	Thermo Fisher Scientific
Penicillin-Streptomycin (10.000 U/ml)	Gibco
Phospate-buffered saline -/- (DPBS)	Gibco
Propidium iodide	Invitrogen
Purple Loading Dye 6X	New England Biolabs
Rat-tail collagen	Gibco
RotiLoad 4X SDS loading buffer	Roth
RPMI 1640	Gibco
SOC outgrowth medium	Invitrogen
Sodium chloride (NaCl)	Roth
Sodium dodecyl sulfate (SDS)	Roth
Sodium hydroxide (NaOH)	Roth
SYBR™ Safe DNA Gel Stain	Invitrogen
TAE buffer (50X)	AppliChem
Tetramethylethylendiamine (TEMED)	BioRad
Tris	Roth
Triton-X100	Roth
Trypsin-EDTA 0,5%	Gibco
Tween-20	Roth
Western Lightning ECL Pro	PerkinElmer
X-tremeGENE HP DNA Transfection Reagent	Roche Diagnostics

8.1.3 Buffers and solutions

Table 3: List of used buffers, solutions and respective recipes.

Buffer/Solution	**Composition**
10X SDS Running Buffer	250 mM Tris, 2 M Glycine, 1% SDS
10X Blotting Buffer	48 mM Tris, 39 mM Glycine, 0.037% SDS, 20% Methanol
Blocking Buffer	5% milk powder in TBS-Tween20

TBS-T	50 mM Tris/Cl; 150 mM NaCl; 0,1% Tween20; pH 7.6
TE buffer	10 mM Tris; 1 mM EDTA; pH 8
Separation gel	375 mM Tris/Cl pH 8.8; 12.5% Acrylamide; 0.1% SDS; 0.075% APS; 0.05% TEMED
5X Separation gel buffer	1.88 mM Tris/Cl pH 8.8
Stacking gel	125 mM Tris/Cl pH 6.8; 5% Acrylamide; 0.1% SDS; 0.1% APS; 0.1% TEMED
4X Stacking gel buffer	0.5 M Tris/Cl pH 6.8

8.1.4 Small Molecules

Table 4: List of used compounds.

Small molecules	**Supplier**
(1S,3R)-RSL3	Sigma-Aldrich
2-TEDC	Tocris Bioscience
9-cis Retinoic Acid	Sigma-Aldrich
a-Tocopherol	MedChemExpress
AGN 193109	Sigma-Aldrich
all-trans Retinal	MedChemExpress
all-trans Retinoic Acid	Sigma-Aldrich
all-trans Retinol	Sigma-Aldrich
Anethole-trithione	Selleck Chemicals
AZD1208	Tocris Bioscience
Cetaben	Santa Cruz Biotechnology
Chenodeoxycholic Acid	LKT Labs
Deferoxamine	MedChemExpress
Dipyridamol	Focus Biomolecules
Ferrostatin-1	Sigma-Aldrich
Fexaramine	MedChemExpress
FIN56	Cayman Chemical
FINO2	Cayman Chemical
Guggulsterone E&Z	Selleck Chemicals
GW6471	Selleck Chemicals
H 89 HCl	Selleck Chemicals
HX 531	Biomol
ICI-89406	Santa Cruz Biotechnology
Idebenone	Sigma-Aldrich
iFSP1	MedChemExpress
Imidazole Ketone Erastin (IKE)	Cayman Chemical
L-778123	TargetMol
LCL161	MedChemExpress
Liproxstatin-1	Sigma-Aldrich
LY231617	Tocris Bioscience

ML210	Focus Biomolecules
Moxisylyte	Santa Cruz Biotechnology
Necrostatin-1	BioVision
Obeticholic Acid	BioVision
Oxymetazoline	Santa Cruz Biotechnology
Seratrodast	MedChemExpress
Staurosporine	TargetMol
Tetradecylthioacetic acid	Sigma-Aldrich
TNFa	biomol
Turofexorate Isopropyl (XL335)	TargetMol
WHI-P154	Selleck Chemicals
Z-VAD-FMK	TargetMol
Zileuton	Santa Cruz Biotechnology

8.1.5 Eukaryotic Cell Lines

Table 5: List of cultured cell lines.

Cell line	**Description**	**Origin**
HT-1080	Fibrosarcoma cancer cell line derived from a 35-year old white male, contains an activated N-ras oncogene	ATCC
HepG2	liver carcinoma cell line derived from a 15-year old caucasian male	ATCC
Mouse embryonic fibroblasts (MEF)	immortalized mouse fibroblasts derived from embryos at 14 days gestation	ATCC
Human hepatocytes	Hepatocytes differentiated from induced pluripotent stem cells, differentiation status was determined by qRT-PCR of typical marker genes	Research Group Human Endogenous Retroviruses, Helmholtz Munich
Murine primary hepatocytes	Primary cells isolated from livers of 41-week old male mice of the strain C57BL/6 (WT and hetero), kept on a normal *ad libitum* diet	Research Group Mitochondrial Toxicity, Helmholtz Munich

8.1.6 Antibodies

Table 6: Primary antibodies with their respective suppliers.

Primary Antibody	**Supplier**
4-Hydroxynonenal	ab46545, Abcam
ACSL3	PA5-114815, Thermo Fisher Scientific
beta-Actin (C4)	sc-47778, Santa Cruz Biotechnology
FSP1 (AIFM2/AMID)	PA5-103183, Thermo Fisher Scientific
GPX4	ab125066, Abcam
NR1H4 (FXR)	ab228949, Abcam
PPARa	MA1-822, Thermo Fisher Scientific
SCD1	ab236868, Abcam

Table 7: Secondary antibodies with their respective suppliers.

Secondary Antibody	**Supplier**
anti-rabbit Alexa 488	A32731, Thermo Fisher Scientific
HRP-conjugated donkey anti-mouse IgG	715-035-150, Jackson ImmunoResearch Laboratories, Biozo
HRP-conjugated donkey anti-rabbit IgG	711-035-152, Jackson ImmunoResearch Laboratories, Biozol

8.1.7 Kits and Enzymes

Table 8: List of used assay kits and enzymes.

Enzyme/ Kit	**Supplier**
Caspase-Glo 3/7 Assay Reagent	Promega
dsDNAse	Thermo Fisher Scientific
Ferrous Iron Chelating (FIC) Assay Kit	amsbio
GSH/GSSG Ratio Detection Assay Kit	Abcam

Maxima H Minus First Strand cDNA Synthesis Kit	Thermo Fisher Scientific
Monarch Total RNA Miniprep Kit	New England BioLabs
NucleoSpin Plasmid Kit	Macherey-Nagel
PowerUp SYBR Green Master Mix	Thermo Fisher Scientific
TBARS (TCA Method) Assay Kit	Cayman Chemical
TrueGuide™ synthetic guideRNA system	Thermo Fisher Scientific

8.1.8 Primers for qRT-PCR

Table 9: List of human qRT-PCR primers.

Primer	**Sequence 5' to 3'**	**Source**
NR1H4 (FXR) forward	acttccgtctgggcattctgac	Origene
NR1H4 (FXR) reverse	gctgtaagcagagcatactcctc	
AIFM2 (FSP1) forward	gactccttccaccacaatgtgg	PMID: 33626342
AIFM2 (FSP1) reverse	cagcaccatctggttcttcagg	
PPARalpha forward	ctatcatttgctgtggagatcg	PMID: 35244215
PPARalpha reverse	aagatatcgtccgggtggtt	
ACSL3 forward	cgaagctgctatttcagcaag	PMID: 33854057
ACSL3 reverse	ctgtcaccagaccagtttca	
SCD1 forward	tctagctcctataccaccacca	PMID: 31847887
SCD1 reverse	tcgtctccaacttatctcctcc	
GPX4 forward	gcaaccagtttgggaggcaggag	PMID: 18762024
GPX4 reverse	cctccatgggaccatagcgcttc	
GAPDH forward	atcccatcaccatcttcc	PMID: 24899804

GAPDH reverse	ccatcacgccacagtttc	
CYP7A1 forward	ccattaggtgttgtgccac	PMID: 21817852
CYP7A1 reverse	catccatcgggtcaatgctt	
NR0B2 (SHP) forward	gacttccttggtttggacaca	PMID: 21817852
NR0B2 (SHP) reverse	gctttcattctcatcccaaga	
RP2 forward	gcaccacgtccaatgacat	Origene
RP2 reverse	gtgcggctgcttccataa	
CYP1A1 forward	gattgagcactgtcaggagaagc	Origene
CYP1A1 reverse	atgaggctccaggagatagcag	
ABCC2 forward	gccaacttgtggctgtgatagg	Origene
ABCC2 reverse	atccaggactgctgtgggacat	
ALB forward	gatgagatgcctgctgacttgc	Origene
ALB reverse	cacgacagagtaatcaggatgcc	
HNF4A forward	gatgtagtcctccaagctcac	PMID 27746336
HNF4A reverse	gccatcatcttctttgaccca	
NTCP forward	tgctcttccccacattgatg	PMID 27746336
NTCP reverse	tcctggttctcattccttgc	
RXRA forward	ggaggtgagggaggagtt	PMID 27746336

RXRA reverse	gcatgagttagtcgcagacat	

Table 10: List of murine qRT-PCR primers.

GAPDH forward	tgtgtccgtcgtggatctga	PMID: 22540009
GAPDH reverse	cctgcttcaccaccttcttgat	
NR1H4 (FXR) forward	cttgatgtgctacaaaagctgtg	PMID: 22540009
NR1H4 (FXR) reverse	actctccaagacatcagcatctc	
NR0B2 (SHP) forward	cgatcctcttcaacccagatg	PMID: 22540009
NR0B2 (SHP) reverse	agggctccaagacttcacaca	
AIFM2 (FSP1) forward	ttggtgactgtgccgatac	PMID: 31952989
AIFM2 (FSP1) reverse	gatctgacccacgccatcat	
PPARalpha forward	tcggcgaactattcggctg	PMID: 27367842
PPARalpha reverse	gcacttgtgaaaacggcagt	
ACSL3 forward	tgcacaggcgtgttttatgt	PMID: 21328461
ACSL3 reverse	tggacctcccagagtagcat	
SCD1 forward	ttcttgcgatacactctggtgc	PrimerBank database
SCD1 reverse	cgggattgaatgttcttgtcgt	ID 31543675a1
GPX4 forward	gagatgagctggggccgtctga	PMID: 34360557
GPX4 reverse	acgcagccgttcttatcaatgagaa	

8.1.9 Plasmids

Table 11: Plasmid with supplier and description.

Plasmid	**Cat.No.**	**Description**
NR1H4 GFP-tagged ORF clone	RG232816, Origene	Overexpression of human Farnesoid X Receptor, GFP-tagged

8.1.10 Guide RNAs

For generation of an FXR-KO cell line, 3 TrueGuide Synthetic sgRNAs were ordered from Thermo Fisher Scientific:

Table 12: Guide RNAs to create a stable CRISPR KO of FXR.

guideRNA	Target sequence	Assay ID
FXR-1	TGTAACAAAGAAGCCCCGCA	CRISPR667888_SGM
FXR-2	GCGAGTATGGTTCCACTTCC	CRISPR667899_SGM
FXR-3	GTTGGAATAATAGGATGACG	CRISPR667889_SGM

8.1.11 siRNAs

For the knock down of different target genes, MISSION endoribonuclease prepared siRNA was ordered from Sigma-Aldrich:

Table 13: Small interfering RNAs for the knock down of different target genes.

siRNA	Cat.No.
NR1H4 (FXR)	EHU133161
eGFP (control)	EHUEGFP

8.1.12 Software

Table 14: Software used for data analysis and visualization.

Software	Company
Adobe Acrobat DC Version 23.001.20177	Adobe Systems Inc.
Adobe Illustrator Version 26.3.1	Adobe Systems Inc.
FlowJo v10.8.1 Software	BD Life Sciences
ImageJ 1.53k	National Institutes of Health
Prism 9.5.1	GraphPad Software
SnapGene Viewer 6.2.1	GSL Biotech LLC
Microsoft Office	Microsoft Corporation
LightCycler 480 Software	Roche Diagnostics
NanoDrop 2000 Software	Thermo Scientific
Columbus	PerkinElmer

8.2 Methods

8.2.1 Cultivation of mammalian cell lines

All adherent cell lines were cultivated in Dulbeccos Modified Eagle Medium (DMEM) containing 10% Fetal Bovine Serum (FBS), 1% Penicillin/Streptomycin and 1% Non-essential amino acids (NEAA). Every 2 to 3 days or when a confluency of approximately 90% was reached, cells were passaged by detaching with Trypsin-EDTA. Cell cultures were mostly grown in T75 or T175 flasks and incubated at 37 °C and 5% CO_2.

Suspension cell lines were cultivated in RPMI 1640 medium supplemented with 10% FBS and 1% Penicillin/Streptomycin in T75 flasks. Every 2 to 3 days, 15 ml cell suspension was discarded and exchanged with fresh medium to maintain optimal cell density. Viability was examined once a week with a Vi-Cell cell counting system.

Primary mouse hepatocytes were isolated by Dr. Banu Akdogan and Tamara Rieder (Research Group Mitochondrial Toxicology, Helmholtz Munich). Before seeding, flasks and plates were coated with 0,01% rat-tail collagen (Gibco). Hepatocytes were cultivated in DMEM high glucose.

Human hepatocytes were differentiated from induced pluripotent stem cells (iPSCs) by Van Lam (Research Group Human Endogenous Retroviruses, Helmholtz Munich) according to a protocol published previously [149]. Hepatocytes were cultivated in growth factor-reduced Matrigel-coated plates and high-glucose DMEM/F12 (gibco) supplemented with 10% KnockOut serum replacement (KOSR), 1% glutamine, 1% non-essential amino acids, 1% Penicillin/Streptomycin and 10^{-7} M Dexamethasone. Medium was changed every day.

For long-term storage, cells were pelleted at 300 x g, 4°C for 5 min, resuspended in Freezing Medium (DMEM or RPMI + 20% FBS + 10% DMSO), transferred into cryovials and frozen at -80 °C. After 24 hours, cryovials were stored in liquid nitrogen.

8.2.2 Compound library screening

To screen for potential ferroptosis-inhibitory compounds, HT-1080 cells were trypsinized and seeded into 384-well plates (CulturPlates, Perkin Elmer) with a density of 750 cells per well by using a MultiFlow Dispenser (BioTek Instruments). After incubation over night, the compound library was transferred in duplicates onto the cell culture plates by a Sciclone G3 Liquid Handler (Perkin Elmer). Ferroptosis was induced with class I ferroptosis inducer IKE. Every plate also contained control wells with cells cotreated with Ferrostatin-1 as a positive control. After an incubation time of 18 hours, a viability assay was performed. Compounds were considered as hits if the viability was higher than the median viability of every compound-treated well of a plate plus 3 times the standard deviation of the viability of these wells.

As a method to evaluate screening quality and reliability, we calculated the Z-prime factor, which is a commonly used measure in high throughput screening [150]:

$$Z = 1 - \frac{3(\sigma_p + \sigma_n)}{|\mu_p - \mu_n|}$$

A value between 0.5 and 1 is considered excellent, proving that controls and screening conditions were chosen adequately and that the obtained hits can be considered reliable [150].

After excluding unwanted compounds, such as frequent hitters, toxic molecules or compounds with no known targets or mode of action, final hits are reordered and validated in follow-up experiments.

8.2.3 Viability Assay

8.2.3.1 Ferroptosis

Cells were seeded into 384-well plates with a density of 750 to 1000 cells per well (according to their growth rate). After approximately 24 hours of incubation, ferroptosis was induced by small molecules and treatment with compounds of interest was performed. Ferrostatin-1 was used as a control treatment for ferroptosis inhibition. 18 hours post-treatment viability was measured by adding 20 µl Celltiter-Glo (Promega) directly into each well. Luminescence was read out with an Envision 2104 plate reader (Perkin Elmer) and normalized to DMSO-treated control wells.

8.2.3.2 Apoptosis

Cells were seeded in the same manner as for the ferroptosis viability assay and incubated for 24 hours. Staurosporine treatment for apoptosis induction was performed before adding compounds of interest. As a positive control for apoptosis inhibition the pan caspase inhibitor zVAD-FMK was used. 18 hours later Caspase-Glo 3/7 Assay Reagent (Promega) was added to the cells and luminescence was read out after one hour incubation time at room temperature with an Envision 2104 plate reader (Perkin Elmer). According to the manufacturer measured luminescence is directly proportional to Caspase 3/7 activity.

8.2.3.3 Necroptosis

Since HT-1080 cells are not sensitive to necroptosis inducers, MEF cells were used instead. They were seeded with 750 cells per well in a 384-well plate and incubated for 24 hours. To induce necroptotic cell death, cells were treated with Tumor Necrosis Factor α (TNFα), zVAD-FMK and SMAC mimetic LCL161. After compounds of interest or Necrostatin-1 as a positive control for necroptosis inhibition were added, cells were incubated for 18 hours. 20 µl Celltiter-Glo (Promega) were added and luminescence was read out with an Envision 2104 plate reader. Luminescence signal was normalized to DMSO-treated control wells.

8.2.4 SDS-PAGE and Western Blotting

For sample preparation, cells were lysed with 2X SDS buffer (RotiLoad), collected with a cell scraper and sonified with a Sonifier U9200S (Hielscher Ultrasonics). Proteins were denatured by heating samples in a Thermoblock at 95 °C for 5 minutes and frozen at -20 °C for long-term storage.

Together with the PageRuler Plus Prestained Protein Ladder (Thermo Scientific), 5-10 µl of cell lysate was run either on a self-cast 12,5% SDS-Polyacrylamide gel (Table **3**) or a pre-cast NuPAGE 4-12% Bis-Tris gel (Invitrogen). Self-cast gels were run in 1X SDS Running Buffer (Table **3**) at 140 V for 1 hour and 40 minutes, whereas pre-cast gels were run in 1X MOPS SDS Running Buffer (Invitrogen) at 190 V for 45 minutes.

Proteins were blotted onto a PVDF membrane by using a semi-dry blotting system (Roth). Three layers of Whatman paper (Roth), soaked in 1X Blotting Buffer (Table **3**), were positioned on the blotting machine, before the acrylamide gel was placed on them and also wetted with Blotting Buffer. The PVDF membrane was activated with 100% methanol for 5 seconds before it was soaked in Blotting Buffer and placed on top of the gel. Finally, the blotting sandwich was closed by an additional layer of 3 Whatman papers soaked in Running Buffer. Protein transfer was achieved by running 15 V and 300 mA for 55 minutes (1 gel) or 160 mA for 1 hour and 20 minutes (2 gels).

To block unspecific binding sites, membrane was incubated in 5% milk in TBS-Tween20 for at least 30 minutes at room temperature on a shaker. Afterwards, incubation with primary antibody (diluted in 2,5% milk in TBS-Tween) was either done overnight at 4 °C or for 2 hours at room temperature on a shaker. Membrane was washed three times for 5 minutes in TBS-Tween, incubated with secondary antibody (diluted 1:7500 in 1,25% milk in TBS-Tween) for 1 hour at room temperature on a shaker and washed another three times for 5 minutes in TBS-Tween.

Since the secondary antibodies are coupled with Horseradish-Peroxidase, membrane was incubated with Western Lightning ECL Pro (Perkin Elmer) and exposed to an X-ray film

(Amersham) in the dark. Films were fixated and developed with a Developer Optimax Typ TR (MS Laboratory Instruments). Blots were analyzed and quantified with ImageJ 1.53k (National Institutes of Health).

8.2.5 RNA extraction

Cells were detached with Trypsin-EDTA, pelleted at 300 x g and 4 °C for 5 minutes and washed with PBS for two times. For optimal lysis, supernatant was removed and pellets were frozen at -80 °C for at least one night. Total RNA was isolated from cell pellets by using the Monarch Total RNA Miniprep Kit (New England BioLabs): cells were resuspended in 300 µl Lysis Buffer and transferred into DNA-binding columns. After centrifugation at 16.000 x g for 30 seconds, columns were discarded and 300 µl of 100% ethanol were added to flowthrough and mixed properly. Mixture was added into RNA-binding columns, centrifuged and flowthrough was discarded. Columns were washed once with 500 µl Priming Buffer, then twice with 500 µl Wash Buffer. After the second wash, columns were centrifuged for 2 minutes at 16.000 x g. RNA was finally eluted with 60 µl nuclease-free water and quantified with a NanoDrop 2000 (Thermo Scientific). Samples were stored at -80 °C to prevent RNA degradation.

8.2.6 cDNA synthesis and qRT-PCR

If possible, 1 µg of RNA was reverse transcribed into complementary DNA by using the Maxima H Minus First Strand cDNA Synthesis Kit (Thermo Fisher Scientific). Residual genomic DNA was digested by DNAse for 2 minutes at 37°C before the provided random hexamer primer, oligo$(dT)_{18}$ primer and dNTPs were added. Mixture was heated to 65°C for 5 minutes to remove possible secondary structures in the RNA. After addition of Reverse Transcriptase and buffer, mixture was incubated for 10 minutes at 25 °C, 30 minutes at 65 °C and 5 minutes at 85 °C. Samples were diluted 1:10 in nuclease-free water and stored at -20 °C.

Quantitative RT-PCR was performed using the PowerUp SYBR Green Master Mix (Thermo Fisher Scientific) in 96-well semi-skirted PCR plates (FrameStar Roche style, 4titude). Each

well contained 5 µl enzyme mix, 1 µl forward primer, 1 µl reverse primer (5 µM each), 2 µl nuclease-free water and 1 µl diluted cDNA. Plate was sealed with adhesive foil (4titude) and measured in a Lightcycler 480 (Roche) with the following program:

Table 15: Lightcycler 480 program for qRT-PCR.

Activation	50 °C	2 min	
Initial Denaturation	95 °C	2 min	
Denaturation Annealing Elongation	95 °C 60 °C 72 °C	15 s 15 s 1 min	40 cycles
Melting curve	65 – 95 °C	15 s	

Levels of mRNA were quantified by applying the delta delta Cp method.

8.2.7 Lipid Peroxidation Assays

8.2.7.1 BODIPY staining microscopy

To image lipid peroxidation after ferroptosis induction, HT-1080 cells were seeded into 6-well plates (400.000 cells per well) or 384-well plates (750 cells per well). After incubation of approximately 24 hours, 1 µM BODIPY 581/591 C11 was added directly into the culture medium, mixed thoroughly and incubated for 30 minutes. Cells were then treated with RSL3 and compounds of interest for at least 2 hours, before culture medium was replaced by PBS.

6-well plates were imaged with an EVOS FL fluorescence microscope (Thermo Fisher Scientific). 384-well plates were imaged with an Operetta high-content system. Image analysis was done with Columbus software (PerkinElmer).

8.2.7.2 BODIPY staining FACS

Cells were seeded into 6-well or 12-well plates with a density of 200.000 cells or 100.000 cells per well. After approximately 24 hours of growth, cells were treated with ferroptosis inducers and compounds of interest for several hours (RSL3 treatment lasted 2-3 hours, IKE treatment 6-7 hours). The time point of staining with BODIPY 581/591 C11 (Thermo Fisher) was chosen depending on the cell morphology observed under the microscope, since it was critical to harvest cells that were ferroptotic but not yet dead. For staining of Reactive Oxygen Species (ROS) and lipid peroxidation, 2 µM BODIPY C11 per well were added directly into the cell culture medium, mixed thoroughly and incubated for 30 minutes, before cells were harvested using Trypsin-EDTA. Samples were pelleted at 500 x g, 4 °C for 5 minutes and washed twice with PBS.

For flow cytometry, cell pellets were resuspended in 300 µl PBS. 15.000 events were measured in the BL-1 channel of an Attune acoustic flow cytometer (Applied Biosystems). FlowJo v10.8.1 Software (BD Life Sciences) was used to analyze and visualize measured data.

8.2.7.3 4-HNE staining and FACS

Cells were seeded and treated in the same manner as for the BODIPY C11 FACS staining. At the exact time point where the cellular morphology looked ferroptotic but not yet dead or detached, cells were harvested using Trypsin-EDTA. Cells were pelleted at 500 x g, 4 °C for 5 minutes and resuspended in 10% normal goat serum (Thermo Fisher Scientific) to block unspecific antibody binding sites. After 30 minutes incubation on ice, cells were centrifuged, supernatant was discarded and pellet resuspended in 100 µl anti-4-Hydroxynonenal antibody (1:50 dilution in 1% BSA in PBS). Cells were incubated for 1 hour on ice before they were washed 3 times by centrifuging at 500 x g, 4 °C for 5 minutes and resuspending in 500 µl PBS. Next, cells were incubated in 100 µl secondary antibody (anti-rabbit Alexa-488, 1:200 dilution in 1% BSA in PBS) for 30 minutes on ice, before they were washed again for 3 times in PBS. After the last wash step, cells were resuspended in 300 µl PBS and 15.000 events per samples

were measured in the BL-1 channel of an Attune acoustic flow cytometer (Applied Biosystems). FlowJo v10.8.1 Software (BD Life Sciences) was used to analyze and visualize measured data.

8.2.7.4 TBARS Assay

The TBARS Assay for measuring Malondialdehyde (MDA) as a byproduct of lipid peroxidation in cells was performed by using the TBARS (TCA Method) Assay Kit (Cayman Chemical).

Since a high number of cells was necessary for reliable results, 2 million HT-1080 cells were seeded into 15 mm dishes and incubated for 48 hours. After ferroptosis induction with RSL3 and treatment with compounds of interest, cellular morphology was observed every 30 minutes under a microscope. When cells appeared to be rounded but not detached, samples were harvested using Trypsin-EDTA and counted. Cell numbers of each sample were adjusted to minimize effects on the assay outcome.

For homogenization, cells were resuspended in PBS and passed through a 26 gauge needle for multiple times. Subsequently, 100 µl of 10% TCA Assay Reagent and 800 µl Color Reagent were added and mixed thoroughly by vortexing. Samples were boiled at 100 °C in a Thermoblock for 1 hour and afterwards cooled in an ice bath for 10 minutes. To collect cellular debris, samples were centrifuged at 1600 x g and 4 °C for 10 minutes. 200 µl of each supernatant were carefully transferred into a black 96-well plate and measured in duplicates at 530 nm excitation and 550 nm emission in an Envision plate reader.

MDA concentrations were calculated with the help of an MDA standard curve that was assayed in parallel to the samples.

8.2.7.5 Lipidomics

To prepare samples for lipidomic analysis, 2 million HT-1080 were seeded into a 100 mm dish and incubated for 24 hours. Cells were treated with RSL3 to induce ferroptosis and co-treated

with Turofexorate or Ferrostatin-1 as a positive control. After 2 hours, cells were harvested using Accutase and pelleted at 500 x g and 4 °C for 5 minutes. Pellets were washed twice with PBS, frozen in liquid nitrogen and stored at -80 °C.

Lipid extraction and global lipidomic profiling were performed by Dr. Constanze Müller at the Research Unit Analytical Biogeochemistry at Helmholtz Munich, according to the protocol described previously [151].

8.2.8 Spheroid experiments

HT-1080 cells were found to be a compatible cell line for the formation of spheroids, since they tolerated high cell densities over several days. 2000 cells per well were seeded into 96-well Round Bottom Ultra Low Attachment Microplates (Corning costar). 48 hours after seeding, spheroid treatment with RSL3 and compounds of interest was performed. After additional 48 hours, Hoechst 33342 was added to the medium in a 1:10.000 dilution and incubated for 1 hour. Spheroids were imaged with an Operetta high-content system. Images were analyzed with Columbus software (Perkin Elmer) by detecting spheroids as “image regions” and calculating properties such as roundness, ratio of width to height or fluorescence intensity.

8.2.9 Cell-free Assays

8.2.9.1 Cell-free BODIPY C11 Assay

The fluorescent dye BODIPY 581/591 C11 was used in a cell-free assay to determine the ROS-scavenging abilities of compounds of interest. The experiment was performed according to a protocol published previously [44].

In short: compounds of interest and Ferrostatin-1 as a gold standard antioxidant were diluted in PBS to a final concentration of 25 µM. As a negative control, DMSO was diluted in PBS as well. Diluted compounds were added to 1,875 µM BODIPY C11 (in PBS) and 7,5 mM 2,2’-Azobis(2-methylpropionamidine) dihydrochloride (AAPH, in PBS, Sigma). The AAPH served as a free radical initiator; a non-oxidized control sample containing only PBS instead of AAPH

was also included. The mixtures were incubated for 30 minutes in the dark at room temperature, before triplicates were transferred into black 96-well plates and fluorescence was detected at 495 nm excitation wavelength and 520 nm emission wavelength in an EnVision 2104 multilabel plate reader (PerkinElmer).

8.2.9.2 DPPH Assay

The antioxidative capacity of different compounds was measured in a cell-free DPPH Assay as described previously [9].

In short: 10 mM of compounds of interest were diluted in 1 ml of o (DPPH, 0,05 mM in methanol, Sigma-Aldrich) to a final concentration of 50 µM. Samples were rotated at room temperature for 10 minutes. Quadruplicates were transferred into a clear 96-well plate and absorbance at 517 nm was measured in an EnVision 2104 Multilabel plate reader (PerkinElmer). Ferrostatin-1 as a strong antioxidant was used as a positive control.

8.2.9.3 Iron Chelator Assay

To determine if compounds can chelate iron and therefore inhibit ferroptosis, the Ferrous Iron Chelating (FIC) Assay Kit (amsbio) was used. This assay is based on the principle that Ferrozine is able to form a highly colored complex together with iron(II) ions. These iron ions are provided by a $FeSO_4$ solution. If an iron chelator is present, the colored complex cannot be formed and therefore less absorbance is measured.

Compounds of interest were diluted in $FeSO_4$ to the same concentrations that were used in cell treatments. DMSO was used as a negative control, EDTA was added as a positive control. Ferrozine was added to start the reaction before samples were incubated at room temperature for 10 minutes. Triplicates were transferred into a clear 96-well plate and absorbance was detected at 562 nm with an EnVision 2104 Multilabel plate reader (PerkinElmer).

8.2.10 Transfection of mammalian cell lines

8.2.10.1 Transient gene knock-down by siRNA

For single gene knock-down experiments, MISSION® predesigned enzymatically prepared siRNA (esiRNA, Eupheria Biotech) were transfected using the Lipofectamine method. Upon arrival, lyophilized esiRNA was resuspended in TE buffer to a concentration of 200 ng/µl and stored in aliquots at -20 °C.

One day before transfection, HT-1080 cells were seeded into 12-well plates with a density of 100.000 cells per well. For each well that should be transfected, the following tubes were prepared:

Tube 1: 50 µl OptiMEM + 3 µl Lipofectamine RNAiMAX transfection reagent (Thermo Fisher Scientific)

Tube 2: 50 µl OptiMEM + esiRNA (concentrations ranging from 40 to 60 nM)

Both tubes were mixed and incubated for 10 minutes at room temperature. In the meantime, cell culture medium was exchanged to 900 µl medium per well. 100 µl of transfection mixture per well were added slowly dropwise to cells, mixed by gentle shaking and incubated for another 10 minutes at room temperature. After 6 hours at 37 °C in the incubator, culture medium was discarded, cells were washed with PBS once and fresh medium was added to avoid cell stress.

48 hours after transfection cells were harvested using Trypsin-EDTA, counted either with a cell viability analyzer ViCell-XR (Beckman Coulter) or with a cell counting chamber and re-seeded into 384-well with a density of 750 cells per well. In parallel, samples for qRT-PCR or Western Blot were taken to verify knock down efficiency. Circa 6 hours after re-seeding, cells were treated for ferroptosis assays and viability was measured after 18 hours using Celltiter-Glo.

8.2.10.2 Transfection of plasmids

For transfection of plasmids into mammalian cell lines, X-tremeGENE HP DNA Transfection Reagent was used. 24 hours before transfection, cells were seeded into 6-well plates with a density of 200.000 cells per well. On the day of transfection, plasmid was diluted in OptiMEM to a concentration of 0,01 µg/µl. Different amounts of Transfection Reagent (1:1 ratio to 4:1 ratio) were added directly into the plasmid dilution and incubated for at least 15 minutes at room temperature. For HT-1080 in 6-well format, 2 µg plasmid in 200 µl OptiMEM together with 4-6 µl Transfection Reagent proved to be a successful ratio. Transfection mixture was pipetted carefully dropwise into each well, before cells were incubated for 48 hours. Transfection success was verified by monitoring GFP fluorescence under an EVOS FL fluorescence microscope (Thermo Fisher Scientific) or by harvesting cells and performing qRT-PCR.

8.2.10.3 Stable gene knock-out via CRISPR-Cas9

To create stable cell lines with a single knock out, the TrueGuide synthetic guideRNA system (Thermo Fisher Scientific) was used. Upon arrival, guideRNAs were resuspended in 15 µl TE buffer to a final concentration of 100 µM, vortexed and incubated at room temperature for 30 minutes, then stored at -20 °C.

One day before transfection, cells were seeded into 6-well plates. Different cell lines preferred different densities and needed to grow nearly confluent to survive transfection. Because of this, HT-1080 cells were seeded with 400.000 cells per well and HepG2 cells were seeded with 250.000 cells per well.

The following tubes were prepared for the transfection (amounts per well):

Tube 1: 125 µl OptiMEM + 6250 ng TrueCut Cas9 Protein v2 + 1200 ng guideRNA + 12,5 µl Lipofectamine Cas9 Plus Reagent

Tube 2: 125 µl OptiMEM + 7,5 µl Lipofectamine CRISPRMAX Reagent

Tube 2 was incubated for 1 minute at room temperature before both tubes were mixed by pipetting up and down. Mixture was incubated for 15 minutes at room temperature, then 250 µl per well were added carefully dropwise to each well.

After 48 hours of incubation, cells were harvested and re-seeded into several 96-well plates with a density of 5 cells per well to generate single cell clones. After 2-3 weeks of growth, clones originating from one single cell were picked, harvested with Trypsin-EDTA and reseeded into T-75 flasks. When the clone was expanded to a cell number high enough to take samples, gene knock out was verified by Western Blot and qRT-PCR.

8.2.11 Plasmid preparation

8.2.11.1 Transformation of *E. coli*

To amplify plasmid DNA quickly, the competent *E. coli* strain TOP10 was used for transformation. 50 µl aliquots of bacteria were thawed on ice before 1-100 ng plasmid DNA was added carefully. After 30 minutes of incubation on ice, bacterial cells were heat shocked at 42 °C in a Thermoblock for 45 seconds and afterwards immediately put on ice for 10 minutes. 250 µl of prewarmed sterile SOC medium was added to the cells, which were then incubated for 1 hour at 37 °C, shaking at 250 rpm. If the plasmid contained an Ampicillin resistance, cells were only incubated for 20 minutes. Different amounts of cell suspension (e.g., 20 µl and 200 µl) were spread on prewarmed LB agar plates containing the proper antibiotic. After an overnight incubation at 37 °C, colonies were picked and inoculated into 2 ml of LB medium. Liquid cultures were incubated for 12 to 18 hours at 37 °C and 200 rpm.

For long-term storage of transformed *E. coli*, a glycerol stock was created by adding 500 µl of overnight liquid bacterial culture to 500 µl 50 % glycerol (in destH_2O) in a cryovial. Bacteria were frozen at -80 °C.

8.2.11.2 Isolation of plasmid DNA

The NucleoSpin Plasmid Kit (Macherey-Nagel) was used to isolate plasmid DNA from *E. coli* LB cultures. Cell suspension was transferred into Eppendorf tubes and centrifuged at 11.000 x g for 30 seconds. Supernatant was discarded and cell pellet lysed by resuspending in 250 µl Lysis Buffer. 250 µl of SDS-containing Buffer A2 were added, mixed by inverting several times and incubated for 5 minutes at room temperature. 300 µl of neutralizing Buffer A3 were added and samples were inverted until the blue color disappeared. The lysate was cleared by centrifuging for 10 minutes at 11.000 x g and subsequently loaded onto a DNA-binding column. After centrifuging at 11.000 x g for 1 minute, flowthrough was discarded and silica membrane was washed with 600 µl ethanol-containing Buffer A4. Membrane was dried by centrifuging at 11.000 x g for 2 minutes. To elute the bound plasmid DNA, 50 µl nuclease-free water were added to the silica membrane, incubated for at least 1 minute at room temperature and centrifuged at 11.000 x g for 1 minute.

Plasmid concentration was determined with a NanoDrop 2000 before samples were frozen at -20 °C.

9. List of Figures

10. List of Tables

11. Supplement

Table S1: Compound concentrations that were used in hit validation experiments.

Screening Hit	**Concentration [µM]**
Ferrostatin-1	0,8
2-TEDC	12
Dipyridamol	6
LY231617	6
Cetaben	6
Anethole-trithione (ATT)	3
Oxymetazoline	12
Moxisylyte	6
Fexaramine	12
Turofexorate	12
L-778123	50
WHI-P154	25
H 89	50
ICI-89406	50
AZD1208	50
Tetradecylthioacetic acid (TTA)	50

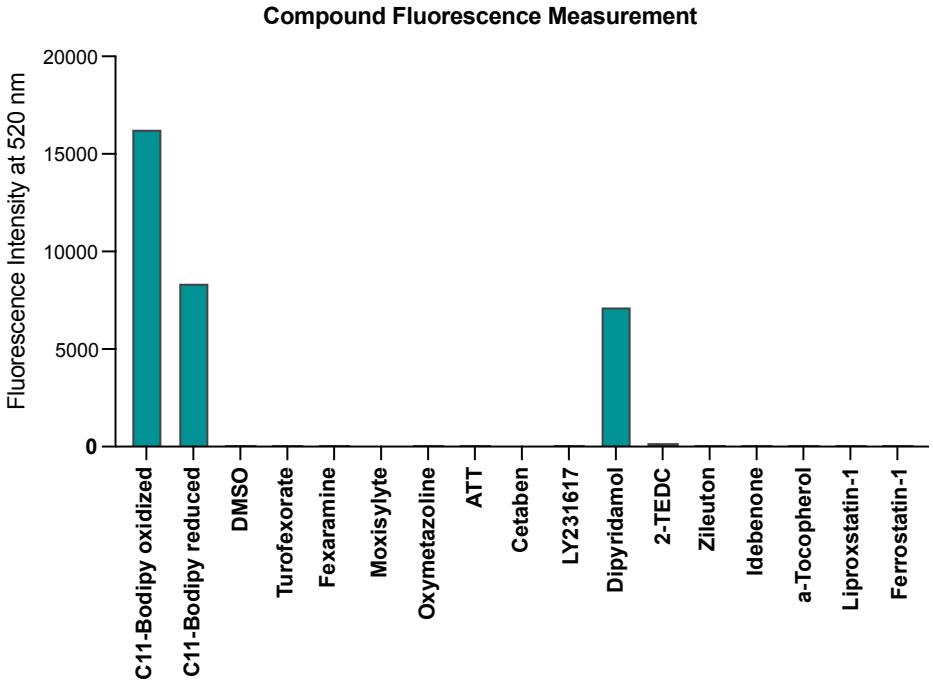

Figure S1: **Fluorescence intensity at 520 nm was measured for each screening compound in a cell-free setting**.

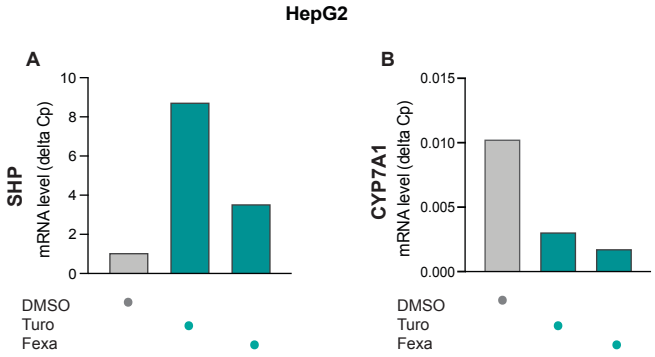

Figure S2: **Expression levels of SHP and CYP7A1 after FXR activation by 12 µM Turo or Fexa.**

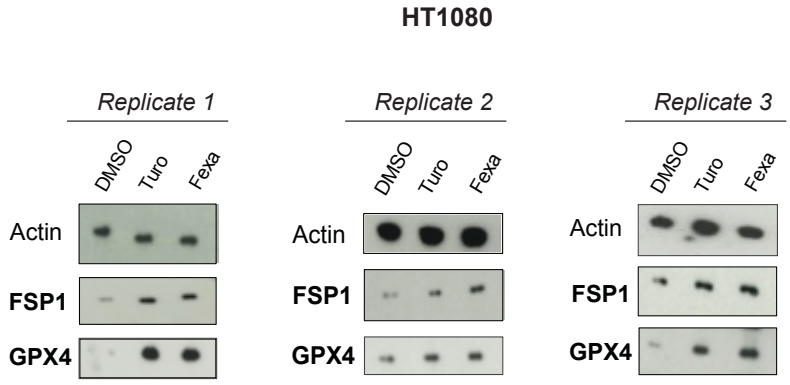

Figure S3: **Biological Western Blot replicates of HepG2 treated with 12 µM Turo or Fexa for 2 hours.**

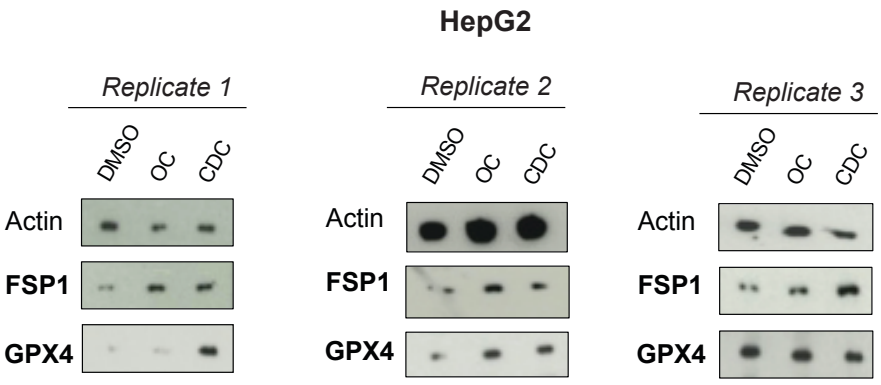

Figure S4: **Biological Western Blot replicates of HepG2 treated with 2 µM obeticholic acid or 20 µM chenodeoxycholic acid for 2 hours.**

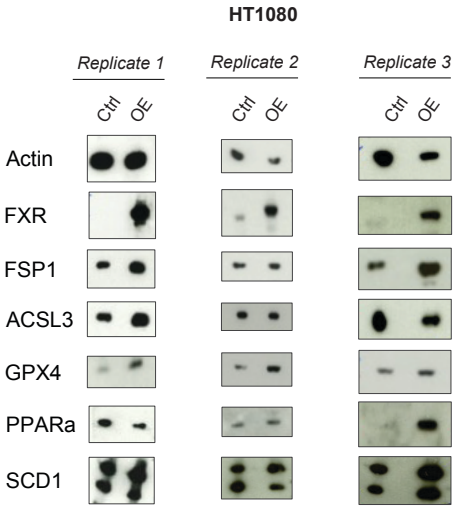

Figure S5: **Biological Western Blot replicates of HT1080 cells overexpressing FXR.**

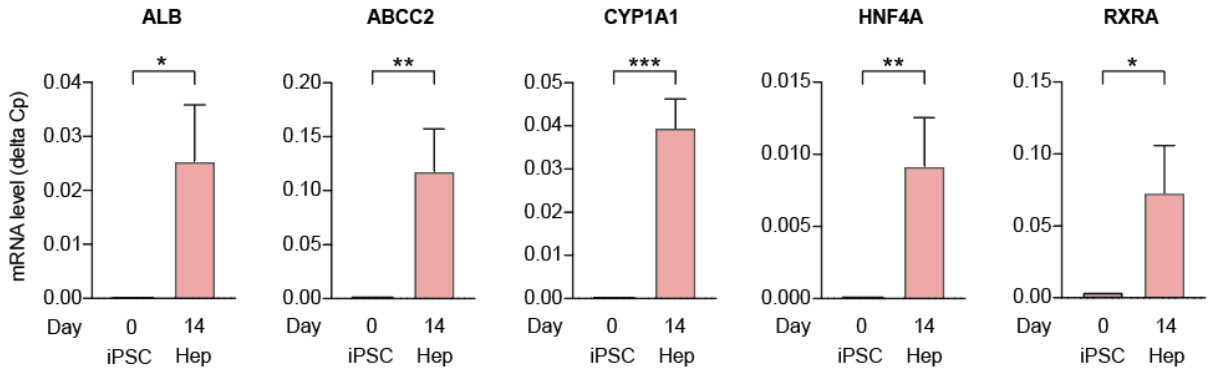

Figure S6: **Expression levels of hepatocyte marker genes after 14 days of differentiation from iPSCs.**

12. Appendix

12.1 Publications

Manuscript **accepted** in July 2023; currently in press:

Tschuck, J., Theilacker, L., Rothenaigner, I., Weiß, S. A. I., Akdogan, B., Lam, V. T., Müller, C., Graf, R., Brandner, S., Pütz, C., Rieder, T., Schmitt-Kopplin, Vincendeau, M., P., Zischka, H., Schorpp, K., and Hadian, K. *Farnesoid X Receptor activation by bile acids suppresses lipid peroxidation and ferroptosis.* Nature Communications, 2023.

Manuscript under revision, pre-print available on bioRxiv:

Tschuck, J.[1] and Padmanabhan Nair, V.[1], Galhoz, A., Ciceri, G., Rothenaigner, I., Tchieu, J., Tai, H-M., Stockwell, B. R., Studer, L., Menden, M. P., and Vincendeau M. and Hadian, K. *Suppression of ferroptosis by vitamin A or antioxidants is essential for neuronal development.* bioRxiv, 2023. ([1] co-first authors)

Manuscript in preparation:

Tschuck, J.[1] and Tonnus, W.[1], Rothenaigner I., Linkermann A., and Hadian, K. *Seratrodast inhibits ferroptosis by suppressing lipid peroxidation.* ([1] co-first authors)

Patent:

Priority Application, *Ferroptosis Inhibitors*, Kamyar Hadian and **Juliane Tschuck**, 2023.

12.2 Acknowledgements

First of all, I would like to thank Prof. Henriette Uhlenhaut for being my doctoral advisor and for reviewing my thesis. Also, many thanks to the members of my thesis advisory committee and examination committee for their time, critical reading of my thesis and useful feedback: PD Dr. Tobias Fromme and Prof. Dr. J. Philipp Benz.

My biggest thanks goes to my direct supervisor Dr. Kamyar Hadian, for providing me with this interesting and fruitful topic and for his intense support in all my projects. Thank you for having trust in me and my abilities and for always confronting me with new challenges that let me grow immensely. You showed me that it is important to dream big, no matter what your competition seems to be.

I am also very grateful for all my colleagues that worked with me during these years at TOXI/SAT: special thanks to Kenji for providing me with never ending wisdom and chocolates or beer at just the right moments. Thank you, Steffi B., Ina and Steffi W., for so many entertaining lunch breaks, shared sweets and shared problems. I would also like to thank the students that I supervised: Lea, Roman and Hui, your work was much appreciated and helped me and my projects a lot.

I also want to thank our collaboration partners, especially Dr. Michelle Vincendeau, Van Thanh Lam, Prof. Hans Zischka and Dr. Banu Akdogan, for their generous help, experience and pleasant cooperation.

And finally: thank you so much, Tom, for all your Klimmzüge, sweets, help with FACS and blot development, memes and everything else.

13. References

1. Stockwell, B.R., *Ferroptosis turns 10: Emerging mechanisms, physiological functions, and therapeutic applications.* Cell, 2022. **185**(14): p. 2401-2421.
2. Murao, A., et al., *Release mechanisms of major DAMPs.* Apoptosis, 2021. **26**(3-4): p. 152-162.
3. Gulbins, E., et al., *Physiology of apoptosis.* Am J Physiol Renal Physiol, 2000. **279**(4): p. F605-15.
4. Hadian, K. and B.R. Stockwell, *The therapeutic potential of targeting regulated non-apoptotic cell death.* Nat Rev Drug Discov, 2023.
5. Yu, T., J.L. Robotham, and Y. Yoon, *Increased production of reactive oxygen species in hyperglycemic conditions requires dynamic change of mitochondrial morphology.* Proc Natl Acad Sci U S A, 2006. **103**(8): p. 2653-8.
6. Cookson, B.T. and M.A. Brennan, *Pro-inflammatory programmed cell death.* Trends Microbiol, 2001. **9**(3): p. 113-4.
7. Degterev, A., et al., *Chemical inhibitor of nonapoptotic cell death with therapeutic potential for ischemic brain injury.* Nat Chem Biol, 2005. **1**(2): p. 112-9.
8. Yang, W.S. and B.R. Stockwell, *Synthetic lethal screening identifies compounds activating iron-dependent, nonapoptotic cell death in oncogenic-RAS-harboring cancer cells.* Chem Biol, 2008. **15**(3): p. 234-45.
9. Dixon, S.J., et al., *Ferroptosis: an iron-dependent form of nonapoptotic cell death.* Cell, 2012. **149**(5): p. 1060-72.
10. Seiler, A., et al., *Glutathione peroxidase 4 senses and translates oxidative stress into 12/15-lipoxygenase dependent- and AIF-mediated cell death.* Cell Metab, 2008. **8**(3): p. 237-48.
11. Dixon, S.J. and B.R. Stockwell, *The Hallmarks of Ferroptosis.* Annual Review of Cancer Biology, Vol 3, 2019. **3**: p. 35-54.
12. Agmon, E., et al., *Modeling the effects of lipid peroxidation during ferroptosis on membrane properties.* Sci Rep, 2018. **8**(1): p. 5155.
13. von Krusenstiern, A.N., et al., *Identification of essential sites of lipid peroxidation in ferroptosis.* Nat Chem Biol, 2023. **19**(6): p. 719-730.
14. Wang, W., et al., *CD8(+) T cells regulate tumour ferroptosis during cancer immunotherapy.* Nature, 2019. **569**(7755): p. 270-274.
15. Xie, Y., et al., *The Tumor Suppressor p53 Limits Ferroptosis by Blocking DPP4 Activity.* Cell Rep, 2017. **20**(7): p. 1692-1704.
16. Jiang, L., et al., *Ferroptosis as a p53-mediated activity during tumour suppression.* Nature, 2015. **520**(7545): p. 57-62.
17. Jenkins, N.L., et al., *Changes in ferrous iron and glutathione promote ferroptosis and frailty in aging Caenorhabditis elegans.* Elife, 2020. **9**.
18. Zheng, H., et al., *Embryonal erythropoiesis and aging exploit ferroptosis.* Redox Biol, 2021. **48**: p. 102175.
19. Distefano, A.M., et al., *Ferroptosis in plants: triggers, proposed mechanisms, and the role of iron in modulating cell death.* J Exp Bot, 2021. **72**(6): p. 2125-2135.
20. Li, L. and Z. Zhu, *Pharmacological modulation of ferroptosis as a therapeutic target for liver fibrosis.* Front Pharmacol, 2022. **13**: p. 1071844.
21. Tang, D., et al., *Ferroptosis: molecular mechanisms and health implications.* Cell Res, 2021. **31**(2): p. 107-125.
22. Conrad, M., S.M. Lorenz, and B. Proneth, *Targeting Ferroptosis: New Hope for As-Yet-Incurable Diseases.* Trends Mol Med, 2021. **27**(2): p. 113-122.
23. Lei, G., L. Zhuang, and B. Gan, *Targeting ferroptosis as a vulnerability in cancer.* Nat Rev Cancer, 2022. **22**(7): p. 381-396.
24. Kajarabille, N. and G.O. Latunde-Dada, *Programmed Cell-Death by Ferroptosis: Antioxidants as Mitigators.* Int J Mol Sci, 2019. **20**(19).
25. Magtanong, L., et al., *Exogenous Monounsaturated Fatty Acids Promote a Ferroptosis-Resistant Cell State.* Cell Chem Biol, 2019. **26**(3): p. 420-432 e9.

26. Hadian, K. and B.R. Stockwell, *SnapShot: Ferroptosis.* Cell, 2020. **181**(5): p. 1188-1188 e1.
27. Wiernicki, B., et al., *Excessive phospholipid peroxidation distinguishes ferroptosis from other cell death modes including pyroptosis.* Cell Death Dis, 2020. **11**(10): p. 922.
28. Koppenol, W.H., *The centennial of the Fenton reaction.* Free Radic Biol Med, 1993. **15**(6): p. 645-51.
29. Li, D. and Y. Li, *The interaction between ferroptosis and lipid metabolism in cancer.* Signal Transduct Target Ther, 2020. **5**(1): p. 108.
30. Feng, H., et al., *Transferrin Receptor Is a Specific Ferroptosis Marker.* Cell Rep, 2020. **30**(10): p. 3411-3423 e7.
31. Esworthy, R.S., et al., *Cloning and sequencing of the cDNA encoding a human testis phospholipid hydroperoxide glutathione peroxidase.* Gene, 1994. **144**(2): p. 317-8.
32. Friedmann Angeli, J.P., et al., *Inactivation of the ferroptosis regulator Gpx4 triggers acute renal failure in mice.* Nat Cell Biol, 2014. **16**(12): p. 1180-91.
33. Smith, A.C., et al., *Mutations in the enzyme glutathione peroxidase 4 cause Sedaghatian-type spondylometaphyseal dysplasia.* J Med Genet, 2014. **51**(7): p. 470-4.
34. Bhabak, K.P. and G. Mugesh, *Functional mimics of glutathione peroxidase: bioinspired synthetic antioxidants.* Acc Chem Res, 2010. **43**(11): p. 1408-19.
35. Yang, W.S., et al., *Regulation of ferroptotic cancer cell death by GPX4.* Cell, 2014. **156**(1-2): p. 317-331.
36. Liu, T., et al., *The Deubiquitylase OTUB1 Mediates Ferroptosis via Stabilization of SLC7A11.* Cancer Res, 2019. **79**(8): p. 1913-1924.
37. Wu, M., et al., *AMID, an apoptosis-inducing factor-homologous mitochondrion-associated protein, induces caspase-independent apoptosis.* J Biol Chem, 2002. **277**(28): p. 25617-23.
38. Doll, S., et al., *FSP1 is a glutathione-independent ferroptosis suppressor.* Nature, 2019. **575**(7784): p. 693-698.
39. Bersuker, K., et al., *The CoQ oxidoreductase FSP1 acts parallel to GPX4 to inhibit ferroptosis.* Nature, 2019. **575**(7784): p. 688-692.
40. Mishima, E., et al., *A non-canonical vitamin K cycle is a potent ferroptosis suppressor.* Nature, 2022. **608**(7924): p. 778-783.
41. Holstein, S.A. and R.J. Hohl, *Isoprenoids: remarkable diversity of form and function.* Lipids, 2004. **39**(4): p. 293-309.
42. Eisenhaber, F., et al., *Prediction of lipid posttranslational modifications and localization signals from protein sequences: big-Pi, NMT and PTS1.* Nucleic Acids Res, 2003. **31**(13): p. 3631-4.
43. Nasser, A. and L.B. Moller, *GCH1 variants, tetrahydrobiopterin and their effects on pain sensitivity.* Scand J Pain, 2014. **5**(2): p. 121-128.
44. Kraft, V.A.N., et al., *GTP Cyclohydrolase 1/Tetrahydrobiopterin Counteract Ferroptosis through Lipid Remodeling.* ACS Cent Sci, 2020. **6**(1): p. 41-53.
45. Soula, M., et al., *Metabolic determinants of cancer cell sensitivity to canonical ferroptosis inducers.* Nat Chem Biol, 2020. **16**(12): p. 1351-1360.
46. Ma, T., et al., *GPX4-independent ferroptosis-a new strategy in disease's therapy.* Cell Death Discov, 2022. **8**(1): p. 434.
47. Hu, Q., et al., *Blockade of GCH1/BH4 Axis Activates Ferritinophagy to Mitigate the Resistance of Colorectal Cancer to Erastin-Induced Ferroptosis.* Front Cell Dev Biol, 2022. **10**: p. 810327.
48. Kubota, C.S. and P.J. Espenshade, *Targeting Stearoyl-CoA Desaturase in Solid Tumors.* Cancer Res, 2022. **82**(9): p. 1682-1688.
49. Paton, C.M. and J.M. Ntambi, *Biochemical and physiological function of stearoyl-CoA desaturase.* Am J Physiol Endocrinol Metab, 2009. **297**(1): p. E28-37.
50. Soupene, E. and F.A. Kuypers, *Mammalian long-chain acyl-CoA synthetases.* Exp Biol Med (Maywood), 2008. **233**(5): p. 507-21.
51. Flowers, M.T. and J.M. Ntambi, *Stearoyl-CoA desaturase and its relation to high-carbohydrate diets and obesity.* Biochim Biophys Acta, 2009. **1791**(2): p. 85-91.

52. Sen, U., C. Coleman, and T. Sen, *Stearoyl coenzyme A desaturase-1: multitasker in cancer, metabolism, and ferroptosis.* Trends Cancer, 2023. **9**(6): p. 480-489.
53. Ndiaye, H., et al., *Immunohistochemical staining reveals differential expression of ACSL3 and ACSL4 in hepatocellular carcinoma and hepatic gastrointestinal metastases.* Biosci Rep, 2020. **40**(4).
54. Doll, S., et al., *ACSL4 dictates ferroptosis sensitivity by shaping cellular lipid composition.* Nat Chem Biol, 2017. **13**(1): p. 91-98.
55. Reed, A., et al., *LPCAT3 Inhibitors Remodel the Polyunsaturated Phospholipid Content of Human Cells and Protect from Ferroptosis.* ACS Chem Biol, 2022. **17**(6): p. 1607-1618.
56. Chen, X., et al., *Iron Metabolism in Ferroptosis.* Front Cell Dev Biol, 2020. **8**: p. 590226.
57. Hentze, M.W., et al., *Two to tango: regulation of Mammalian iron metabolism.* Cell, 2010. **142**(1): p. 24-38.
58. Lane, D.J., et al., *Cellular iron uptake, trafficking and metabolism: Key molecules and mechanisms and their roles in disease.* Biochim Biophys Acta, 2015. **1853**(5): p. 1130-44.
59. Wang, W., et al., *Serum ferritin: Past, present and future.* Biochim Biophys Acta, 2010. **1800**(8): p. 760-9.
60. Hou, W., et al., *Autophagy promotes ferroptosis by degradation of ferritin.* Autophagy, 2016. **12**(8): p. 1425-8.
61. Zhang, S., et al., *Double-edge sword roles of iron in driving energy production versus instigating ferroptosis.* Cell Death Dis, 2022. **13**(1): p. 40.
62. Dolma, S., et al., *Identification of genotype-selective antitumor agents using synthetic lethal chemical screening in engineered human tumor cells.* Cancer Cell, 2003. **3**(3): p. 285-96.
63. Zhang, Y., et al., *Imidazole Ketone Erastin Induces Ferroptosis and Slows Tumor Growth in a Mouse Lymphoma Model.* Cell Chem Biol, 2019. **26**(5): p. 623-633 e9.
64. Gout, P.W., et al., *Sulfasalazine, a potent suppressor of lymphoma growth by inhibition of the x(c)- cystine transporter: a new action for an old drug.* Leukemia, 2001. **15**(10): p. 1633-40.
65. Dixon, S.J., et al., *Pharmacological inhibition of cystine-glutamate exchange induces endoplasmic reticulum stress and ferroptosis.* Elife, 2014. **3**: p. e02523.
66. Weiwer, M., et al., *Development of small-molecule probes that selectively kill cells induced to express mutant RAS.* Bioorg Med Chem Lett, 2012. **22**(4): p. 1822-6.
67. Eaton, J.K., et al., *Selective covalent targeting of GPX4 using masked nitrile-oxide electrophiles.* Nat Chem Biol, 2020. **16**(5): p. 497-506.
68. Shimada, K., et al., *Global survey of cell death mechanisms reveals metabolic regulation of ferroptosis.* Nat Chem Biol, 2016. **12**(7): p. 497-503.
69. Gaschler, M.M., et al., *FINO(2) initiates ferroptosis through GPX4 inactivation and iron oxidation.* Nat Chem Biol, 2018. **14**(5): p. 507-515.
70. Hendricks, J.M., et al., *Identification of structurally diverse FSP1 inhibitors that sensitize cancer cells to ferroptosis.* Cell Chem Biol, 2023.
71. Zilka, O., et al., *On the Mechanism of Cytoprotection by Ferrostatin-1 and Liproxstatin-1 and the Role of Lipid Peroxidation in Ferroptotic Cell Death.* ACS Cent Sci, 2017. **3**(3): p. 232-243.
72. Devisscher, L., et al., *Discovery of Novel, Drug-Like Ferroptosis Inhibitors with in Vivo Efficacy.* J Med Chem, 2018. **61**(22): p. 10126-10140.
73. Conrad, M. and D.A. Pratt, *The chemical basis of ferroptosis.* Nat Chem Biol, 2019. **15**(12): p. 1137-1147.
74. Estrov, Z., et al., *In vitro and in vivo effects of deferoxamine in neonatal acute leukemia.* Blood, 1987. **69**(3): p. 757-61.
75. Hall, J.E., *Guyton and Hall Textbook of Medical Physiology*. 2015: Elsevier Health Sciences.
76. Ordonez-Moran, P. and A. Munoz, *Nuclear receptors: genomic and non-genomic effects converge.* Cell Cycle, 2009. **8**(11): p. 1675-80.

77. Scholtes, C. and V. Giguere, *Transcriptional control of energy metabolism by nuclear receptors.* Nat Rev Mol Cell Biol, 2022. **23**(11): p. 750-770.
78. De Bosscher, K., et al., *Nuclear receptor crosstalk — defining the mechanisms for therapeutic innovation.* Nature Reviews Endocrinology, 2020. **16**(7): p. 363-377.
79. O'Malley, B.W. and N.J. McKenna, *Coactivators and corepressors: what's in a name?* Mol Endocrinol, 2008. **22**(10): p. 2213-4.
80. Olefsky, J.M., *Nuclear receptor minireview series.* J Biol Chem, 2001. **276**(40): p. 36863-4.
81. Petkovich, M. and P. Chambon, *Retinoic acid receptors at 35 years.* J Mol Endocrinol, 2022. **69**(4): p. T13-T24.
82. Forman, B.M., et al., *Identification of a nuclear receptor that is activated by farnesol metabolites.* Cell, 1995. **81**(5): p. 687-93.
83. Anderson, K.M. and C.P. Gayer, *The Pathophysiology of Farnesoid X Receptor (FXR) in the GI Tract: Inflammation, Barrier Function and Innate Immunity.* Cells, 2021. **10**(11).
84. Fiorucci, S., et al., *Immunomodulatory functions of FXR.* Mol Cell Endocrinol, 2022. **551**: p. 111650.
85. Fang, S., *Bile Acid Receptor Farnesoid X Receptor: A Novel Therapeutic Target for Metabolic Diseases* Journal of Lipid and Atherosclerosis, 2017. **6**(1): p. 1-7.
86. Stofan, M. and G.L. Guo, *Bile Acids and FXR: Novel Targets for Liver Diseases.* Front Med (Lausanne), 2020. **7**: p. 544.
87. Hoeke, M.O., et al., *Human FXR Regulates SHP Expression through Direct Binding to an LRH-1 Binding Site, Independent of an IR-1 and LRH-1.* PLOS ONE, 2014. **9**(2): p. e88011.
88. Miao, J., et al., *Ligand-Dependent Regulation of the Activity of the Orphan Nuclear Receptor, Small Heterodimer Partner (SHP), in the Repression of Bile Acid Biosynthetic CYP7A1 and CYP8B1 Genes.* Molecular Endocrinology, 2011. **25**(7): p. 1159-1169.
89. Ricketts, M.L., et al., *The cholesterol-raising factor from coffee beans, cafestol, as an agonist ligand for the farnesoid and pregnane X receptors.* Mol Endocrinol, 2007. **21**(7): p. 1603-16.
90. Copple, B.L. and T. Li, *Pharmacology of bile acid receptors: Evolution of bile acids from simple detergents to complex signaling molecules.* Pharmacol Res, 2016. **104**: p. 9-21.
91. Peddicord, S., *FDA approves Ocaliva for rare, chronic liver disease*, U.S.F.a.D. Administration, Editor. 2016

.
92. Evans, M.J., et al., *A synthetic farnesoid X receptor (FXR) agonist promotes cholesterol lowering in models of dyslipidemia.* Am J Physiol Gastrointest Liver Physiol, 2009. **296**(3): p. G543-52.
93. Szapary, P.O., et al., *Guggulipid for the treatment of hypercholesterolemia: a randomized controlled trial.* JAMA, 2003. **290**(6): p. 765-72.
94. Giguere, V., et al., *Identification of a receptor for the morphogen retinoic acid.* Nature, 1987. **330**(6149): p. 624-9.
95. Petkovich, M., et al., *A human retinoic acid receptor which belongs to the family of nuclear receptors.* Nature, 1987. **330**(6147): p. 444-50.
96. Germain, P., et al., *International Union of Pharmacology. LX. Retinoic Acid Receptors.* Pharmacological Reviews, 2006. **58**(4): p. 712-725.
97. Mangelsdorf, D.J. and R.M. Evans, *The RXR heterodimers and orphan receptors.* Cell, 1995. **83**(6): p. 841-50.
98. Kiser, P.D., M. Golczak, and K. Palczewski, *Chemistry of the Retinoid (Visual) Cycle.* Chemical Reviews, 2014. **114**(1): p. 194-232.
99. Westin, S., et al., *Interactions controlling the assembly of nuclear-receptor heterodimers and co-activators.* Nature, 1998. **395**(6698): p. 199-202.
100. Germain, P., et al., *Co-regulator recruitment and the mechanism of retinoic acid receptor synergy.* Nature, 2002. **415**(6868): p. 187-92.

101. Ghyselinck, N.B. and G. Duester, *Retinoic acid signaling pathways.* Development, 2019. **146**(13).
102. Rakhshandehroo, M., et al., *Peroxisome proliferator-activated receptor alpha target genes.* PPAR Res, 2010. **2010**.
103. Blaner, W.S., I.O. Shmarakov, and M.G. Traber, *Vitamin A and Vitamin E: Will the Real Antioxidant Please Stand Up?* Annu Rev Nutr, 2021. **41**: p. 105-131.
104. Bi, G., et al., *Retinol saturase mediates retinoid metabolism to impair a ferroptosis defense system in cancer cells.* Cancer Res, 2023.
105. Li, D., et al., *Idebenone attenuates ferroptosis by inhibiting excessive autophagy via the ROS-AMPK-mTOR pathway to preserve cardiac function after myocardial infarction.* Eur J Pharmacol, 2023. **943**: p. 175569.
106. Dogne, J.M., et al., *Pharmacological characterization of N-tert-butyl-N'-[2-(4'-methylphenylamino)-5-nitrobenzenesulfonyl]urea (BM-573), a novel thromboxane A2 receptor antagonist and thromboxane synthase inhibitor in a rat model of arterial thrombosis and its effects on bleeding time.* J Pharmacol Exp Ther, 2004. **309**(2): p. 498-505.
107. Rolin, S., B. Masereel, and J.M. Dogne, *Prostanoids as pharmacological targets in COPD and asthma.* Eur J Pharmacol, 2006. **533**(1-3): p. 89-100.
108. McNaught, A.D. and A. Wilkinson, *IUPAC. Compendium of Chemical Terminology, 2nd ed.*, in *the „Gold Book“*. 1997, Blackwell Scientific Publications: Oxford.
109. Dhuriya, Y.K. and D. Sharma, *Necroptosis: a regulated inflammatory mode of cell death.* J Neuroinflammation, 2018. **15**(1): p. 199.
110. Clifford, B.L., et al., *FXR activation protects against NAFLD via bile-acid-dependent reductions in lipid absorption ll FXR activation protects against NAFLD via bile-acid-dependent reductions in lipid absorption.* Cell Metabolism, 2021. **33**: p. 1-14.
111. Mitsopoulos, C., et al., *canSAR: update to the cancer translational research and drug discovery knowledgebase.* Nucleic Acids Res, 2021. **49**(D1): p. D1074-D1082.
112. Makishima, M., et al., *Identification of a nuclear receptor for bile acids.* Science, 1999. **284**(5418): p. 1362-5.
113. Shah, R., M.S. Shchepinov, and D.A. Pratt, *Resolving the Role of Lipoxygenases in the Initiation and Execution of Ferroptosis.* ACS Cent Sci, 2018. **4**(3): p. 387-396.
114. Goodwin, B., et al., *A regulatory cascade of the nuclear receptors FXR, SHP-1, and LRH-1 represses bile acid biosynthesis.* Mol Cell, 2000. **6**(3): p. 517-26.
115. Wang, Y.D., et al., *FXR: A metabolic regulator and cell protector.* Cell Research, 2008. **18**(11): p. 1087-1095.
116. Hendricks, J.M., et al., *Identification of structurally diverse FSP1 inhibitors that sensitize cancer cells to ferroptosis.* bioRxiv, 2022: p. 2022.12.14.520445.
117. Li, Y., et al., *Ischemia-induced ACSL4 activation contributes to ferroptosis-mediated tissue injury in intestinal ischemia/reperfusion.* Cell Death Differ, 2019. **26**(11): p. 2284-2299.
118. Stockwell, B.R., et al., *Ferroptosis: A Regulated Cell Death Nexus Linking Metabolism, Redox Biology, and Disease.* Cell, 2017. **171**(2): p. 273-285.
119. Ursini, F., Maiorino, M., Valente, M., Ferri, L., Gregolin, C., *Purification from pig liver of a protein which protects liposomes and biomembranes from peroxidative degradation and exhibits glutathione peroxidase activity on phosphatidylcholine hydroperoxides.* Biochimica et biophysica acta, 1982. **710**(2): p. 197-211.
120. Linkermann, A., et al., *Synchronized renal tubular cell death involves ferroptosis.* Proc Natl Acad Sci U S A, 2014. **111**(47): p. 16836-41.
121. Noack, V., et al., *An Antioxidant Screen Identifies Candidates for Protection of Cochlear Hair Cells from Gentamicin Toxicity.* Front Cell Neurosci, 2017. **11**: p. 242.
122. Ernster, L. and G. Dallner, *Biochemical, physiological and medical aspects of ubiquinone function.* Biochim Biophys Acta, 1995. **1271**(1): p. 195-204.
123. Nowicka, B. and J. Kruk, *Occurrence, biosynthesis and function of isoprenoid quinones.* Biochim Biophys Acta, 2010. **1797**(9): p. 1587-605.
124. Lenaz, G.G., M. L., *Quinones*, in *Encyclopedia of Biological Chemistry*, W.J.L. Lennarz, M. D. , Editor. 2004, Elsevier. p. 621-627.

125. Hao, Y., et al., *Seratrodast, a thromboxane A2 receptor antagonist, inhibits neuronal ferroptosis by promoting GPX4 expression and suppressing JNK phosphorylation.* Brain Res, 2022. **1795**: p. 148073.
126. Shah, R., et al., *Beyond DPPH: Use of Fluorescence-Enabled Inhibited Autoxidation to Predict Oxidative Cell Death Rescue.* Cell Chem Biol, 2019. **26**(11): p. 1594-1607 e7.
127. Stenton, S.L., et al., *Impaired complex I repair causes recessive Leber's hereditary optic neuropathy.* J Clin Invest, 2021. **131**(6).
128. Jakaria, M., et al., *Vitamin A metabolites inhibit ferroptosis.* Biomed Pharmacother, 2023. **164**: p. 114930.
129. Bi, G., et al., *Retinol Saturase Mediates Retinoid Metabolism to Impair a Ferroptosis Defense System in Cancer Cells.* Cancer Res, 2023. **83**(14): p. 2387-2404.
130. Chen, Y., F. Derguini, and J. Buck, *Vitamin A in serum is a survival factor for fibroblasts.* Proc Natl Acad Sci U S A, 1997. **94**(19): p. 10205-8.
131. Dinkova-Kostova, A.T. and P. Talalay, *Direct and indirect antioxidant properties of inducers of cytoprotective proteins.* Mol Nutr Food Res, 2008. **52 Suppl 1**: p. S128-38.
132. Levin, A.A., et al., *9-cis retinoic acid stereoisomer binds and activates the nuclear receptor RXR alpha.* Nature, 1992. **355**(6358): p. 359-61.
133. Deluao, J.C., et al., *OXIDATIVE STRESS AND REPRODUCTIVE FUNCTION: Reactive oxygen species in the mammalian pre-implantation embryo.* Reproduction, 2022. **164**(6): p. F95-F108.
134. McDougall, M., et al., *Vitamin E deficiency during embryogenesis in zebrafish causes lasting metabolic and cognitive impairments despite refeeding adequate diets.* Free Radic Biol Med, 2017. **110**: p. 250-260.
135. Jaeschke, W., et al., *Role of Oxidative Stress in Liver Disorders.* Livers, 2022. **2**: p. 283-314.
136. Venkatesh, D., et al., *MDM2 and MDMX promote ferroptosis by PPARalpha-mediated lipid remodeling.* Genes Dev, 2020. **34**(7-8): p. 526-543.
137. Xing, G., et al., *PPARa alleviates iron overload-induced ferroptosis in mouse liver.*
138. Kim, D.-H., et al., *Farnesoid X receptor protects against cisplatin-induced acute kidney injury by regulating the transcription of ferroptosis-related genes.* Redox Biology, 2022. **54**: p. 102382-102382.
139. Heisterkamp, N., et al., *The human gamma-glutamyltransferase gene family.* Hum Genet, 2008. **123**(4): p. 321-32.
140. Xu, Y., et al., *Glutathione-S-transferase protects against oxidative injury of endothelial cell tight junctions.* Endothelium, 2007. **14**(6): p. 333-43.
141. Dai, C., et al., *Transcription factors in ferroptotic cell death.* Cancer Gene Ther, 2020. **27**(9): p. 645-656.
142. Ma, Q., *Role of nrf2 in oxidative stress and toxicity.* Annu Rev Pharmacol Toxicol, 2013. **53**: p. 401-26.
143. Dodson, M., R. Castro-Portuguez, and D.D. Zhang, *NRF2 plays a critical role in mitigating lipid peroxidation and ferroptosis.* Redox Biol, 2019. **23**: p. 101107.
144. Sun, X., et al., *Activation of the p62-Keap1-NRF2 pathway protects against ferroptosis in hepatocellular carcinoma cells.* Hepatology, 2016. **63**(1): p. 173-84.
145. Roh, J.L., et al., *Nrf2 inhibition reverses the resistance of cisplatin-resistant head and neck cancer cells to artesunate-induced ferroptosis.* Redox Biol, 2017. **11**: p. 254-262.
146. Li, S., et al., *Obeticholic acid and ferrostatin-1 differentially ameliorate non-alcoholic steatohepatitis in AMLN diet-fed ob/ob mice.* Front Pharmacol, 2022. **13**: p. 1081553.
147. Ramirez-Perez, O., et al., *The Role of the Gut Microbiota in Bile Acid Metabolism.* Ann Hepatol, 2017. **16 Suppl 1**: p. S21-S26.
148. Upadhyayula, P.S., et al., *Dietary restriction of cysteine and methionine sensitizes gliomas to ferroptosis and induces alterations in energetic metabolism.* Nat Commun, 2023. **14**(1): p. 1187.
149. Xia, Y., et al., *Human stem cell-derived hepatocytes as a model for hepatitis B virus infection, spreading and virus-host interactions.* J Hepatol, 2017. **66**(3): p. 494-503.

150. Zhang, J.H., T.D. Chung, and K.R. Oldenburg, *A Simple Statistical Parameter for Use in Evaluation and Validation of High Throughput Screening Assays.* J Biomol Screen, 1999. **4**(2): p. 67-73.
151. Xin, S., et al., *MS4A15 drives ferroptosis resistance through calcium-restricted lipid remodeling.* Cell Death Differ, 2022. **29**(3): p. 670-686.